ESTERIFICATION OF FREE FATTY ACID AND OIL WITH FATTY ACID CONTENT OVER ACIDIC HETEROGENEOUS CATALYST

Miss Sirima Jeenpadiphat

A Thesis Submitted in Partial Fulfillment of the Requirements for the Degree of
Doctor of Philosophy Program in Nanoscience and Technology
(Interdisciplinary Program)
Graduate School
Chulalongkorn University
Academic Year 2012

เอสเทอริฟิเคชันของกรดไขมันอิสระและน้ำมันที่มีกรดไขมันเป็นองค์ประกอบโดยใช้ตัวเร่งปฏิกิริยาวิวิธพันธุ์ชนิดกรด

นางสาวศิริมา จีนปฏิพัทธิ์

วิทยานิพนธ์นี้เป็นส่วนหนึ่งของการศึกษาตามหลักสูตรปริญญาวิทยาศาสตรดุษฎีบัณฑิต
สาขาวิชาวิทยาศาสตร์นาโนและเทคโนโลยี (สหสาขาวิชา)
บัณฑิตวิทยาลัย จุฬาลงกรณ์มหาวิทยาลัย
ปีการศึกษา 2555

Thesis Title	ESTERIFICATION OF FREE FATTY ACID AND OIL WITH FATTY ACID CONTENT OVER ACIDIC HETEROGENEOUS CATALYST
By	Miss Sirima Jeenpadiphat
Field of Study	Nanoscience and Technology
Thesis Advisor	Duangamol Tungasmita, Ph.D.

Accepted by the Faculty of Graduate School, Chulalongkorn University in Partial Fulfillment of the Requirements for the Doctoral Degree

….....Dean of the Graduate School

(Associate Professor Amorn Petsom, Ph.D.)

THESIS COMMITTEE

……...Chairman

(Associate Professor Vudhichai Parasuk, Ph.D.)

……...Thesis Advisor

(Duangamol Tungasmita, Ph.D.)

……Examiner

(Assistant Professor Sukkaneste Tungasmita, Ph.D.)

……Examiner

(Ratthapol Rangkupan, Ph.D.)

……External Examiner

(Anurak Winitsorn, Ph.D.)

ศิริมา จีนปฏิพัทธ์ : เอสเทอริฟิเคชันของกรดไขมันอิสระและน้ำมันที่มีกรดไขมันเป็นองค์ประกอบโดยใช้ตัวเร่งปฏิกิริยาวิวิธพันธุ์ชนิดกรด (ESTERIFICATION OF FREE FATTY ACID AND OIL WITH FATTY ACID CONTENT OVER ACIDIC HETEROGENEOUS CATALYST) อ. ที่ปรึกษาวิทยานิพนธ์หลัก: ดร. ดวงกมล ตุงคะสมิต, 131 หน้า.

ได้ศึกษาปฏิกิริยาเอสเทอริฟิเคชันของแอลกอฮอล์และน้ำมันที่มีกรดไขมันเป็นองค์ประกอบสูงโดยใช้ตัวเร่งปฏิกิริยาวิวิธพันธุ์ชนิดกรด โดยมีเมทานอล เอทานอล กลีเซอรอล กรดปาล์มิติก กรดโอเลอิก น้ำมันสบู่ดำ น้ำมันปาล์มที่ผ่านการใช้งานแล้วและน้ำมันผสมระหว่างกรดโอเลอิกร้อยละ 15 โดยน้ำหนักกับน้ำมันปาล์มกลั่นเป็นสารตั้งต้นในปฏิกิริยาเอสเทอริฟิเคชัน ความแตกต่างทางรูปร่างสัณฐานวิทยาและขนาดรูพรุนของสารเอสบีเอ-15 ซิลิการูพรุนขนาดกลางที่เติมหมู่กรดโพรพิลซัลโฟนิก ดินเบนโทไนต์ที่ถูกทำให้เป็นกรด และดินพิลลาร์เบนโทไนต์ที่ถูกทำให้เป็นกรดได้ถูกเตรียมขึ้นและศึกษาประสิทธิภาพในการเป็นตัวเร่งปฏิกิริยาของสารเหล่านี้ โดยสารที่เตรียมนี้ถูกนำไปตรวจสอบลักษณะเฉพาะด้วยเทคนิคการเลี้ยวเบนของรังสีเอกซ์ การดูดซับแก๊สไนโตรเจน การเรืองแสงของรังสีเอกซ์ กล้องจุลทรรศน์แบบส่องกราด และกล้องจุลทรรศน์แบบส่องผ่าน ตัวเร่งปฏิกิริยาเอสบีเอ-15 ที่มีลักษณะเป็นเกลียวเชือกที่มีหมู่กรดโพรพิลซัลโฟนิกแสดงประสิทธิภาพการเป็นตัวเร่งปฏิกิริยาสูงที่สุดในการเปลี่ยนกรดโอเลอิกและให้ผลผลิตไตรกลีเซอไรด์สูงที่สุดเนื่องด้วยตัวเร่งปฏิกิริยานี้มีความเป็นกรดและมีพื้นที่ผิวในการเกิดปฏิกิริยาสูง นอกจากนี้วิธีการที่เหมาะสมในการเพิ่มความเป็นกรดให้ดินเบนโทไนต์มีผลทำให้ดินเบนโทไนต์นี้แสดงประสิทธิภาพในการให้ผลผลิตเมทิลโอลีเอทสูงถึง 100 เปอร์เซ็นต์และสามารถเปลี่ยนกรดไขมันอิสระได้สูงถึง 99 เปอร์เซ็นต์ในปฏิกิริยาเอสเทอริฟิเคชันของกรดโอเลอิกในน้ำมันปาล์มกับเมทานอล นอกจากนี้ดินพิลลาร์เบนโทไนต์ถูกเตรียมได้สำเร็จและมีพื้นที่ผิวเพิ่มมากขึ้นอย่างมีนัยสำคัญกว่าดินเบนโทไนต์ตั้งต้น 20 เท่า ตัวเร่งปฏิกิริยากรดพิลลาร์เบนโทไนต์นี้มีประสิทธิภาพในการเร่งปฏิกิริยาได้ดีกว่าดินเบนโทไนต์ตั้งต้นและตัวเร่งปฏิกิริยาทางการค้าเรซิ่นชนิดกรดอีกด้วย

สาขาวิชา วิทยาศาสตร์นาโนและเทคโนโลยี ลายมือชื่อนิสิต .....

ปีการศึกษา 2555 ลายมือชื่อ อ. ที่ปรึกษาวิทยานิพนธ์หลัก .....

53878656: MAJOR NANOSCIENCE AND TECHNOLOGY
KEYWORDS: HETEROGENEOUS / ESTERIFICATION / BIODIESEL / CATALYST / MESOPOROUS SILICA / ACID ACTIVATION / CLAY
SIRIMA JEENPADIPHAT: ESTERIFICATION OF FREE FATTY ACID AND OIL WITH FATTY ACID CONTENT OVER ACIDIC HETEROGENEOUS CATALYST. ADVISOR: DUANGAMOL TUNGASMITA, Ph.D., 131 pp.

The esterification of alcohol with high acid content oil was investigated with different acidic heterogeneous catalysts. The methanol, ethanol, glycerol, palmitic acid, oleic acid, Jatropha oil, waste cooking palm oil and mixed refined palm oil with 15 wt.% oleic acid were used as esterification starting materials. The different morphology and pore size of propyl sulfonic functionalized mesoporous silica SBA-15, acid-activated clay and acid-activated pillar bentonite materials were prepared and studied their catalytic activities. The characterization of the synthesized materials was conducted by XRD, nitrogen adsorption, XRF, SEM and TEM analysis. The rope-like propyl sulfonic functionalized SBA-15 catalyst showed highest catalytic activity in case of oleic acid conversion and tri-glyceride yield, due to its high acid amount and surface area. Moreover, an appropriated bentonite treatment could increase acidity, resulting that bentonite catalyst exhibited high methyl oleate yield as 100% and 99% of FFA conversion in the esterification of oleic acid in palm oil with methanol. Finally, the pillar bentonite was successfully prepared and significantly increased the specific surface area 20-fold compared with the parent material. The acid-activated pillar bentonite catalyst provided higher catalytic activity than bentonite parent and commercial acidic resin catalyst.

Field of Study Nanoscience and Technology Student's Signature .....

Academic year 2012 Advisor's Signature .....

ACKNOWLEDGEMENTS

The success of this thesis can be attributed to the extensive support, valuable suggestion and assistance from my thesis advisor, Dr. Duangamol Tungasmita. I deeply thank her for kindness throughout this study.

I would like to give my gratitude to the chairperson, Associate Professor Dr. Vudhichai Parasuk and member of this thesis committee, Assistant Professor Dr. Sukkaneste Tungasmita, Dr. Ratthapol Rangkupan and Dr. Anurak Winitsorn, respectively, for all of their kindness and useful advice in the research.

I would like to gratefully thank to the financial support from PTT Public Company Limited. Moreover, I am grateful to Program of Nanoscience and Technology, Faculty of Graduate School, Chulalongkorn University for the valuable knowledge and experience. I also would like to thank the members of Materials Chemistry and Catalysis Research Unit and my friends for their encouragement and friendship.

Finally, I would like to express my deepest gratitude to my family for their entirely care, understanding and financial support.

CONTENTS

Page

Page

Page

Page

Page

Page

LIST OF TABLES

LIST OF FIGURES

Figure **Page**

Figure **Page**

Figure **Page**

Figure **Page**

LIST OF SCHEMES

.

LIST OF ABBREVIATIONS

Btu	British thermal unit
K	Kelvin
°C	Degree Celsius
µm	Micrometer
nm	Nanometer
mL	Milliliter (s)
ppm	Part per million
M	Molar
Å	Angstrom unit
CCD	Couple charge detector
eV	Electron volt
R.T.	Room temperature
CCT	Charge transfer
XRD	X-ray diffraction
NMR	Nuclear magnetic resonance
GC	Gas chromatography
SEM	Scanning electron microscopy
BET	Brunauer, Emmett and Teller equation
BJH	Barret-Joyner-Halender equation
h	Hour or hours
^{o}C	Degree Celsius
min	Minute or minutes
wt%	Percent by weight
mole%	Percent by mole
FFAs	Free fatty acids
CMC	Critical micelle concentration
MPTMS	(3-mercaptopropyl)trimethoxysilane
TEOS	Tetraethyl orthosilicate
Std.	Standard

CHAPTER I

INTRODUCTION

1.1 Background

Diesel fuel is one fraction from crude oil refinery process containing C_{14} - C_{25} hydrocarbon complexes that used in transportation and agricultural goods. The diesel fuel demand has been increasing as well as the economic growth. The world diesel consumption is about 100 billion liters per year. Currently, about 2.2 million barrels of diesel fuel is consumed everyday in the U.S. road transportation market. Thailand imports more than 100 million liters of foreign oil each year of which 46% is diesel which is the most consumption. Thailand imports more than 100 million liters of foreign oil each year of which 46% is diesel which is the most consumption [1-3]. The total world energy consumption and production in 1980-2030 was shown in the Figures 1.1.

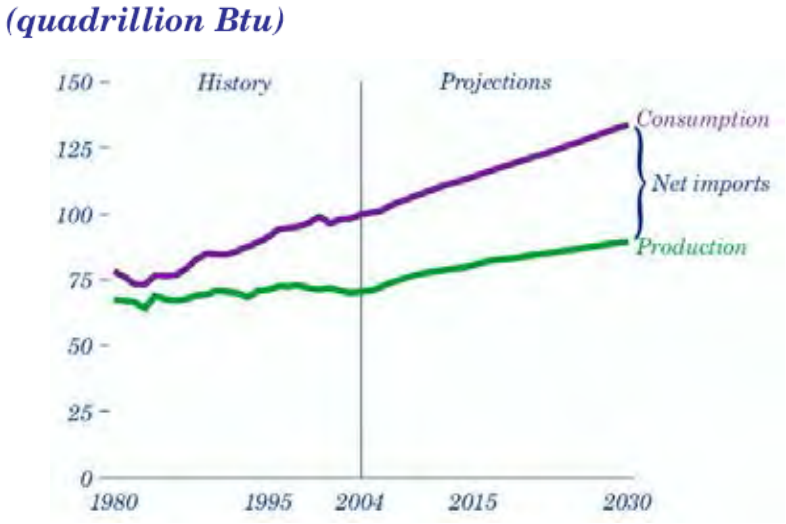

Figure 1.1 The total world energy consumption [1].

Biodiesel is an alternative, renewable and sustainable energy for replacement of the non-renewable petroleum diesel. Biodiesel is an fatty acid alkyl ester (FAME), which was produced from either transesterification of triglyceride from vegetable oils and animal fats (Figure 1.2) or esterification of free fatty acid (FFA) (Figure 1.3) react with short chain alcohols such as methanol and ethanol in the presence of catalyst to create a complex mixture of fatty acid methyl ester (FAME) and glycerol or water as by-products [5-8]. The advantages of biodiesel are bio-degradable, non-toxic in nature, low emission profile thus help reducing global warming, friendly environment and essentially free from sulfur and aromatics [9-12].

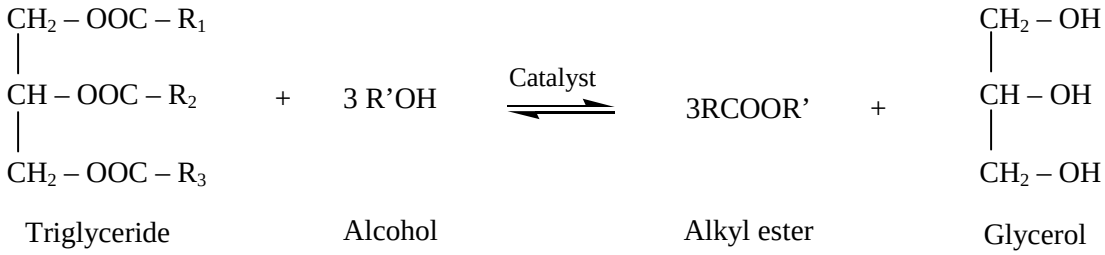

Figure 1.2 Transesterification of triglyceride and alcohol.

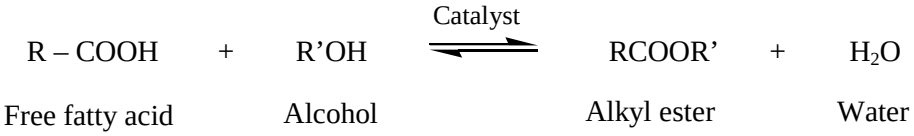

Figure 1.3 Esterification of free fatty acid and alcohol.

Catalytic using for the transesterification and esterification are categorized as homogeneous catalyst, enzyme [6, 7, 13, 14] and heterogeneous catalyst, but conventional processing mostly involves a homogeneous alkali catalyzed process. Because basic catalyzed process is less corrosive than the homogeneous acidic catalysts and proceeds at higher rate. The alkali catalysts including sodium hydroxide, sodium methoxide, potassium hydroxide and potassium methoxide, etc. are effective

[15] but the alkali catalyst is unsatisfied for high free fatty acid feed stocks because of soap formation.

Although transesterification using a basic catalyzed process exhibits high methyl esters yield in short times but the catalyst has difficult to remove from the product. Therefore, the heterogeneous catalyst was used as catalyst to replace homogeneous catalyst in transesterification of triglycerides. This catalyst shows greatly simplify the post-treatment of the products (separation and purification). They can be easily separated from the system at the end of the reaction run and can also be reused. The wide use of heterogeneous catalysts has been reported by many researchers, including enzymes, zeolites, clays, and ion-exchange resins [10].

However, pretreatment process using acidic catalyst exhibits high yield and high quality of biodiesel product. These techniques have been provided to permit biodiesel production from soap stock and high free fatty acid content oils that are waste matter. Moreover, the procedures are very sensitive to the presence of water and free fatty acid [16]. One methodology for enhancing the processing of high free fatty acid oils is free fatty acid esterification to produce alkyl esters in the presence of an acidic catalyst. This pretreatment step has been successfully done using sulfuric acid catalyst. Unfortunately, using of the homogeneous sulfuric acid catalyst is difficult to neutralization, separation and reuse. Therefore, it would be required to carry out the esterification pretreatment step using a heterogeneous acidic catalyst [17].

Since Santa Barbara researchers [18] has contributed largely to the development of the heterogeneous mesoporous silica material that was SBA-15. The SBA-15 material was performed using amphiphilic triblockcopolymers, poly(ethylene oxide) - poly(propylene oxide) - poly(ethylene oxide) as a structure directing agent (template). This material contains long range-ordered hexagonal structure (Figure 1.4), high surface areas, large uniform mesopore (up to approximately 30 nm). Moreover, mesoporous SBA-15 allows bulky molecules to enroll into their pores and because of high pore wall thickness so this material is higher thermal stable than other

materials. Due to their controllable pore size, the ordered mesoporous materials have a large potential as catalyst in organic chemistry reactions, as well as for the production of biodiesel industry.

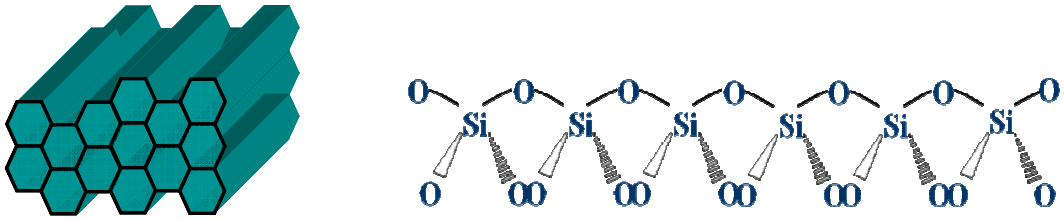

Figure 1.4 Hexagonal structure of mesoporous SBA-15 [18].

Mesoporous silica SBA-15 can be incorporated with hydrophobic hydrocarbon such as propyl (-Pr-) and inorganic sulfonic acid group (-SO_3H) via two different synthesis procedures that are direct synthesis and post-synthesis grafting procedure. The direct synthesis procedure often required a specialized synthesis conditions depending on the respective structures of the materials, and the incorporation of propyl sulfonic acid into the silica matrix usually caused a decrease in the structural ordering [19].

The development of a simple post-synthesis grafting method for the propyl sulfonic acid functionalized mesoporous SBA-15 become an appealing alternate choice. The grafting method provides the well-ordered functionalized mesoporous materials. However, this method often creates irregularly distributed organic groups because the surface hydroxyls, which needed for the functionalization, are randomly distributed above the surface [20].

In addition, clay catalysts are novel materials not only because of the low cost raw materials and less harmful environment but also because of their properties, such as mechanical and thermal stability and ion-exchange capacity. Furthermore, acid-activation is process that can be used to modify in clays. The advantages of acid-activation are rising in surface area, porosity and number of acidic sites compared to

the parent clays [21]. Bentonite can be used both in natural form and after some property treatments according to the application areas [22, 23]. Major clay minerals in bentonites are montmorillonite, beidellite, saponite, nontronite, and hectorite [24]. Acid-activated bentonite was used in many applications depend on the treatment conditions [25].

1.2 Literature reviews on catalyst

1.2.1 Mesoporous silica catalyst

In the recent year the interest in large mesoporous silica has increased. Some of these materials possess improved catalytic properties in comparison with the classical zeolite. Many studies have been carried out to synthesize highly pure mesoporous silica and modified mesoporous silica materials. In the synthesis routes of mesoporous silica, many parameters were concerned.

In 1998, Stucky *et al.* [18] successfully synthesized a mesoporous molecular sieves, SBA-15, using amphiphilic triblockcopolymers, poly(ethylene oxide)-poly(propylene oxide) - poly(ethylene oxide) as surfactant under acidic conditions. SBA-15 has the pore size in the range of 50 to 300 Å, wall thickness about 31 to 64 Å that refers to hydrothermal stability.

Moreover, many researchers indicated that MCM-41 had lower hydrothermal stability than SBA-15 thus MCM-41 was not suitable for catalytic reaction at high temperature. However, the SBA-15 consists of pure silica frameworks which limited to use for acid catalytic application. Generally, incorporation of heteroatom has been implemented in order to create active site and ion-exchange capacity [26].

Because the SBA-15 has less acidity, therefore in 2000, Melero *et al.* [27] investigated the new procedure in the synthesization of sulfonic acid functionalized mesostructure materials. They improved the direct synthesis method to create propyl sulfonic acid functionalized SBA-15 (SBA-15-Pr-SO_3H). This

procedure involved an one-step co-condensation of tetraethyl orthosilicate (TEOS) and (3-mercaptopropyl) trimethoxysilane (MPTMS) in the presence of Pluronic P123 and hydrogen peroxide in HCl aqueous solution. This approach allowed in-situ oxidation of the thiol groups to sulfonic acid groups.

In 2002, Melero *et al*. used the same route for the preparation of ordered SBA-15 comprising aryl sulfonic acid groups [28]. The synthesis strategy involved the co-condensation of 2-(4-chlorosulfonylphenyl)ethyltrimethoxysilane (CSPETMS) and TEOS using Pluronic P123 as template under acidic conditions. Hydrolysis of the chlorosulfonyl groups (-$SOCl_2$) to the conforming sulfonic acid groups was achieved under acidic condensation reaction. The resultant material showed large uniform pore sizes (*ca.* 60 Å) with large surface areas (*ca.* 650 m^2/g), good mesoscopic ordering, and thick walls.

In 2005, Luo *et al*. [29] studied the increasing acidity of SBA-15 by grafting sulfonic acid group (-SO_3H) on the surface using post-synthesis grafting method. The effects of time and amount of oxidizing agent were investigated. The resultant material showed the highest acidity when oxidized with 30% H_2O_2 for 24 h. Moreover, SBA-15-Pr-SO_3H exhibited high specific surface areas (600 m^2/g) and uniform pore sizes (6 nm).

In 2008, Cheng *et al*. [30] studied arene and propyl sulfonic acid dual-functionalized mesoporous silica materials. These samples were synthesized by co-condensation of TEOS and organosilane precursors in the presence of Pluronic P123 tri-block copolymer under acidic condition. The various concentrations of the organosilane precursors in synthesis gel were performed and sulfur contents in prepared materials were determined. The arene and propyl sulfonic acid dual-functionalized SBA-15 catalyst exhibited higher catalytic activity than the single arene sulfonic acid functionalized in condensation of phenol and acetone to produce bisphenol-A.

In 2009, Kureshy *et al*. [31] studied organo sulfonic acid functionalized mesoporous material. From the results, the propyl sulfonic acid functionalized SBA-15 material was an excellent dehydrating heterogeneous acidic catalyst for the reaction of chromanol to produce chromenes. This catalyst showed high chromanols conversion as 99% in 10 min reaction time and gave 10 times catalytic reusability. Moreover, the acidic heterogeneous propyl sulfonic acid functionalized SBA-15 provided higher catalytic efficiency than acidic homogeneous p-toluene sulfonic acid (pTSA) catalyst due to simple preparation, easy recovery and reusability.

1.2.2 Acid-activated clay catalyst

The use of clay mineral as catalyst has expanded rapidly in recent years as well as their properties, such as mechanical stability, thermal stability, high surface area and ion-exchange capacity. In 1995, Galarneau *et al.* [32] suggested a different route to achieve thermal stability materials from the cationic layer clays in three steps. Firstly, the cationic surfactant and neutral amine co-surfactants were added in the interlayer space of the host clay creating micelle structures. Secondly, in-situ polymerization of a silica source around the micelle structures was performed to form silica pillars, and then finally the calcination was used to remove organic surfactants from the material. This process obtained a new class of materials (porous pillar clays) with a high specific surface area with micro and mesoporous structures

In 2011, Nascimento *et al.* [33] studied the esterification of oleic acid with methanol for biodiesel production over acid-activated metakaolin catalyst. The kaolin was treated at 950 °C and activated with 4 M sulfuric acid solutions to produce acid-activated metakaolin. This material exhibited high acidic sites (250.5 μmol/g) and offered larger conversion values. The effect of temperature and time were examined. From the catalytic results, kaolin was found to be an encouraging raw material for the creation of new acidic heterogeneous catalyst in the esterification of FFA.

In 2011, Moraes et al. [34] studied the esterification of acetic acid and 1-propanol using propyl sulfonic acid functionalized bentonite catalyst. This material was synthesized by using post synthesis grafting method. Functionalization was performed by anchoring, oxidation and acid activation of (3-mercaptopropyl)trimethoxysilane. The preparation provided acid properties to the raw bentonite. This catalyst enhanced the reaction rate and product yield when compared to the no catalyst reaction. The propyl sulfonic acid functionalized bentonite catalyst exhibited 65% acetic conversion at 100^{o}C for 10 h.

1.3 Literature reviews on esterification of vegetable oils and free fatty acids

Zirconium sulfate was supported on silica (ZS) with 10-50 wt% loading was studied as the solid acid catalyst in esterification reaction of oleic acid. The reaction was shown that the zirconium supported ZS provided a higher activity than bulk ZS, Amberlyst-15 and conventional acid resins at reaction temperature 120^{o}C for 4 h and amount of catalyst 5 wt% based on oleic free fatty acid (94% conversion) [35]. After that, Ni, *et al.* [36] considered the esterification of free fatty acid (palmitic acid) with methanol over silica-supported Nafion® resin (SAC-13) and sulfated zirconia using batch and fixed bed-reactors.

Marchetti, J. M. *et al.* [37] used basic resins (Dowex monosphere 550A and Dowex upcore Mono A-625) to perform the esterification reaction into biodiesel from frying oils with a certain high amount of free fatty acids. The effect of the reaction temperature 30-55^{o}C, ethanol to oil mole ratio 4:1-6:1, amount of catalyst 2-7% and amount of free fatty acids (oleic acid) 2-27 fed with the oil have been studied. The final conversion was obtained of 80%.

In 2010, Morales *et al.* [38] reported the polystyrene sulfonic acid functionalized mesoporous silica material was used as catalyst in acylation of anisole with acetic anhydride, Fries rearrangement of phenyl acetate and esterification of oleic acid with n-butanol. This catalyst was synthesized by using direct co-condensation of styrylethyl-trimethoxysilane (STETMOS) and tetraethyl-orthosilicate (TEOS) in one-pot synthesis. As the results, the polystyrene sulfonic functionalized

mesoporous silica materials provided well-ordered hexagonal structure with high surface area and narrow pore size distribution. For esterification of oleic acid with n-butanol, the poly styrene sulfonic functionalized SBA-15 catalyst exhibited 85% oleic acid conversion that was higher than commercial Amberlyst-15 and SAC-13 resin under 1:1.2 oleic acid to butanol mole ratio, 115^{o}C for 3 h and 2 wt.% catalyst amount condition.

In 2010, Melero *et al.* [39] studied biodiesel production from high free fatty acid content palm oil using sulfonic acid-functionalized SBA-15 materials. The results showed that sulfonic acid functionalized mesoporous silica materials were higher active than conventional ion-exchange sulfonic resins (Amberlyst-36 and SAC-13) in esterification reaction. The reused propyl-SO_3H and arene-SO_3H-functinalized mesoporous catalysts provided high stability. However, ionic-exchange sulfonic acid resins demonstrated low conversion in the second run. Moreover, arene-SO_3H functionalized SBA-15 catalyst with hydrophobic trimethylsilyl groups enhanced its catalytic performance. This catalyst gave FAME yield of 95% in 4 h at methanol to oil mole ratio of 20:1, 140^{o}C and a catalyst amount of 6 wt.% based on reactants.

From literatures that were mentioned above, the acidic heterogeneous catalyst was suitable for esterification reaction both in catalytic activity and separation process. Therefore, in this study we utilize organo-sulfonic acid functionalized mesoporous silica and acid-activated clay as acidic heterogeneous catalysts in esterification of FFA and high acid content oil with methanol or ethanol for pre-treatment in biodiesel production. Furthermore, some properties, such as crystal structure, chemical composition, morphology, specific surface area, pore volume and pore diameter of prepared SBA-15-Pr-SO_3H and acid-treated clay were investigated. The catalytic activities of reuse and regenerated catalysts were also performed.

1.4 Objectives

1.4.1 To prepare SBA-15-Pr-SO_3H and acid-treated clay catalysts by using easy and low cost method

1.4.2 To characterize the synthesized catalysts by using XRD, N_2-adsorption, SEM, TEM, XRF, acidic-base titration and CHNS/O techniques

1.4.3 To compare catalytic activities of prepared materials in esterification of oleic acid, palmitic acid, palm olein oil, Jatropha oil and waste cooking palm oil with methanol or ethanol at low temperature and small amount of alcohol

1.4.4 To investigate the optimum conditions in esterification reaction of FFA

1.4.5 To test reuseability and regeneration of catalysts

1.5 Scope

This research studies about mesoporous SBA-15 and modified mesoporous SBA-15 synthesis and clay acid-activation process, characterization of synthesized materials, catalytic activity testing in esterification of FFAs and high acid content oil with methanol or ethanol. In addition, the reuseability and regeneration of catalysts will be investigated.

CHAPTER II

THEORY

2.1 Catalyst

Industrial catalysts comprise wide variety of materials that was manufactured by a variety of methods. Many catalysts or porous structure were studied. The commercially useful catalyst particle size is determined by the process in which to be used, fixed beds and fluidized beds. In fluidized beds reactors, usually present in the catalyst powder supplied. The particles present generally range from about 20-300 μm in diameter. For fixed beds particles generally range from about 0.0625-0.5 inches in diameter. In general, 60% of commercially produced chemical products involve catalyst at some stage in the process of their manufacture [40].

2.2 Types of catalysts

Catalysts can be distributed into two categories, heterogeneous and homogeneous catalysts. Heterogeneous catalyst is presence in different phases from the starting materials; whereas, homogeneous catalyst is in the same phase.

2.2.1 Homogeneous catalysts

The material, which present in the same phase of reactants, is homogeneous catalysts. The catalyst begins reaction with reactants to produce intermediate materials and products. Following steps induce to the formation of products and to the reuse and regeneration of the catalyst. Typically, everything will be presence as gas or contained in a single liquid phase.

2.2.2 Heterogeneous catalysts

Heterogeneous catalyst is presented in different phases from the reactants. A heterogeneous catalysis can be occurred on the surface of catalyst and then the reactants are adsorbed. The mechanism of heterogeneous catalysis comprises five steps [41].

(1) The reactants over the catalyst particle are diffused.

(2) The reactants on the catalyst are adsorbed.

(3) The reactants on the surface of catalyst are interacted.

(4) The products from the catalyst particle are desorbed.

(5) The products into the surrounding medium are diffused.

2.3 Porous materials

Porous materials are used in many applications including catalysis due to high surface area, large pore volume, and uniformity in pore size. Porous materials can be classified based on the IUPAC pore diameter into three groups that was shown in table 2.1.

Table 2.1 IUPAC classification of porous materials [42]

Porous material	**Pore diameter (nm)**
Microporous	up to 2
Mesoporous	2-50
Macroporous	50 to up

2.4 Clay

Clay contain of phyllosilicate minerals, metal oxides and organic matter. Moreover, the shale, mudstone, metamorphic slate and phyllite can be found in clay mineral. Examples of clay minerals are kaolinite, smectite and sepiolite. Generally, the smectite is mentioned to as bentonite, which is being the whole rock term. Smectite contains sodium and calcium montmorillonites. The clay minerals are used in many applications such as useful industrial minerals. The kaolinite, smectite and sepiolite clay minerals are used in various industrial applications and in most cases quite different depend on theirs physical structure and chemical composition properties. The structure and composition of kaolin, smectites, and sepiolite are very distinct although each includes octahedral and tetrahedral sheets as their basic

building blocks. The important characteristics and properties of kaolin, smectite, and sepiolite are shown in Table 2.2. The applications of the clay minerals depend on particle size, shape, and morphology properties. Moreover, the surface chemistry, surface area, and surface charge are very important properties for clay application [43].

The smectite contains of a 2:1 layer clay mineral and two silica tetrahedral (T) sheets attached to an alumina octahedral (O) sheet that was show in Figure 2.1. The negative charge anion of the 2:1 (TOT) layers is balanced by the positive charge cation such as Na^{+} and Ca^{2+}.

Table 2.2 Some important properties of clay minerals that relate to their applications

Kaolin	**Smectite**	**Sepiolite**
1:1 layer	2:1 layer	2:1 layer inverted
White or near white	Tan, olive green, gray or white	Light tan or gray
Little substitution	Octahedral and tetrahedral substitutions	Octahedral substitution
Minimal layer charge	High layer charge	Moderate layer charge
Low base exchange capacity	High base exchange capacity	Moderate base exchange capacity
Pseudo-hexagonal flakes	Thin flakes and laths	Elongate
Low surface area	Very high surface area	High surface area
Very low absorption capacity	High absorption capacity	High absorption capacity
Low viscosity	Very high viscosity	High viscosity

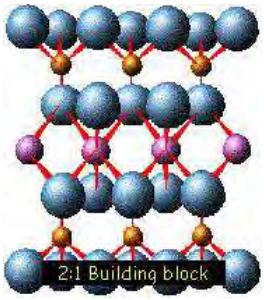

Figure 2.1 Clay structure [43].

2.5 Mesoporous materials

Mesoporous materials are a type of molecular sieves, such as silicas or modified layered materials such as pillared clays and silicates. The mesoporous silica has been contained of 2 to 50 nm uniform pore sizes and has been found that good utility as catalysts due to the regular arrays of uniform channels.

2.5.1 Classification of mesoporous materials

Mesoporous materials can be classified by different synthetic procedures into three categories as described in Table 2.3.

Table 2.3 Classification of mesoporous materials by synthesis procedure

Assembly	Template	Media	Material
(a) Electrostatic	quaternary ammonium salt	base or acid	MCM-41
(b) H-bonding	primary amine	neutral	HMS
(c) H-bonding	amphiphilic triblock copolymer	acid (pH<2)	SBA-15

2.5.2 Synthesis strategies of mesoporous materials

Crystalline molecular sieves are generally obtained by hydrothermal crystallization. The reaction gel, usually, contains cation (e.g. Si^{4+} for silicate materials, Al^{3+} for aluminate materials) to form the framework; anionic species (e.g. OH^- and F^-); organic template and solvent (generally water). Typically, the nature of

template can be considered into two parts that are hydrophobic tail on the alkyl chain side and hydrophilic head on the other side. The examples of template used are primary, secondary tertiary and quaternary amines, alcohols, crown or linear ethers, and as well as polymer. An understanding of how organic molecules interact with each other and with the inorganic frameworks would increase the ability to design rational routes to molecular sieve materials. The organic templates are frequently occluded in the pores of the synthesized material.

2.5.2.1 The behavior of surfactant molecules in an aqueous solution

In a simple binary system of water-surfactant, surfactant molecules, at a particular concentration can aggregate to form micelles in various types. The shapes of micelle strongly depend on the concentrations as shown in Figure 2.2.

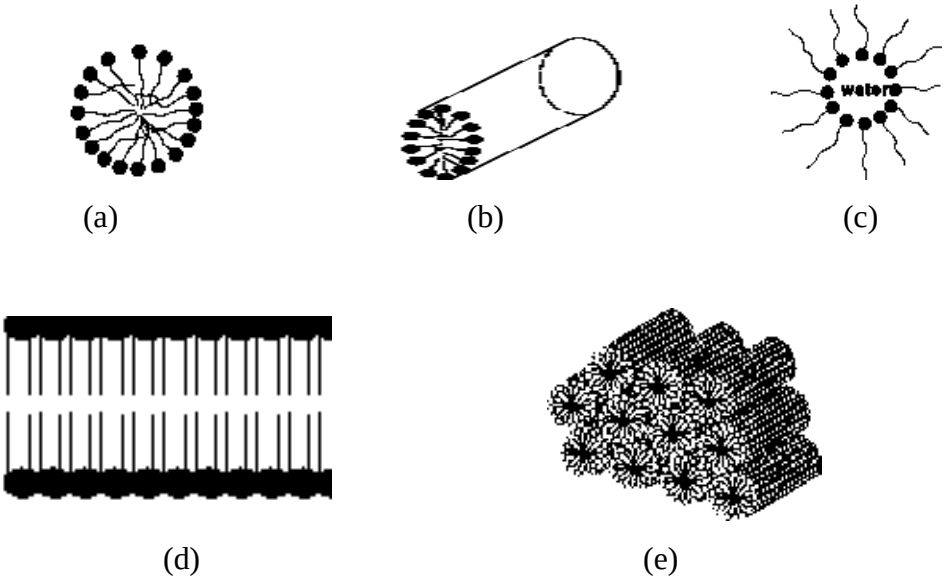

Figure 2.2 Phase sequence of the surfactant-water binary system (a) spherical micelle, (b) rod-shaped micelle, (c) reverse micelle, (d) lamellar phase, and (e) hexagonal phase [44].

At low concentration, they energetically exist as isolated molecules. With rising concentration, surfactant combined together to form isotropic spherical

and rod shaped micelles by directing the hydrophobic tails inside and turning the hydrophilic heads outside in order to decrease the system entropy. The initial concentration threshold at which those molecules aggregate to form isotropic micelle is called critical micelle concentration (CMC). The CMC determines thermodynamic stability of the micelles. When the concentration is continuously increased, the micellar shape changes from sphere or rod shape to hexagonal, lamellar, and inverse micelles. Moreover the ionic strength, pH value, and temperature including other additives are the factors determining the shape of micelles.

2.5.2.2 Interaction between inorganic species and surfactant micelles

The major components of framework structure, mainly silicate, present in aqueous solution as inorganic species. To acquire the desired structure, firstly the template forms the proper shape, and then the inorganic soluble species interact with the surfactant as shown in Table 2.4.

Table 2.4 Example routes for interactions between the surfactant and the inorganic soluble species

Surfactant type	Inorganic type	Interaction type	Example materials
Cationic (S^+)	I^-	S^+I^-	MCM-41, MCM-48
	I^+X^-	$S^+X^-I^+$	SBA-1, SBA-2, zinc phosphate
	I^0F^-	$S^+F^-I^0$	silica
Anionic (S^-)	I^+	S^-I^+	Al, Mg, Mn, Ga
	I^-M^+	$S^-M^+ I^-$	alumina, zinc oxide,
Neutral S^0 or N^0	I^0	S^0I^0 or N^0I^0	HMS, MSU-X, aluminum oxide
	I^+X^-	$S^0X^-I^+$	SBA-15

Where S^x or N^x : surfactant with charge of X

I^x : inorganic species with charge of X

X^- : halogenide anions

F^- : fluoride anion

M^{n+} : with charge of X

In case of ionic surfactant (S^+ and S^-), the hydrophilic head mainly binds with inorganic species through electrostatic interactions. There are two possible formation routes. Firstly, direct pathway: surfactant and inorganic species of which charges are opposite interact together directly (S^+I^- and S^-I^+). Another is the indirect pathway, occurring when the charges of surfactant and inorganic species are the same, so the counter ions in solution get involved as charge compensating species, in the present of halogenide anions (X^- = Cl^- or Br^-) and the S^-M^+ I^- route is the individual of basic media, in the existence of alkaline cation (M^+ = Na^+ or K^+). Figure 2.3 shows the possible hybrid inorganic-organic interfaces. Using non-ionic surfactant (S^0 or N^0), the main interaction between template and inorganic species is hydrogen bonding or dipolar, which is called neutral path i.e. S^0I^0 and $S^0F^-I^+$.

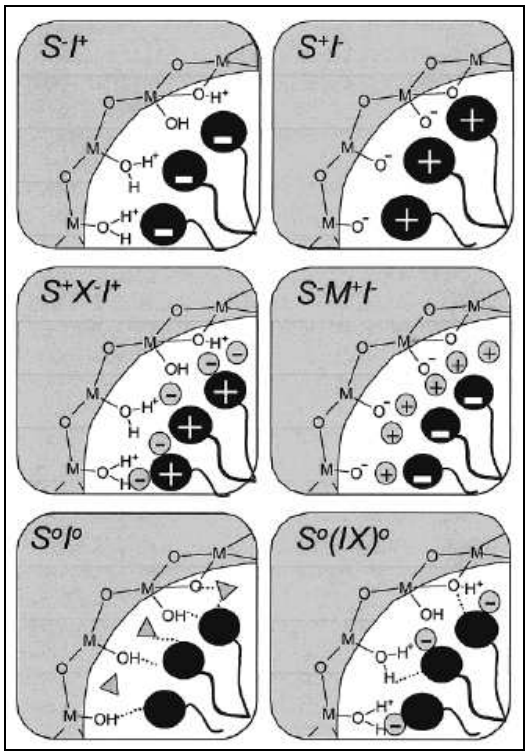

Figure 2.3 Schematic representation of the different types of silica-surfactant interfaces. Dashed line corresponded to H-bonding interactions [44].

2.5.2.3 Mechanism formation of mesoporous materials

Mechanism of mesoporous formation can be classified on the basis of synthetic route into three types exhibited in Figure 2.4:

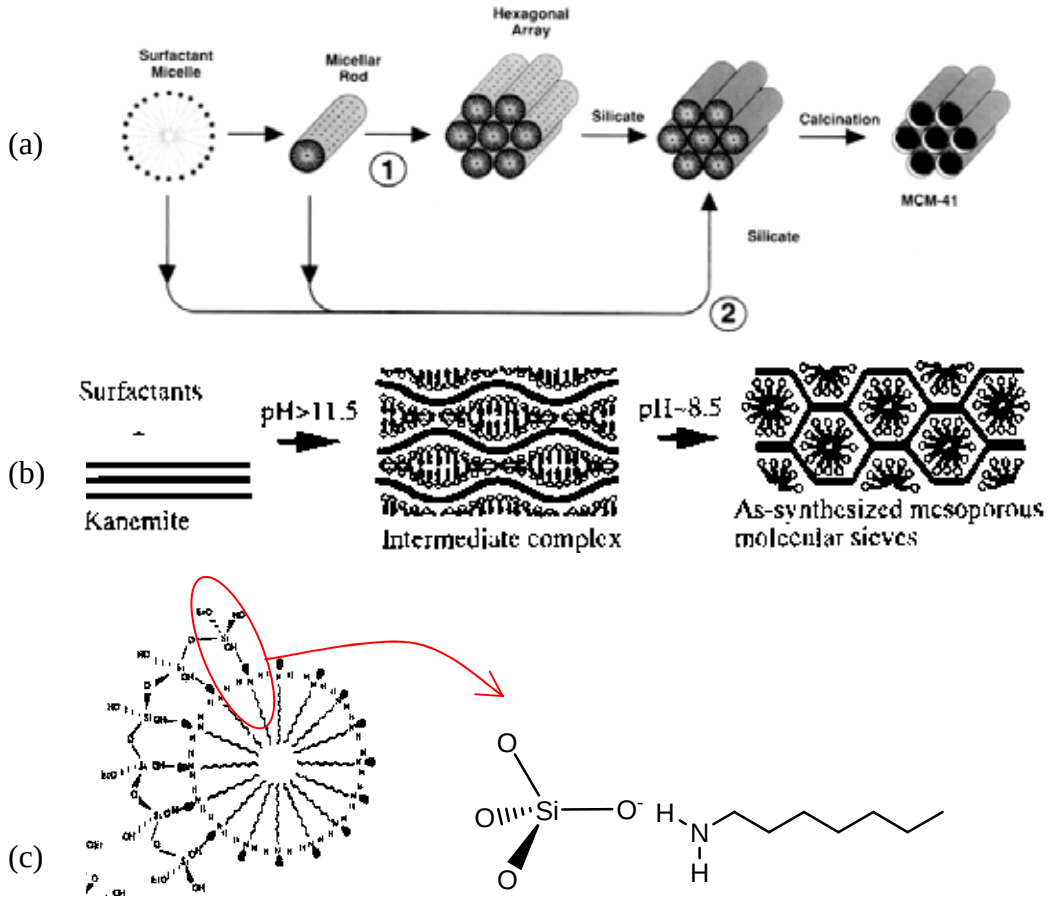

Figure 2.4 Mechanism of mesoporous formation (a) LCT of MCM-41 formation, (b) Folding sheet formation of FSM-16 and (c) H-bonding interaction in HMS formation [45].

(a) *Liquid crystal Templating mechanism*: i.e. MCM-41. From Figure 2.10(a) there are two main pathways; firstly, liquid crystal phase was complete before silicate species were added or another pathway the ordering of the subsequent silicate-encased surfactant micelles was aggregated by adding silica.

(b) *Folding sheet formation*: i.e. FSM-16. The intercalation of ammonium surfactant into hydrate sodium silicate, which composes of single layered silica sheets called "kanemite" (ideal composition $NaHSi_2O_5.3H_2O$), produced the lamellar-to-hexagonal phase in FSM-16. Then the templates were ion exchange into the layer of structure and condense into a hexagonal structure.

(c) *Hydrogen-bonding interaction*: The neutral template generated mesoporous materials with higher thermal stability than the LCT-derived silicates.

Although some of mesoporous as described above have the same hexagonal structure, they are different in the properties as shown in Table 2.5. Since the thermal and hydrothermal stability of material are based on the wall thickness, therefore, from Table 2.5 SBA-15 possesses and exhibits significantly higher thermal and hydrothermal stability than other materials. Furthermore, its pore size can be expanding up to 300 Å which allow the bulky molecule to diffuse into their pores.

Table 2.5 Properties of some hexagonal mesoporous materials

Material	**Pore size (Å)**	**Wall thickness (nm)**	**BET specific surface area (m^2/g)**
MCM-41	15-100	1	>1000
HMS	29-41	1-2	640-1000
FSM-16	50-300	no report	680-1000
SBA-15	15-32	3-6	630-1000

2.5.3 Synthesis strategy of mesoporous material using block-copolymer as structure directing agent

In the synthesis of mesoporous materials such as MCM-41, FSM-16 ionic surfactant i.e. the cationic, alkyltrimethyl ammonium (C_nTA^+, $8<n<18$), and anionic surfactant, tertiary amine ($C_nH_{2n+1}N^+(CH_3)_3$) are used as template, respectively. These syntheses were done in extreme (alkaline) pH condition and the

obtained materials having pore size between 15 to 100 Å only. However, by this mean, two limitations occurred:

(1) The lower stability of the obtained materials: because of the thinner pore wall of materials (8-13 Å).
(2) Difficult to expanding the pore size: the ionic surfactants give a limited pore size. The only way to expand the pore size is using swelling agents such as 1,3,5-trimethyl benzene, involving complicate synthesis.

Thus, the block copolymer has been used to solve these problems. Generally, amphiphilic block copolymer has been used in the field of surfactants, detergent manufacturing, emulsifying, coating, etc. Figure 2.5 shows typical block copolymer used as templates.

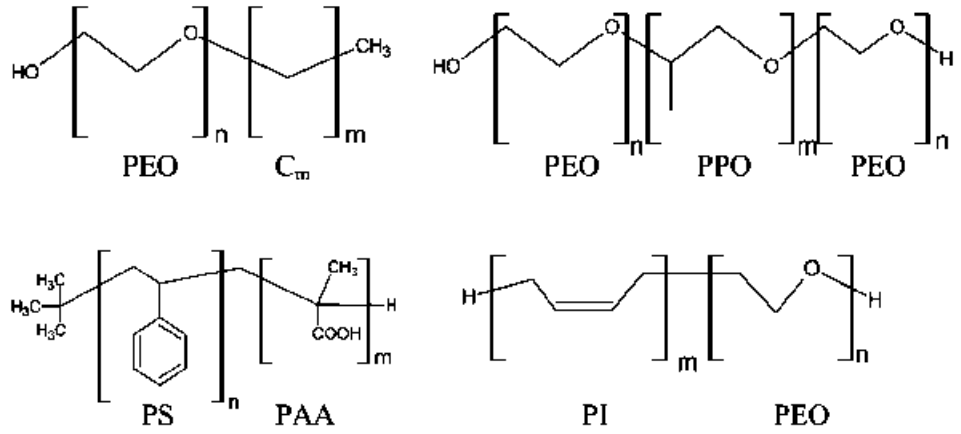

Figure 2.5 Block copolymer used in mesostructured generation [46].

Some advantages of using these block copolymer are:

(1) The thicker wall thickness (about 15-40 Å), enhancing hydrothermal and thermal stability of materials.
(2) Pore diameter can be tuned easier by varying type or concentration of polymer.

(3) Easier to eliminate from framework by calcination or solvent extraction. Due to the hydrogen bonding interaction between surfactant and inorganic framework, therefore, it is simple to separate as compared to ionic templates (electrostatic interaction).

Interaction between block copolymer template and inorganic species, called hybrid interphase (HI), is particularly important. Different possible interactions that occur at the HI are showed in Figure 2.6. Most of the fine HI characterization has been done on PEO-based (di or triblock) templates. Melosh *et al*. [46] performed that in F127-templated silica monoliths, organization arose for polymer weight fractions higher than 40%. For lower polymericsilica ratios, non-ordered gels were created.

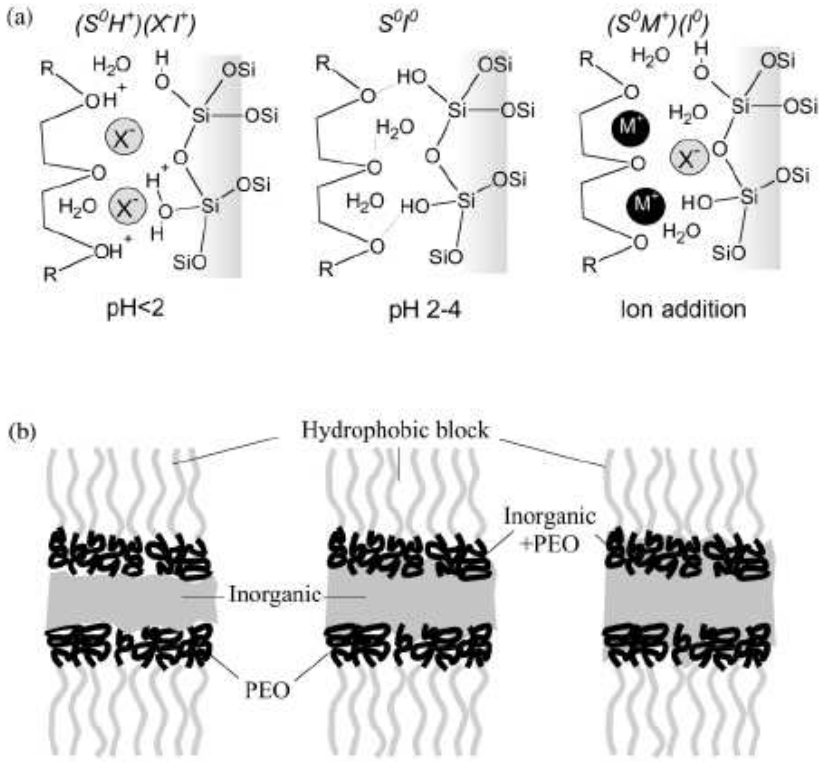

Figure 2.6 (a) Schematic view of the $(S^0H^+)(X^-I^-)$, S^0I^0, and $(S^0M^+)(X^-I^0)$ hybrid interphases (HIs) (b) Three possible structures of a HI composed by a nonionic polymer and an inorganic framework [46].

2.6 Mesoporous silica SBA-15

2.6.1 Structure and properties of SBA-15

The SBA-15 mesoporous material was prepared under acidic solution using tri-block copolymer template. This novel material exhibited higher thermal stability than MCM-41 due to higher pore wall thickness (3.1-6.4 nm). Furthermore, SBA-15 also provided uniform pore size and hexagonal-structured channel similar to MCM-41 as shown in Figure 2.7. Some properties of MCM-41 and SBA-15, two well-known materials, are compared as described in Table 2.6. According to the properties listed in Table 2.6 SBA-15 show a better performance than MCM-41 in almost of properties.

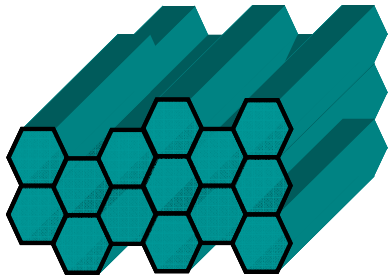

Figure 2.7 Hexagonal mesoporous structure.

Table 2.6 Comparison of two well-known mesoporous materials, MCM-41 and SBA-15 in their characteristic properties [47]

Properties	**MCM-41**	**SBA-15**
pore size (Å)	20-100	46-300
pore volume (ml/g)	>0.7	0.8-1.23
surface area (m^2/g)	>1000	690-1040
wall thickness (Å)	10-15	31-64

2.6.2 Synthesis of SBA-15 and mechanism formation

Zhao *et al*. [18] reported the aging time and temperature are important factors to synthesize SBA-15 sample. The aging of the precursor in the mother liquors induces to an enhancement on the pore size distribution (Figure 2.8).

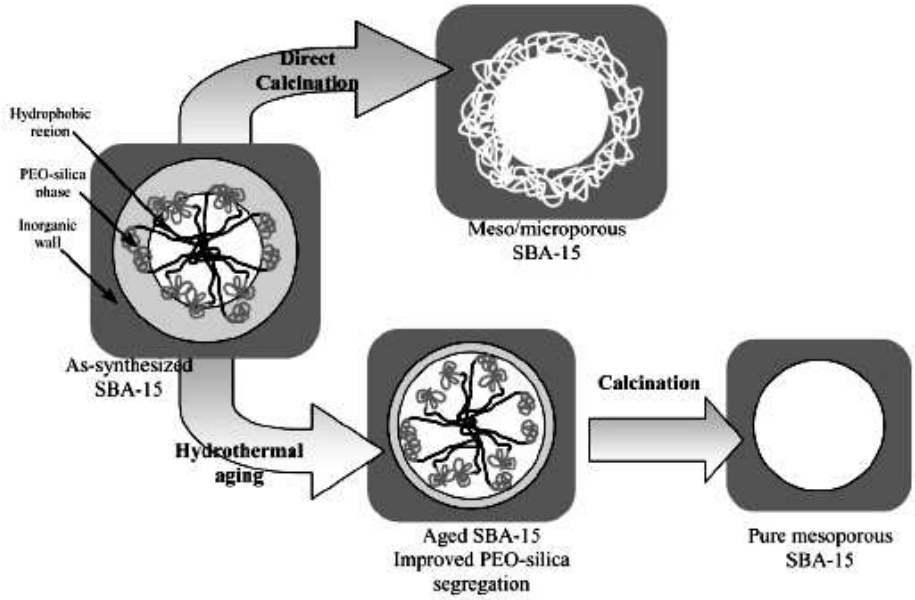

Figure 2.8 Pore evolution upon thermal treatment, depending on pre-treatment and aging [48].

For a mechanism, firstly alkoxysilane species (TMOS or TEOS) are hydrolyzed as [48]:

$$Si(OEt)_4 + nH_3O^+ \xrightarrow[pH<2]{\text{hydrolysis}} Si(OEt)_{4-n}(H_2O^+)_n + n\ EtOH$$

This is followed by partial oligomerization at the silica. Furthermore, at this condition, the PEO parts of surfactant associate with hydronium ions as followed:

$$-PEO_m- + yHX \xrightarrow{H_2O} -PEO_{m-y}[(EO).3H_2O^+]_y\ ----X_y^-$$

Next, coordination sphere expansion around the silicon atom by anion coordination of the form $X^{-}SiO_2^{+}$ may play an important role. The hydrophilic PEO blocks are used to interact with the protonated silica and thus be closely associated with the inorganic wall. During the hydrolysis and condensation of the silica species, intermediate mesophase is sometimes observed and further condensation result in the formation of the lowest energy silica-surfactant mesophase structure allowed by solidifying network.

2.7 Biodiesel

Biodiesel is alkyl esters that can be achieved from vegetable oil or animal fats. Mostly, biodiesel is produced by using esterification and transesterification reactions. However, biodiesel can be combined with diesel oil using in modern engines. Normally, the gel point of biodiesel is higher than diesel oil; thus, this can be improved by using a biodiesel and diesel blend. The biodiesel was used as an additive in low-sulfur formulations of diesel to rise the lubricity lost when the sulfur is removed [49].

2.7.1 The production of biodiesel

2.7.1.1 Direct use and blending

All researchers reported the vegetable oils that used to feed diesel engine exhibited coking formation on the injectors. The direct use of vegetable oils in diesel engines has been many problems such as decrease in power output and thermal efficiency of the engine. Other drawbacks to the use of vegetable oils and animal fats are the high viscosity (about 11-17 times higher than diesel fuel) and lower volatility, which affect to the carbon deposits in engines due to incomplete combustion.

2.7.1.2 Transesterification

Transesterification or alcoholysis is the movement of alcohol from ester. A basic catalyst is used to enhance the reaction rate and yield. Because the reaction can be reversed, so the excess alcohol is used shift the equilibrium to the

product side [4]. The transesterification reaction diagram of triglycerides is showed in the Figure 2.9.

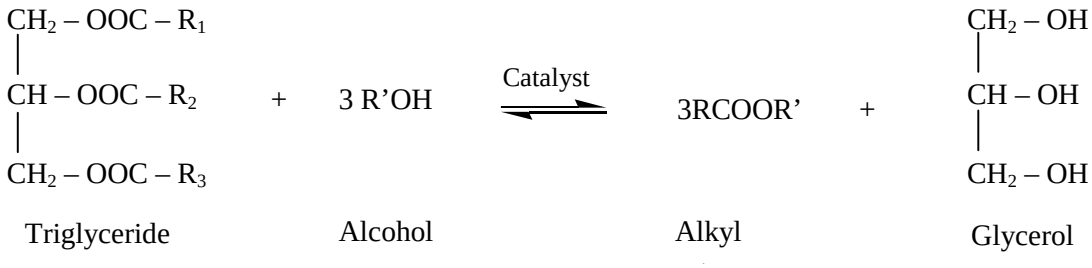

Figure 2.9 Transesterification reaction of triglyceride and alcohol**.**

2.7.1.2.1 Transesterification kinetics and mechanism

The fatty acid alkyl ester, di-glyceride and mono-glyceride intermediates, and glycerol by-product can be prepared from transesterification of tri-glycerides and alcohol. The stoichiometric reaction needs 1 mole of tri-glyceride and 3 mole of alcohol to produce 3 mole of ester and 1 mole of glycerol. The forward reaction is pseudo-first order in presence of excess alcohol and the reverse reaction is found to be second-order. It was noted that transesterification is faster when using alkali catalyst. The mechanism of acid and alkali-catalyzed transesterification is described in Figures 2.10 and 2.11, respectively [50].

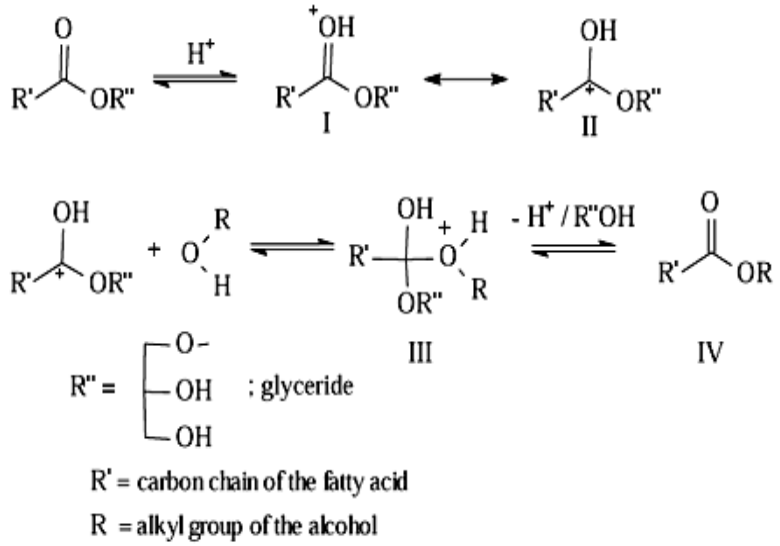

Figure 2.10 Mechanism of acid catalyzed transesterification reaction.

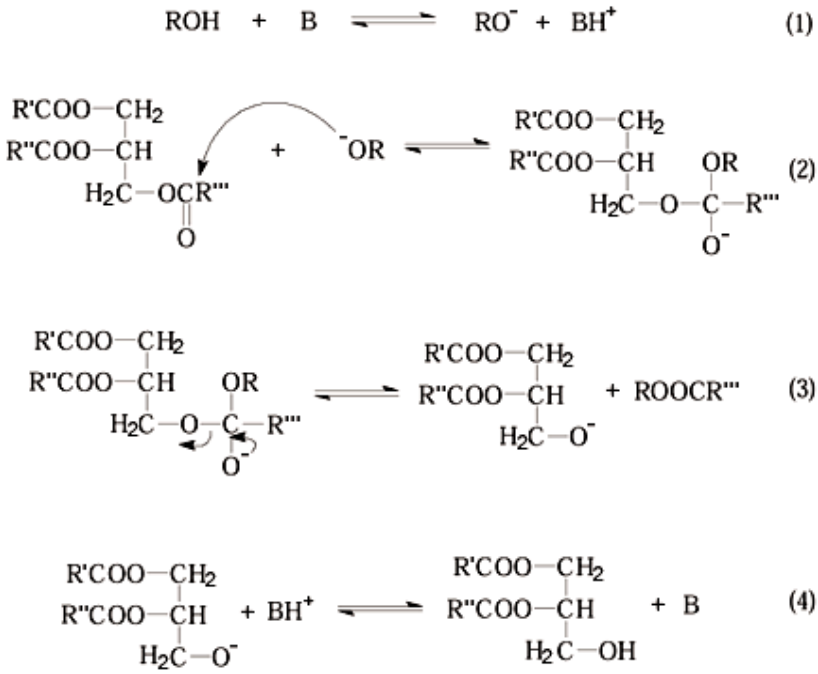

Figure 2.11 Mechanism of base catalyzed transesterification reaction.

2.7.1.3 Esterification

Esterification is common method for making esters from carboxylic acid or free fatty acid with short chain alcohol. Esterification is among the

simplest and most often performed organic transformations. The esterification reaction diagram of free fatty acid is shown in the Figure 2.12. The mechanism of acid and alkali catalyzed esterifications are presented in Figure 2.13 and 2.14, respectively [51].

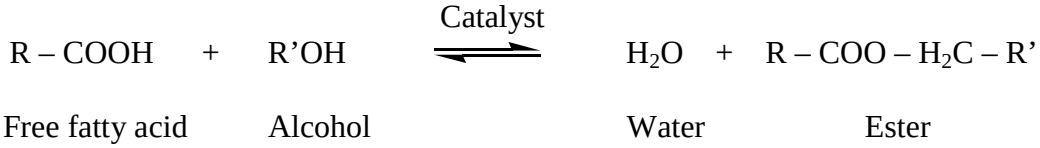

Figure 2.12 Typical esterfication diagram of free fatty acid.

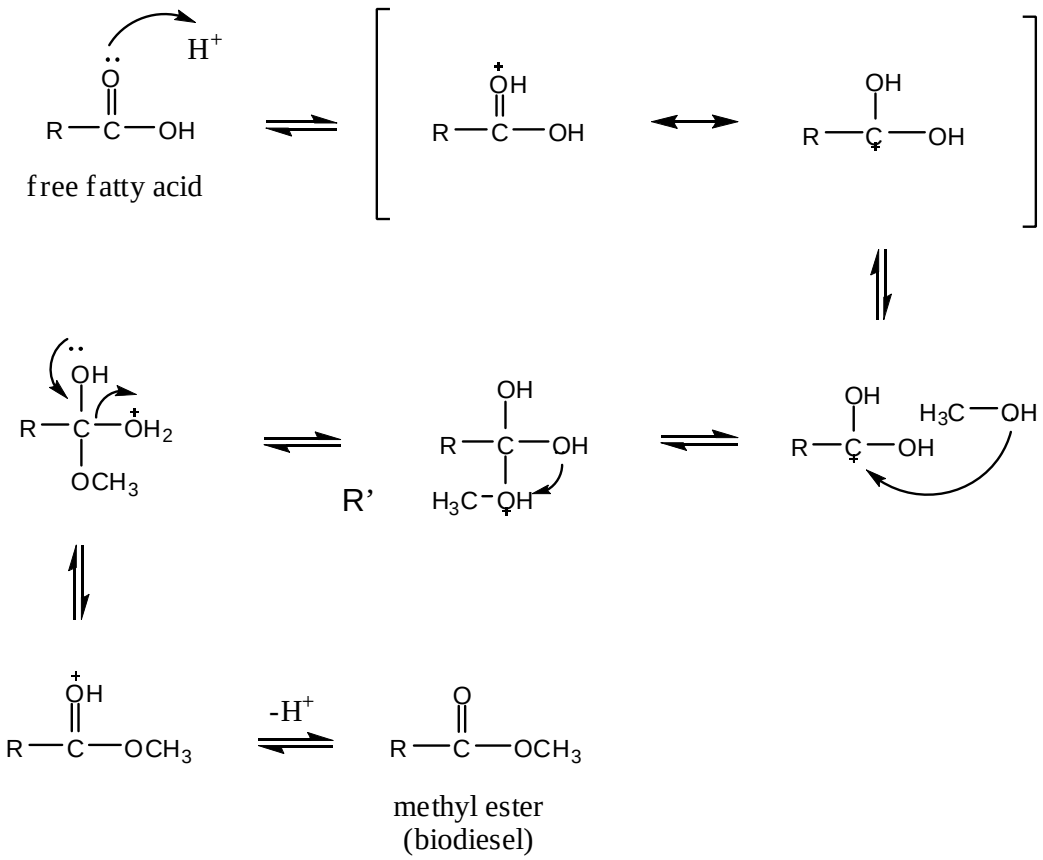

Figure 2.13 Mechanism of acid catalyzed esterification of fatty acid.

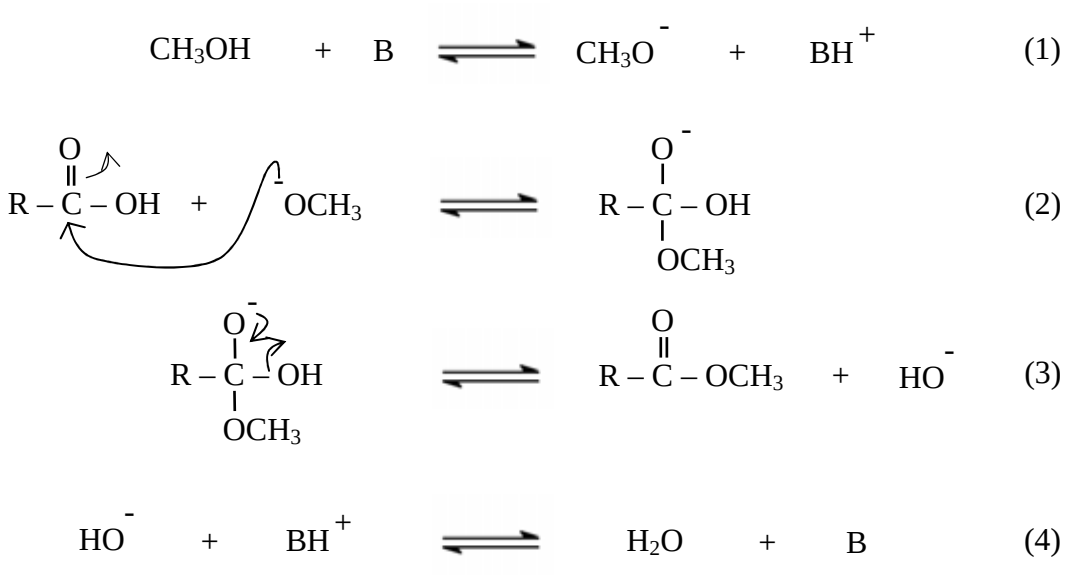

Figure 2.14 Mechanism of base catalyzed esterification of fatty acid.

2.7.1.3.1 Esterification parameters

The most relevant variables that influence the esterification reactions are the following: [52]

(a) Molar ratio of alcohol to free fatty acid

The molar ratio is associated with the type of catalyst. Higher molar ratios show high fatty acid methyl ester yield in a short time.

(b) Catalyst type and concentration

Catalysts in esterification reaction are classified as alkali, acid, or enzyme. Acid-catalyzed reaction is more efficient and less side reaction than alkali-catalyzed. It is suitable if the glycerides contain high free fatty acid content and more water. Acid catalysts include sulfuric acid (H_2SO_4), hydrochloric acid (HCl) and phosphoric acid (H_3PO_4)

(c) Reaction time

The conversion rate and fatty acid methyl ester yield are increase with increase reaction time.

(d) Reaction temperature

Esterification can be done at different temperature, depending on the oil used and catalyst types. Temperature clearly influenced the reaction rate and yield of esters.

2.8 Characterization of materials

2.8.1 Powder X-ray diffraction (XRD)

X-ray powder diffraction (XRD) is a technique used for characterization of minerals, as well as other crystalline materials. XRD is a technique in which a collimated beams of nearly monochromatic. X-rays is directed onto the flat surface of a relatively thin layer of finely ground material. XRD can provide additional information beyond basic identification. If the sample is a mixture, XRD data can be analyzed to determine the proportion of the different minerals present. Other obtained information can include the degree of crystallinity of the minerals present, possible deviations of the minerals from their ideal compositions, the structural state of the minerals and the degree of hydration for minerals that contain water in their structure.

The main components of XRD instrument are an X-ray source, a specimen holder and a detector. The record results are showed in a respectable powder diffraction pattern [53]. The information from XRD pattern and diffraction of x-ray were showed in Table 2.7 and in Figure 2.15, respectively.

Table 2.7 Information from powder x-ray diffraction pattern

Feature	**Information**
Peak positions (2θ values)	Unit cell dimensions
Non-indexable lines	Presence of a crystalline impurity
Systematicallly absent reflections	Symmetry
Background	Presence (or absence) of amorphous material
Width of peaks	Crystallite (domain) size, stress/strain and stacking faults
Peak intensities	Crystal structure

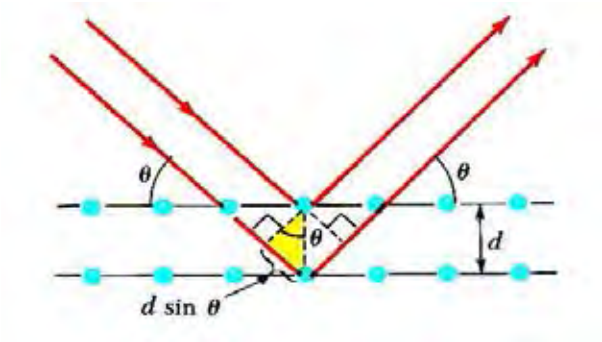

Figure 2.15 Diffraction of X-rays by a crystal.

Figure 2.17 shows a monochromatic beam of X-ray incident on the surface of crystal at angle θ. The scattered intensity can be measured as a function of scattering angle 2θ.

$$n\lambda = 2d \sin\theta$$

From the Bragg equation (above), *d* is the distance between equivalent atomic planes, θ is the angle between the incident beam and these planes, n is an

integer and λ is the wavelength of X-ray source. Then from XRD results, it is able to determine the interplanar spacing of the sample.

2.8.2 N_2 adsorption-desorption technique

A great deal of very useful information is derived from measurement of the physical adsorption of gases on porous solids. The monolayer capacity of non-porous solid, measured by chemisorption, or by physisorption well above the boiling point of the adsorbing gas, can be easily translated into a surface area. Adsorption amount depends on gas pressure, adsorption temperature, and properties of adsorptive gas and adsorbent solid. In nitrogen adsorption isotherm measurement, temperature is constant and gas is limited, thus the isotherm changes according to the property of solid. Several forms of isotherm besides the langmuir type have been shown in Figure 2.16. According to the IUPAC definition, microporous materials show a Type I adsorption-desorption isotherm. Nonporous or macroporous exhibit types II, III, and VI and mesoporous exhibits types IV and V. Moreover, adsorption isotherms were shown in Table 2.8.

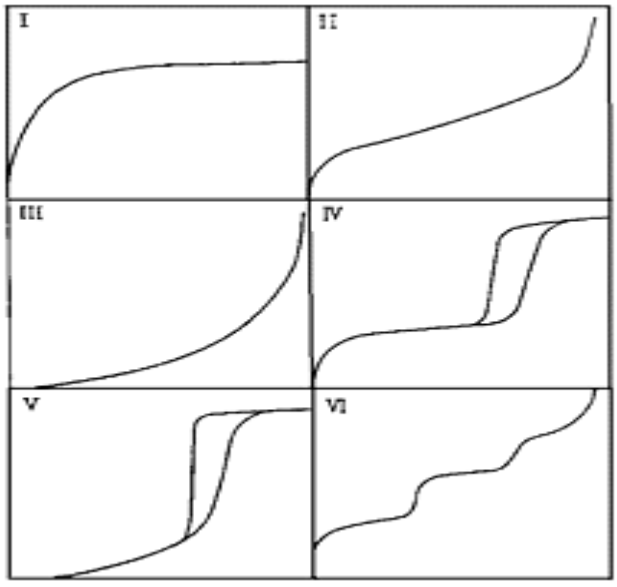

Figure 2.16 The IUPAC classification of adsorption isotherm.

Table 2.8 Features of adsorption isotherms [42]

Type	Features	
	Interaction between sample surface and gas adsorbate	**Porosity**
I	Relatively strong	Micropores
II	Relatively strong	Nonporous
III	Weak	Nonporous
IV	Relatively strong	Mesopore
V	Weak	Micropores or Mesopore
VI	Relatively strong Sample surface has an even distribution of energy	Nonporous

The t-plot method was invented by Lippens and de Boer. Standard isotherm shows the relationship between relative pressure and thickness of adsorption layer. Specific surface area, a_s (m^2/g) can be calculated from the equation 2.3 with the slope of t-plot [42].

$$a_s = \frac{s \times 0.354}{22414} \times L \times \sigma = 1.541 \times s$$

Where L is Avogadro constant and σ is cross sectional area of adsorptive. There are 3 different types of t-plot isotherm. If t-plot is a linear curve the original point, and thus the adsorbent is considered to be non-porous material. If t-plot has 2 slopes, the one is a sharp slope passing the original point and the other is more gradual slope, it means that the adsorbent has homogenized sized micropores. And the last isotherm that draws a sharp strength line but become smoother curve from some point, it is considered to have mesopores.

MP method measures distribution from the curvature of t-plot. v_p is an integrated value of pore volume (v_1), which can be obtained from below equation.

$$v_1 = (a_1 - a_2) \times (t_1 + t_2)/2 \times 10^{-3}$$

Although d_{peak} is the peak position it is not suitable for MP method analysis when d_{peak} is below 0.71 nm, due to the same reason for the fact that average pore diameter is not accurate unless 2 or more adsorption layers are formed in pores.

CHAPTER III

EXPERIMENTAL

3.1 Instruments, apparatus and analytical techniques

3.1.1 Centrifuge

The separation and collection of prepared solid sample after hydrothermal crystallization and acid activation were processed by a Sanyo Centaur 2 centrifuge at speed of 6,000 rpm. In addition, this equipment was used in recovering the catalyst after esterification reaction.

3.1.2 Oven and furnace

Crystallization of SBA-15 during the synthesis was performed at 100^{o}C using a UM-500 oven as heater. Calcination of the solid catalysts at elevated temperature was achieved in a Carbolite RHF 1600 muffle furnace in air with programmable heating rate of 1^{o}C/min. Calcination method was conducted in order to remove template, moisture and some impurities from material. The temperature program used for the calcination of mesoporous silica sample was shown in Scheme 3.1.

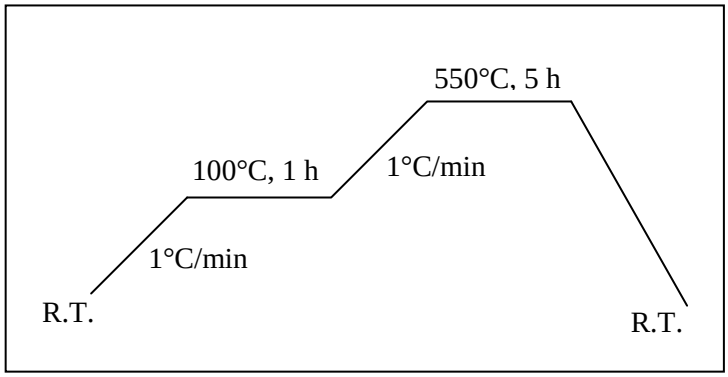

Scheme 3.1 The temperature program for the calcination of SBA-15 catalyst.

3.1.3 Powder X-ray diffraction (XRD)

The structure of prepared samples were characterized using a Rigaku D/MAX-2200 Ultima+ X-ray diffractometer (XRD) equipped with Cu Kα radiation (40 kV 30 mA) and a monochromater at 2 theta angle between 0.5 to 50 degrees. The scattering slit, divergent slit and receiving slit were fixed at 0.5 degree, 0.5 degree, and 0.15 mm, respectively.

3.1.4 Scanning electron microscopy (SEM)

SEM image was done to observe the morphology using a JEOL JSM-5410 LV scanning electron microscope. All samples were coated with spluttering gold under vacuum.

3.1.5 Surface area analyzer

Characterization of catalyst porosity in terms of nitrogen adsorption-desorption isotherms, BET specific surface area, and pore size distribution of the catalysts was carried out using a BEL Japan, BELSORP-mini instrument.

3.1.6 X-Ray fluarescence Spectrometer (XRF)

The chemical compositions of clay sample were investigated by using X-Ray Fluarescence Spectrometer.

3.1.7 Transmission electron microscopy (TEM)

The hexagonal mesostructure of SBA-15 and modified SBA-15-Pr-SO_3H was investigated by using JEOL; JEM-2100 transmission electron microscopy.

3.1.8 Acid-base titration technique

The acid amount of acid materials was quantified by using acid-base titration technique. A 0.05 g of the material was mixed with 15 ml of the NaCl solution and permitted to equilibrate for 30 min. After that, it was titrated by dropwise addition of 0.01 M NaOH aqueous solution.

3.1.10 Gas chromatography analysis (GC)

The methyl ester yield can be analyzed by Gas Chromatography which was carried out on a VARIAN CP-3800 chromatography equipped with split ratio 1:50, flame ionization detector (FID, N_2 as a carrier gas and a 30 m in length of CP-sil-8 column equivalent to HP-5 with a 0.25-mm outer diameter and a 0.25 µm film thickness. The capillary column has been had maximum temperature limit of 300^{o}C. The mono-, di and tri-glyceride yield values were determined by using Metal biodiesel column with guard column. Eicosane 1.2 x 10^{-1} M was used as an internal standard for analysis. Samples were prepared for GC analysis by silylation method (Fat and oil derivatives-Fatty Acid Methyl Ester (FAME) - Determination of free and total glycerol and mono-, di-, triglyceride contents (BS EN 14105:2003)) and 1 µL of sample was injected into the column. The GC temperature program for product analysis was 152^{o}C hold for 2 min, programmed at 2.5^{o}C/min up to 204^{o}C, programmed at 10^{o}C/min up to 240^{o}C, final temperature hold for 5 min, it was shown in Scheme 3.2.

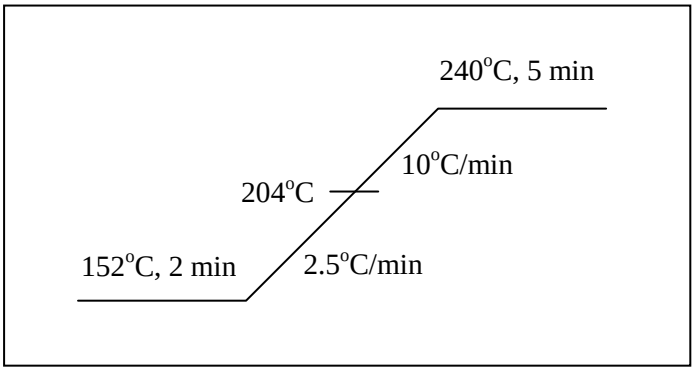

Scheme 3.2 The temperature program used for GC analysis of fatty acid methyl ester compounds.

3.1.11 PARR reactor

The esterification reaction of free fatty acids (palmitic acid and oleic acid) was performed in 100 ml PARR reactor. The temperature program for the reaction was shown in Scheme 3.3.

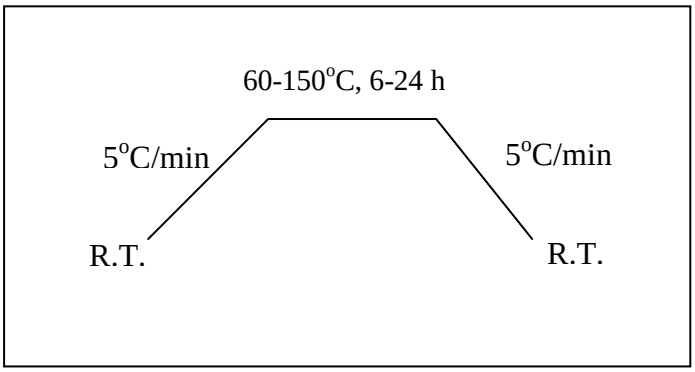

Scheme 3.3 The temperature program for esterification reaction.

3.2 Chemicals

1. Tetraethyl orthosilicate, TEOS (Fluka)
2. Tri-block copolymer pluronic P123 ($EO_{20}PO_{70}EO_{20}$) (Aldrich)
3. 1-hexadecylamine (Aldrich)
4. Cetyltrimethylammonium bromide, CTAB (Aldrich)
5. 3-mercaptopropyltrimethoxysilane (Aldrich)
6. 30 wt. % H_2O_2 (Merck)
7. Refined palm oil (Olein Co., Ltd., Thailand)
8. *Jatropha Curcas* oil (Lam Soon (Thailand) Public Company Limited, Thailand)
9. Waste cooking palm oil (Chester's Grill, Thailand)
10. Palmitic acid, $C_{16}H_{32}O_2$ (Fluka, ≥97%)
11. Oleic acid, $C_{18}H_{34}O_2$ (Aldrich, 90%)
12. Methanol, CH_3OH (Merck, 99.9%)
13. Ethanol, $C2H_5OH$ (Merck, 99.9%)
14. Glycerol (Merck)
15. Eicosane, $C_{20}H_{42}$ (Fluka, ≥97%)

16. N-methyl-N-trimethylsilyltrifluoroacetamide (MSTFA), (Fluka, ≥97%)
17. Methyl palmitate standard, $C_{17}H_{34}O_2$ (Fluka, ≥97.%)
18. Methyl oleate standard, $C_{19}H_{36}O_2$ (Aldrich, 99%)
19. Mono-, di- and tri-glyceride standard, (Aldrich, 99%)
20. Acetone, C_3H_6O (Merck, 99.5%)
21. Hydrochloric acid, HCl (CARLO ERBA, 37%)
22. Nitric acid, HNO_3 (Merck, 65%)
23. Sulfuric acid, H_2SO4 (Merck, 92-95%)
24. Bentonite clay (Siam Valclay Co., Ltd. (Thailand))
25. Kaolin clay (Industrial Mineral Development Ltd. (Thailand))
26. Amberlyst-15 in dry form (Rohm & Haas, France)

3.3 Catalyst preparation

3.3.1 Rope mesoporous SBA-15

The rope mesoporous SBA-15 synthesis process was modified from the procedure reported by Zhao et al. [18] under hydrothermal condition. A 4.0 g of pluronic P123 template was dissolved with stirring in 30 g of water and 120 g of 2.0 M of HCl solution at room temperature. Subsequently, 8.50 g of tetraethyl orthosilicate (TEOS) was added, stirred for 1 h. The solution was aged at 40^{o}C for 24 h under stirring, after that moved to a Teflon-lined autoclave for hydrothermal crystallization at 100^{o}C for 48 h without stirring. As-synthesized rope mesoporous SBA-15 was recovered by filtration, washed with deionized water, and dried in the air. The white powder material was obtained. The synthesized material was removed template by calcination method at 550^{o}C for 5 h. The molar gel composition of rope mesoporous material was 1.0 TEOS : 0.0165 P123 : 6.95 HCl : 140 H_2O and this material was denoted as rp-SBA-15. The procedure for preparing the rp-SBA-15 was shown in Scheme 3.4.

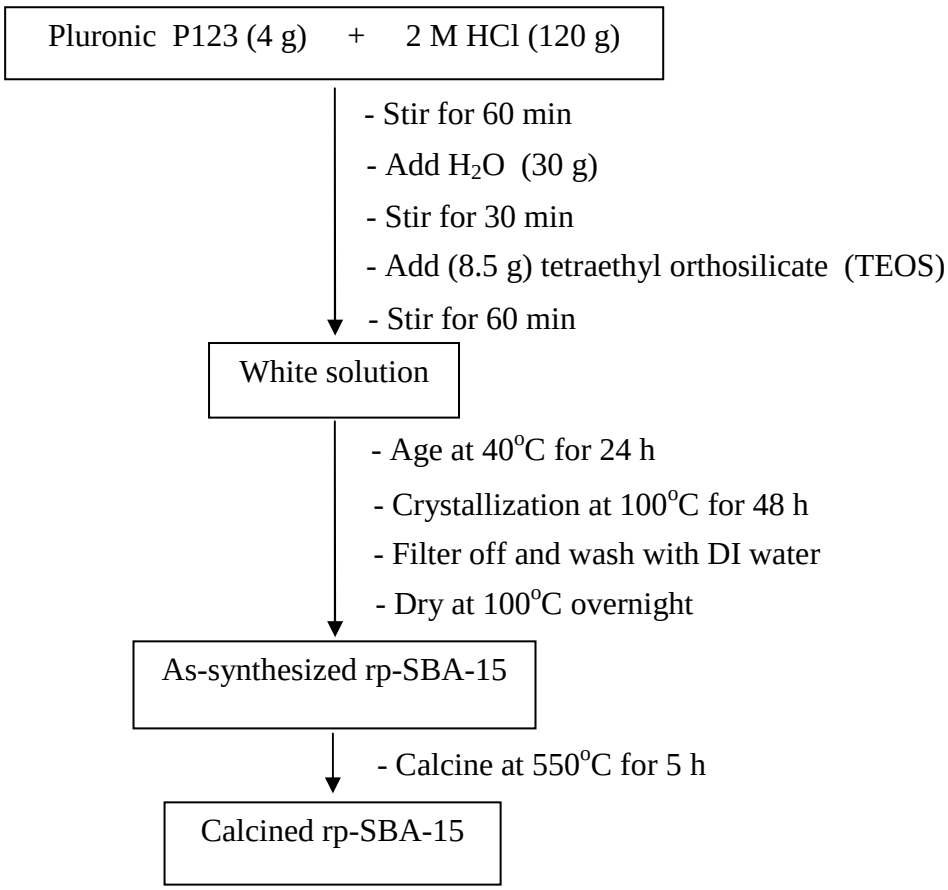

Scheme 3.4 Diagram of mesoporous rp-SBA-15 synthesis.

Figure 3.1 Apparatus for mesoporous rp-SBA-15 synthesis.

3.3.2 Rod, fiber mesopore SBA-15 and MCM-41

The large mesoporous silica rod and fiber materials were synthesized according to Johansson et al. using triblock copolymer pluronic P123, ammonium fluoride, tetraethyl orthosilicate, heptane and hydrogen peroxide as starting materials under hydrochloric acid solution [54, 55]. The heptane to P123 ratio was varied to study particle rod or fiber shape and pore size. The rod and fiber mesoporous SBA-15 samples were denoted as rd-SBA-15 and f-SBA-15, respectively. For MCM-41 sample, the hexadecylamine (HDA) surfactant and TEOS silica precursor under hydrochloric acid solution were used to prepare MCM-41 hexagonal mesoporous silica following the literature procedure reported by Tuel and Gontier [56]. The solution was autoclaved hydrothermal at 120^{o}C during 24 h. Moreover, the surfactant was removed by calcinations at 550^{o}C in air for 12 h.

3.3.3 Propyl sulfonic acid functinalized mesoporous silica SBA-15 (mesoporous silica-Pr-SO_3H)

Incorporation of propyl sulfonic acid group onto rp-SBA-15 was performed two different methods. First method was a direct synthesis and secondary method was a post synthesis grafting.

3.3.3.1 Direct synthesis method

The propyl sulfonic acid functinalized rp-SBA-15 material was synthesized according to Melero *et al*. [28]. The pluronic P123 template was dissolved under stirring in 1.9 M HCl solution at room temperature. Subsequently, TEOS was added dropwise and stirred at 40°C for 45 min. Then, 30 wt% H_2O_2 and 3-mercaptopropyltrimethoxysilane (MPTMS) were added and stirred for 1 h and then aged at 40^{o}C for 20 h under stirring. The product was moved to a Teflon-lined autoclave for hydrothermal crystallization at 100^{o}C for 24 h. As-synthesized rp-SBA-15-Pr-SO_3H was separated by filtration, washed with deionized water and dried overnight. The template was removed by refluxing with ethanol for 24 h (1 g of as-synthesized rp-SBA-15-Pr-SO_3H per 400 mL of ethanol). Then the solid product was acidified by 0.2 M H_2SO_4 solution for 2 h. The molar gel composition of directed propyl sulfonic acid fuctionalized rp-SBA-15 material was 0.0369 TEOS: 0.0041

MPTMS: 0.0369 H_2O_2: 0.24 HCl: 6.9046 H_2O: 0.0007 P123. The propyl sulfonic acid functinalized SBA-15 sample, which was synthesized from direct method, was denoted as (d) rp-SBA-15-Pr-SO_3H. The process for preparation this sample was illustrated in Scheme 3.5.

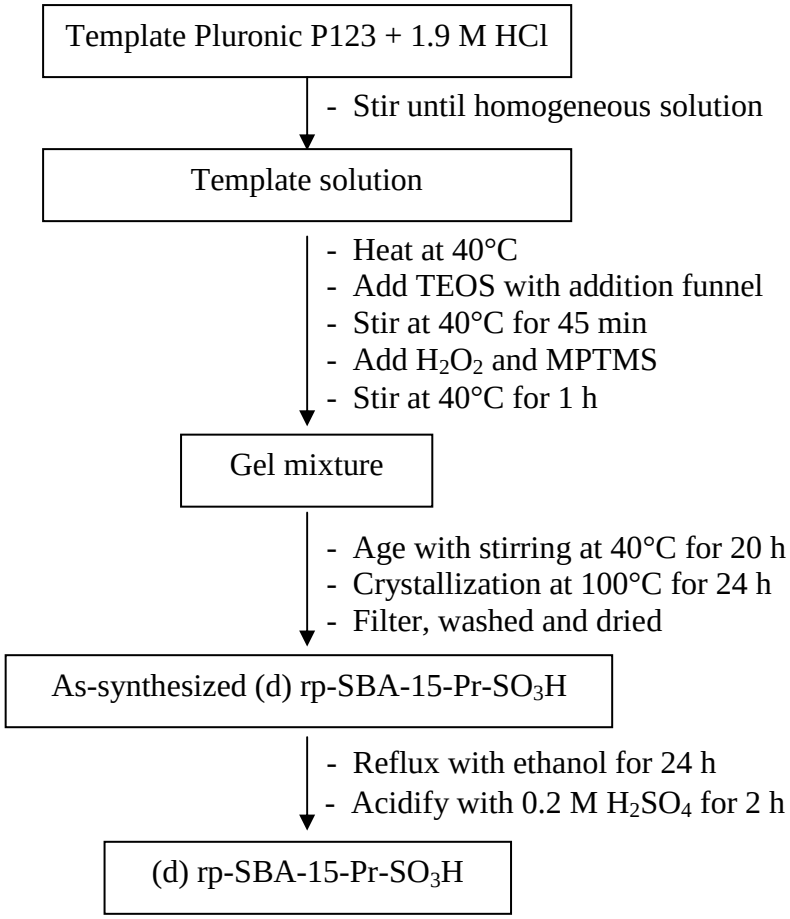

Scheme 3.5 Diagram of (d) rp-SBA-15-Pr-SO_3H synthesis.

3.3.3.2 Post synthesis grafting method

The propyl sulfonic acid functionalized mesoporous silica preparation process was modified from Raju et al. [57]. A mixture of 3.0 g calcined mesoporous silica (rp-SBA-15, rd-SBA-15, f-SBA-15 or MCM-41) and 5.3 g 3-mercaptopropyltrimethoxysilane (MPTMS) was refluxed in 50 mL of dry toluene at 60^{o}C for 6 h. The solid was filtered off and oxidation with 30 mL of 30 wt. % H_2O_2 at 60^{o}C for 24 h. The solid was filtered off and washed with water. The synthesized material was acidified under continuous stirring with 50 mL of 0.2 M H_2SO_4 at room

temperature for 2 h, then filtered off and dried at 100^{o}C for 4 h. The propyl sulfonic acid functinalized mesoporous silica samples, which were prepared from rp-SBA-15, rd-SBA-15, f-SBA-15 and MCM-41 by post synthesis grafting method, were denoted as (p) rp-SBA-15-Pr-SO_3H, (p) rd-SBA-15-Pr-SO_3H, (p) f-SBA-15-Pr-SO_3H and (p) MCM-41-Pr-SO_3H, respectively. The procedure for synthesizing this material was showed in Scheme 3.6.

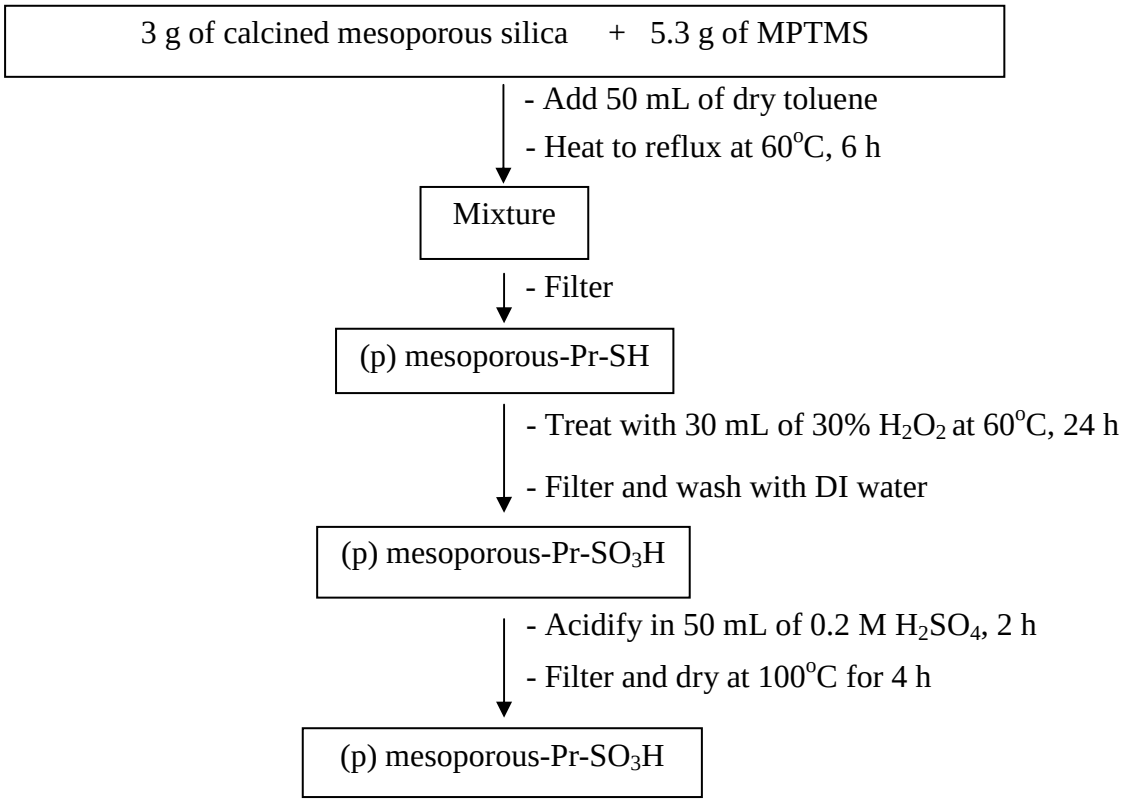

Scheme 3.6 Diagram of propyl sulfonic acid functionalized mesoporous silica synthesis.

3.3.4 Acid-activated clay

The clay samples (bentonite or kaolin) were prepared by using acid-activation method with either H_2SO_4 at varying concentrations from 0.25 to 2.0 M or with 0.5 M HNO_3. The acid-activated bentonite was performed by refluxing dried bentonite powder with H_2SO_4 or HNO_3, 120^oC for 1 h at a bentonite: acid solution ratio of 1.0 g: 30 ml. At the end of each run, the mixture was separated by centrifugation and then the collected bentonite was refluxed twice more as above with a fresh sample at the same acid type / concentration. Finally, the acid-activated bentonite was dried in air at 100^oC overnight. The activated bentonite samples as above with 0.25, 0.5, 1.0 and 2.0 M H_2SO_4 were denoted as TBS-0.25, TBS-0.5, TBS-1.0 and TBS-2.0, respectively, whilst that activated with 0.5 M HNO_3 was denoted as TBN-0.5. The activated kaolin samples with 0.5 M H_2SO_4 and 0.5 M HNO_3 were denoted as TKS-0.5 and TKN-0.5, respectively. The preparation process was shown in Scheme 3.7.

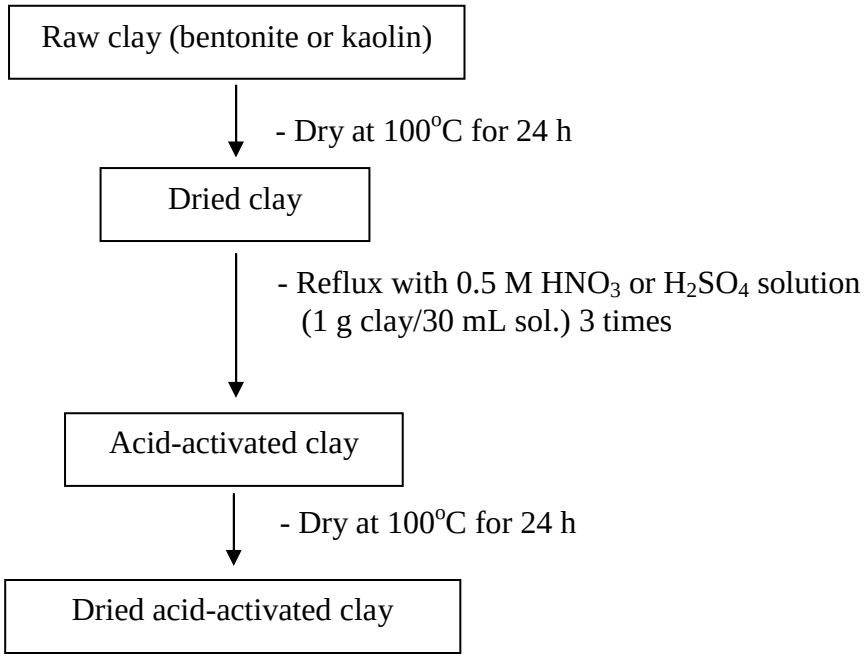

Scheme 3.7 Diagram of acid-activated clay preparation.

3.3.5 Pillar bentonite and acid-activated pillar bentonite

Six gram of dried bentonite was added to 100 mL of 0.1 M CTAB surfactant solution and stirred at 50^{o}C for 24 h. Then, the clay (CTAB-Bent) was separated from the solution and 50 g of TEOS was added at 50^{o}C under stirring for 4 h. Then modified bentonite was separated from the solution, washed with ethanol, dried at room temperature and finally calcined at 600^{o}C for 6 h, which was denoted as PilB-T-C. For other pillar clay matters, 20 g of HDA co-surfactant was added together with TEOS and then proceeded same as previous, which was denoted as PilB-HT-C. Moreover, the HDA and TEOS modified sample was refluxed with 0.1 M of hydrochloric acid in ethanol for 24 h and calcined at 150^{o}C for 6 h, which was denoted as PilB-HT-RC, for completely surfactant removal. In addition, the PilB-HT-RC sample was acid-activated with 0.5 M sulfuric acid solution three times under refluxing. After that, the acid-activated pillar bentonite was dried overnight, which was denoted as H-PilB-HT-RC. The preparation process was shown in Scheme 3.8.

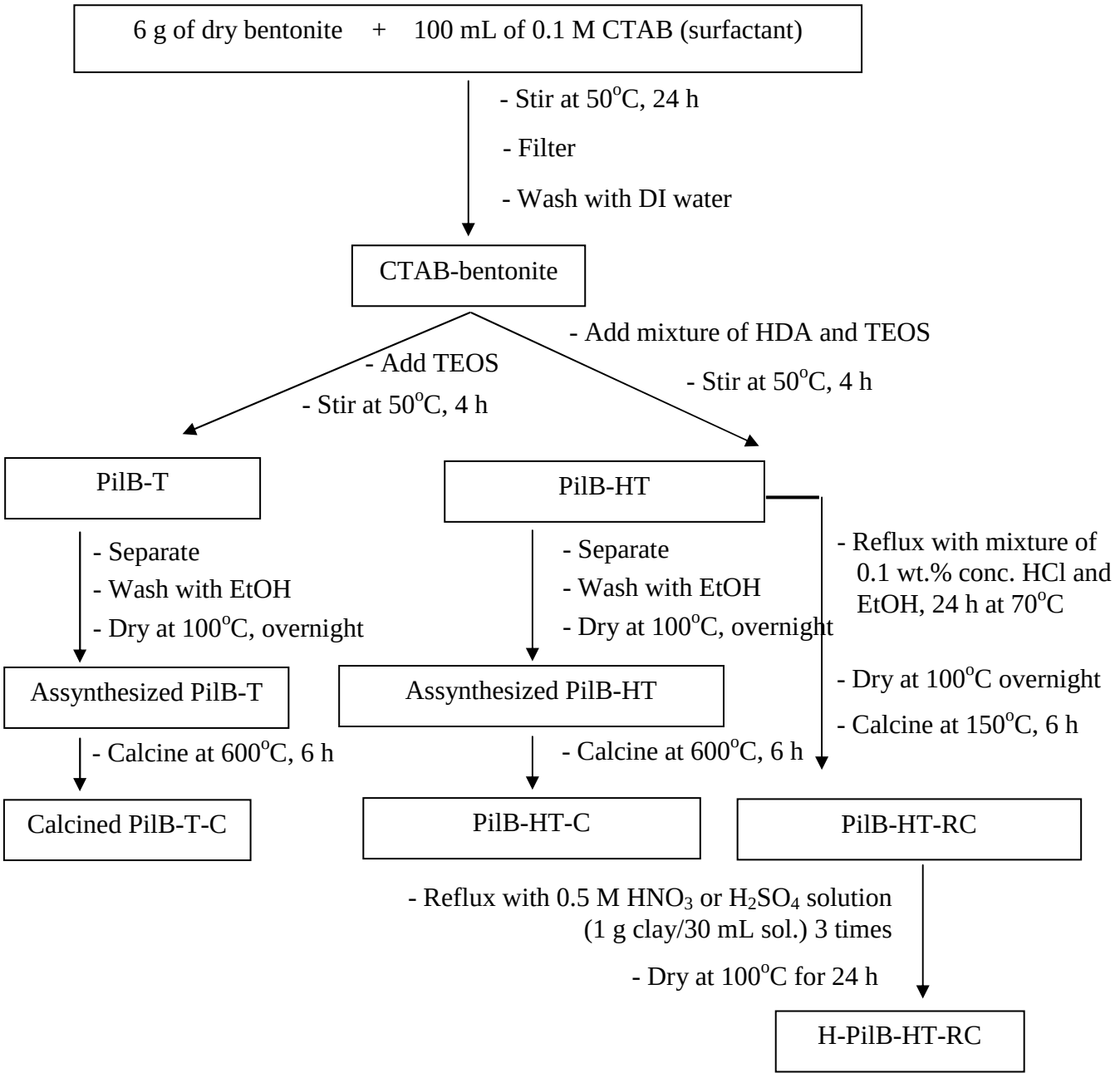

Scheme 3.8 Diagram of pillar and acid-activated pillar bentonite preparation.

3.4 Catalytic activity of synthesized catalysts in esterification

In this work, the palmitic acid and oleic acid free fatty acids were chosen to starting material for the esterification reaction. Because of in Thailand, palm oil tree is cultivated higher than another oil tree. Palm oil contains a large quantity of oleic, palmitic and linoleic free fatty acid. Free fatty acid composition was shown in Table 3.1. The esterification will be used to handle free fatty acid commonly found in crude palm oil, used cooking oil, crude jatropha oil. The biodiesel process can be done with esterification instead of deacidification during pretreatment.

Table 3.1 Typical free fatty acid composition in palm oil (OLEEN, Co., Ltd.)

Fatty acid	C no. : DB	FW	% wt
Oleic acid	C18 : 1	282.46	45.22
Palmitic acid	C16 : 0	256.42	37.94
Linoleic acid	C18 : 2	280.45	10.89
Stearic acid	C18 : 0	284.48	3.84
Myristic acid	C14 : 0	228.37	1.19
Lauric acid	C12 : 0	220.39	0.67
Linolenic acid	C18 : 3	278.43	0.25

C: carbon, DB: double bond, FW: formula weight

3.4.1 Esterification of free fatty acid

The esterification was carried out in a 100 mL stainless steel autoclave batch reactor with a stirrer (Figure 3.2) using palmitic acid or oleic acid free fatty acid (FFA) and methanol as starting materials. The reaction was done in the presence of prepared catalyst at 60^{o}C. The FFA and methanol (FFA to methanol mol ratio of 1:9) were added into the reactor with 10 wt. % of catalyst based on reactant weight under stirring at 200 rpm. After reaction, the sample chamber was cooled down to room temperature and the used catalyst was separated from the liquid phase by

centrifugation. The reaction mixture was separated free fatty acid methyl ester phase (bottom phase) from mixed water and methanol phase (top phase) by separate funnel. After that, the free fatty acid methyl ester was silylated with N-methyl-N-trimethylsilyltrifluoroacetamide (MSTFA) and reaction mixture was analyzed by a Varian CP-3800 gas chromatography (GC) with CP-8 column (following EN 14105:2003). Percentage of methyl ester yield was calculated based on eicosane internal standard. The used catalyst was washed with acetone and dried for reuse and regeneration. The esterification of free fatty acid procedure was illustrated in Scheme 3.9.

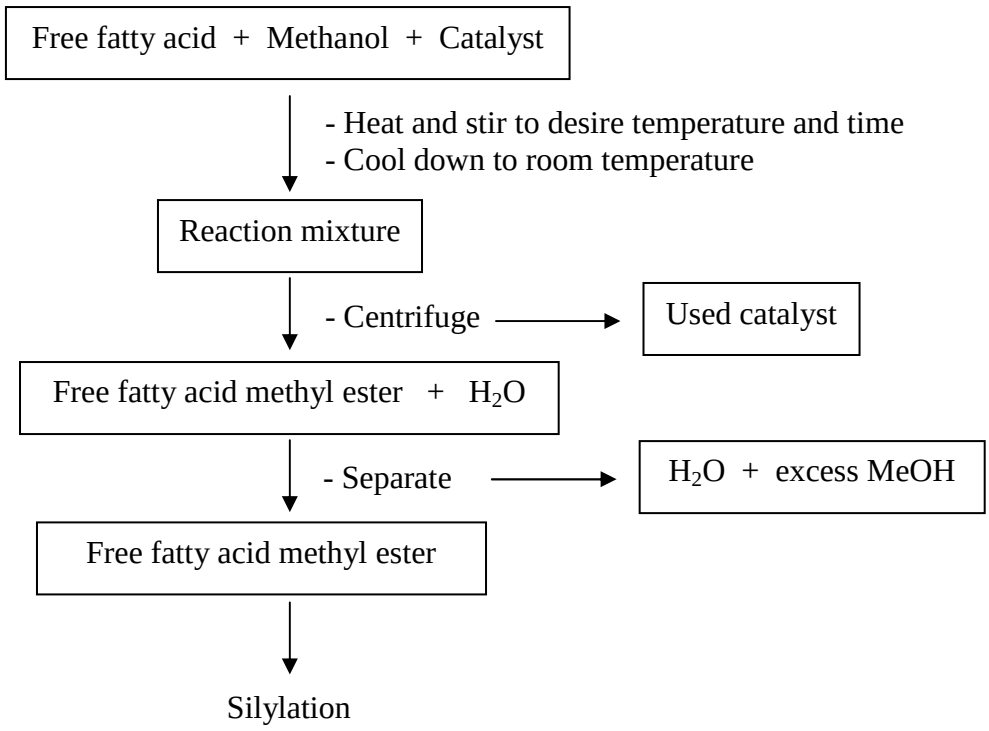

Scheme 3.9 Diagram of esterification of free fatty acid with methanol.

Figure 3.2 Apparatus for esterification reaction.

3.4.2 Esterification of vegetable oil

The esterification of vegetable oil (mixed of 15 wt.% oleic acid and refined palm oil, Jatropha oil and waste cooking palm oil) was done in a 100 mL round-bottom flask equipped with a magnetic stirrer and water cooling condenser. The reaction of vegetable oil and methanol was studied at various molar ratios of oil to methanol (1:9, 1:23, 1:30, 1:50 and 1:70), reaction times (15, 30, 45 and 60 h) and catalytic amounts (0.5, 1, 5 and 10 wt.%). After reaction, the used catalyst was separated from the liquid phase by centrifugation and the sample was determined free fatty acid content by titration technique following AOCS official Method Ca 5a-40.

3.4.3 Silylation procedure [ASTM D 6584 and BS EN 14103:2003]

One hundred milligrams of free fatty acid methyl ester was sillylated with 100 µL of MSTFA. Then, shaken vigorously and stored at room temperature for 15 minutes. The MSTFA helped reduce clumping due to agitation and freezing of the free fatty acid methyl ester (biodiesel). After that, one gram of internal standard stock solution (estimated 1.2 x 10^{-1} M eicosane in THF) and 8 mL of THF were added before gas chromatography analysis. Each GC run contained 1 µL of solution. A modified temperature profile was defined above (3.1.9). The silylation procedure was illustrated in Scheme 3.10.

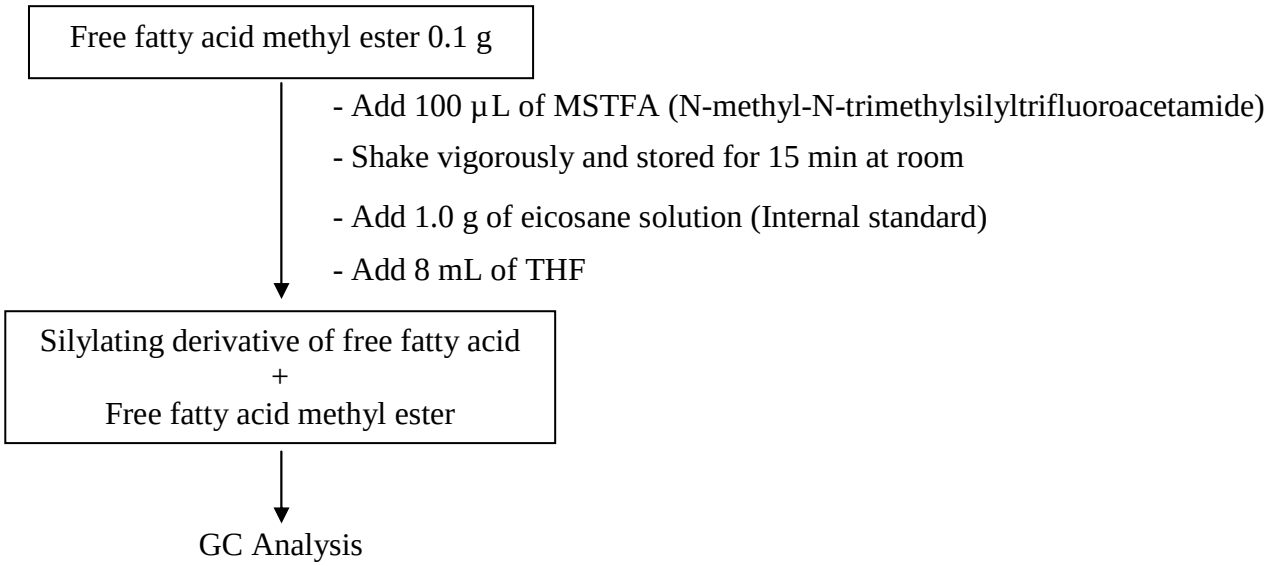

Scheme 3.10 Diagram of silylation of free fatty acid.

3.5 Parameters affecting esterification reaction

3.5.1 Effect of catalyst amount

The effect of catalyst loading was also studied in esterification reaction. The catalyst amounts to reaction mixture were varied in range of 0-10 wt%.

3.5.2 Effect of methanol to free fatty acid mol ratio

The esterification reaction was performed at various methanol to oil mole ratios according to the general procedure described above. The effect of methanol to FFA mole ratios was investigated at the value of 6:1-70:1.

3.5.3 Effect of reaction time

The reaction time was studied in range of 0.5-24 h.

3.5.4 Effect of reaction temperature

To investigate the effect of temperature and time in esterification reaction, the reaction was also performed at various temperatures as the general procedure above. The reaction temperature was varied in range of 60-120^{o}C.

3.5.5 Activity of reuse catalyst

The used catalysts were tested for their activity again without any treatment except washing with acetone and dry in air at 60-100^{o}C for 24 h before reuse in next batch reaction.

3.5.6 Regeneration catalyst

For regeneration of (p) rp-SBA-15-Pr-SO_3H, the used catalyst was washed with acetone, dried at 60^{o}C for 24 h and incorporated with propyl sulfonic acid group by using post synthesis grafting method, which was described in topic 3.3.2.2. For regeneration of acid-treated clay, the used catalyst was washed with acetone, dried at 100^{o}C for 24 h and acid activated by 0.5 M H_2SO_4 aqueous solution that was described in topic 3.3.3.

CHAPTER IV

RESULTS & DISCUSSIONS

4.1 Rope-like mesoporous silica (rp-SBA-15) and propyl sulfonic acid rope-like mesoporous silica (rp-SBA-15-Pr-SO_3H) catalysts

4.1.1 Characterization of catalyst

4.1.1.1 X-ray diffractometry (XRD)

The XRD patterns of as-synthesized and calcined mesoporous rp-SBA-15 were shown in Figure 4.1. Both materials exhibited the typical pattern of hexagonal structure [18], as-synthesized rp-SBA-15 provided the peak positions located at two-theta of 0.8^o, 1.5^o and 1.7^o for plane (100), (110) and (200) respectively. After remove the template, the calcined sample showed higher intensity at all reflections than as-synthesized sample because the mesoporous template in pores was completely removed. In addition, the XRD pattern of the calcined sample was slightly shifted to the larger angle because the unit cell shrinks after sample was heated at high temperature (about 550^oC) [58].

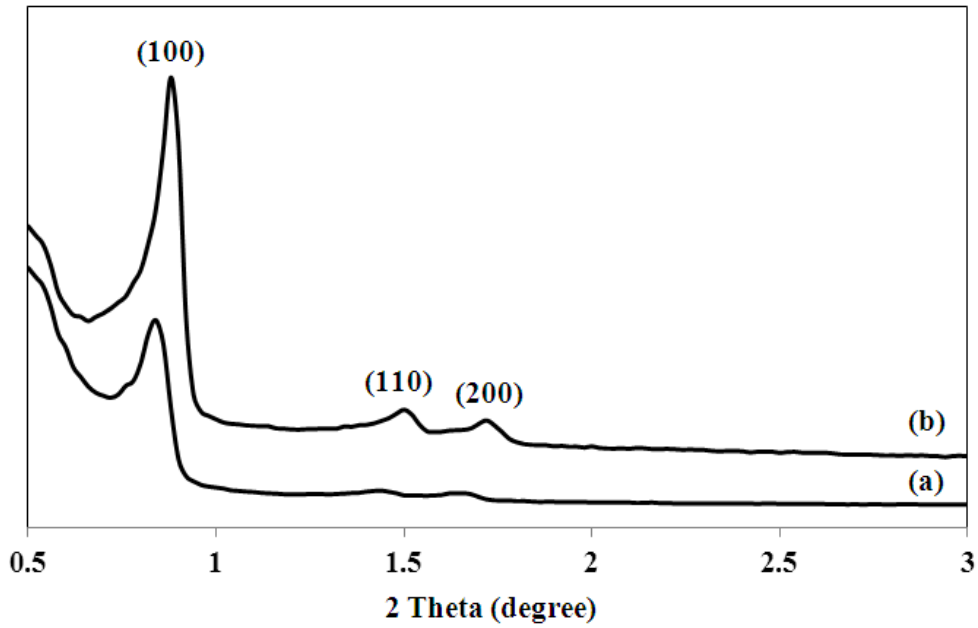

Figure 4.1 Representative XRD patterns of (a) as-synthesized rp-SBA-15 and (b) calcined rp-SBA-15.

Low angle XRD patterns of propyl sulfonic functionalized mesoporous rp-SBA-15 materials (rp-SBA-15-Pr-SO_3H) were showed in Figure 4.2. After propyl sulfonic functionalized, all samples still exhibited one very intense peak and two weak peaks indexed to (100), (110) and (200) diffractions, respectively similar to parent rp-SBA-15, indicating the prepared materials contained well-ordered hexagonal structure corresponding to pure rp-SBA-15 [18]. In comparison with Rb-SBA-15, the diffraction peaks of propyl sulfonic functionalized rp-SBA-15 materials were slightly shifted to lower 2 theta values, indicating the presence of bulky functional group on the surface of rp-SBA-15 would decrease void volume, then *d*-spacing was increased. The (p) rp-SBA-15-Pr-SO_3H sample that was prepared from post grafting method showed higher crystal structure than direct synthesized material. The crystal structure of (p) rp-SBA-15-Pr-SO_3H sample was decreased after used in reaction because the reactants and products could be adsorbed in pore of material. However, the used (p) rp-SBA-15-Pr-SO_3H was regenerated by wash with acetone and graft with propyl sulfonic acid, indicating the crystal structure was increased.

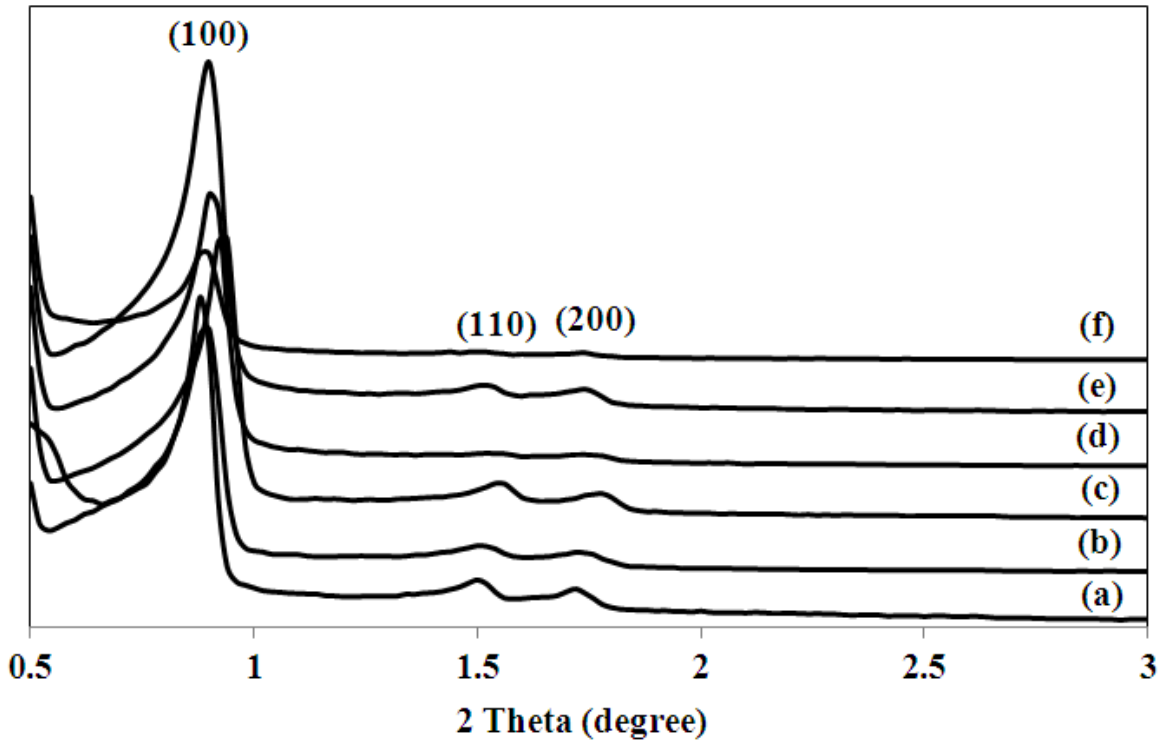

Figure 4.2 Representative XRD patterns of (a) calcined rp-SBA-15, (b) (d) Rp-SBA-15-Pr-SO_3H, (c) (p) rp-SBA-15-Pr-SO_3H, (d) used (p) Rp-SBA-15-Pr-SO_3H, (e) regenerated (p) rp-SBA-15-Pr-SO_3H and (f) used regenerated (p) rp-SBA-15-Pr-SO_3H.

4.1.1.2 Sorption properties and acid amount analysis

The specific BET surface area (A) and total pore volume (V) of samples were obtained from the standard BET (Brunauer, Emmett and Teller) method and the Barret-Joyner-Halender (BJH) equation, respectively. Moreover, the internal surface area was obtained from *t-plot* equation. The textural properties of rp-SBA-15 and propyl sulfonic functionalized rp-SBA-15 materials were shown in Table 4.1. The Rb-SBA-15 provided BET surface area as 874 m^2/g with large internal surface area as 820 m^2/g and an average pore size diameter as 9.2 nm. After propyl sulfonic functionalization, the BET surface area, internal surface area, pore volume and pore diameter were decreased whereas pore wall thickness was increased due to the presence of bulky functional group on the surface and in the pore of rp-SBA-15. The (p) rp-SBA-15-Pr-SO_3H contained BET surface area of 733 m^2/g, internal surface

area 699 m^2/g and an average pore diameter of 8.0 nm that were higher compared to (d) rp-SBA-15-Pr-SO_3H, which was prepared from direct synthesis. For post synthesis grafting, the MPTMS propyl sulfonic groups were introduced onto the pore wall surface and onto surface of material whereas for direct synthesis, the MPTMS groups were incorporated during the synthesis of the material. Furthermore from XRD and nitrogen adsorption analysis, the (p) rp-SBA-15-Pr-SO_3H gave higher pore wall thickness than direct synthesized (d) rp-SBA-15-Pr-SO_3H resulting in high thermal stability. The decrease in the BET surface area, the internal surface area and the pore size of (p) rp-SBA-15-Pr-SO_3H after catalyzed esterification indicated that the reactants could be reacted in mesoporous structure and on the mesoporous surface at the same time. The physicochemical properties of post synthesized (p) rp-SBA-15-Pr-SO_3H could be increased by regeneration.

The acid amount values of the parent rp-SBA-15 and propyl sulfonic functionalized rp-SBA-15 materials were shown in Table 4.1. It was significant that acid amount values of the materials were found to increase when functionalized with sulfonic acid groups by both direct synthesis and post synthesis grafting methods. After propyl sulfonic acid functionalization, the acid amount of direct and post synthesized samples ((d) rp-SBA-15-Pr-SO_3H and ((p) rp-SBA-15-Pr-SO_3H) were increased almost 5-7 fold from 0.24 to 1.25 and 1.58 mmol/g, respectively compared to parent rp-SBA-15. However, (p) rp-SBA-15-Pr-SO_3H that was prepared by post synthesis grafting method showed a highest acid amount value than by direct synthesis method. The acid amount value of used catalyst after catalyzed reaction was decreased due to leaching out of sulfonic acid active site. The regenerated (p) rp-SBA-15-Pr-SO_3H exhibited nearly acid amount with fresh (p) rp-SBA-15-Pr-SO_3H.

Table 4.1 BET surface area, total pore volume, average pore diameter and acid strength of propyl sulfonic acid functionalized mesoporous silica and Amberlyst-15 samples.

Catalyst	**BET surface area (m^2/g) (A)**	**Internal surface area (m^2/g)**	**Total pore volume (cm^3/g) (V)**	**Average pore diameter (nm)**	**Wall thickness (nm)**	**Acid amount (mmol/g)**
rp-SBA-15	874	820	1.14	9.2	1.69	0.24
(d) rp-SBA-15-Pr-SO_3H	708	675	0.79	8.0	2.02	1.25
(p) rp-SBA-15-Pr-SO_3H	733	699	1.04	8.0	2.83	1.58
Used (p) rp-SBA-15-Pr-SO_3H	320	578	0.51	7.0	2.12	0.72
Regenerated (p) rp-SBA-15-Pr-SO_3H	538	650	0.72	8.1	2.32	1.32
Used regenerated (p) rp-SBA-15-Pr-SO_3H	354	440	0.51	8.1	2.04	0.48
Amberlyst-15	37	12	0.06	2.4	-	3.00

As shown in Figure 4.3, nitrogen adsorption-desorption isotherm curves for the parent rp-SBA-15 and propyl sulfonic functionalized rp-SBA-15 provided isotherm type IV of IUPAC classification and exhibited a hysteresis loop H1-type which was characteristic of large-pore mesoporous materials with narrow pore size distribution. A slight hysteresis loop and sharp adsorption step at relative pressures around 0.6-0.8 identify characteristic of this isotherm [18]. Moreover, pore size of prepared materials has also been confirmed by adsorption-desorption isotherm.

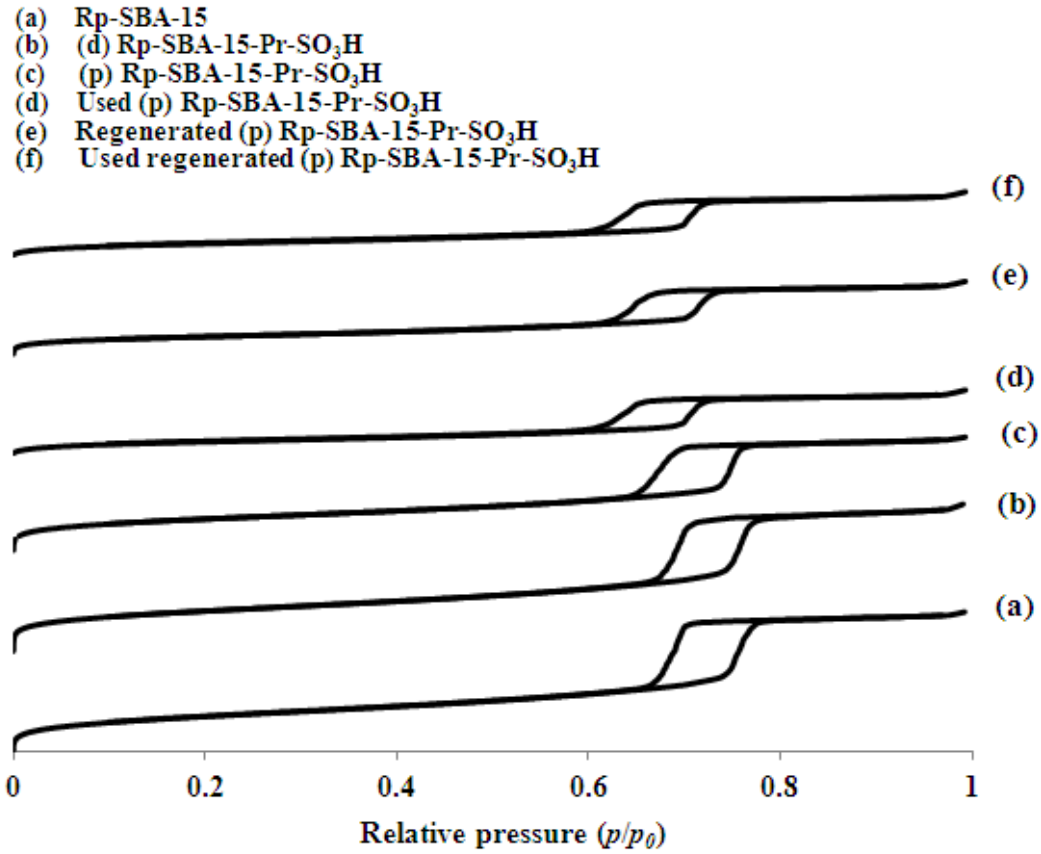

Figure 4.3 Representative N_2 adsorption/desorption isotherms of parent rp-SBA-15, direct and post synthesis propyl sulfonic functionalized, used and regenerated post synthesis materials.

4.1.1.3 Scanning electron microscopy (SEM)

The SEM images of parent rp-SBA-15 and propyl sulfonic functionalized rp-SBA-15 samples at 10,000 magnification were shown in Figure 4.4**.** Pure silica rp-SBA-15 performed regular dispersion containing small rod particles about 0.9 × 1.2 µm which agglomerated to rope-liked structure. The propyl sulfonic functionalized rp-SBA-15 samples that were prepared by direct and post synthesis method (Figure 4.4 (b-c)) were aggregated particles with rope-like structure similar to parent rp-SBA-15. However, direct synthesized (d) rp-SBA-15-Pr-SO_3H provided larger formation particle than post grafting sample, resulting to lower surface area (as showed in Table 4.1). The used post synthesized (p) rp-SBA-15-Pr-SO_3H sample,

which was catalyzed in esterification, showed more aggregate and segregative particle due to the effect of stir in the reaction.

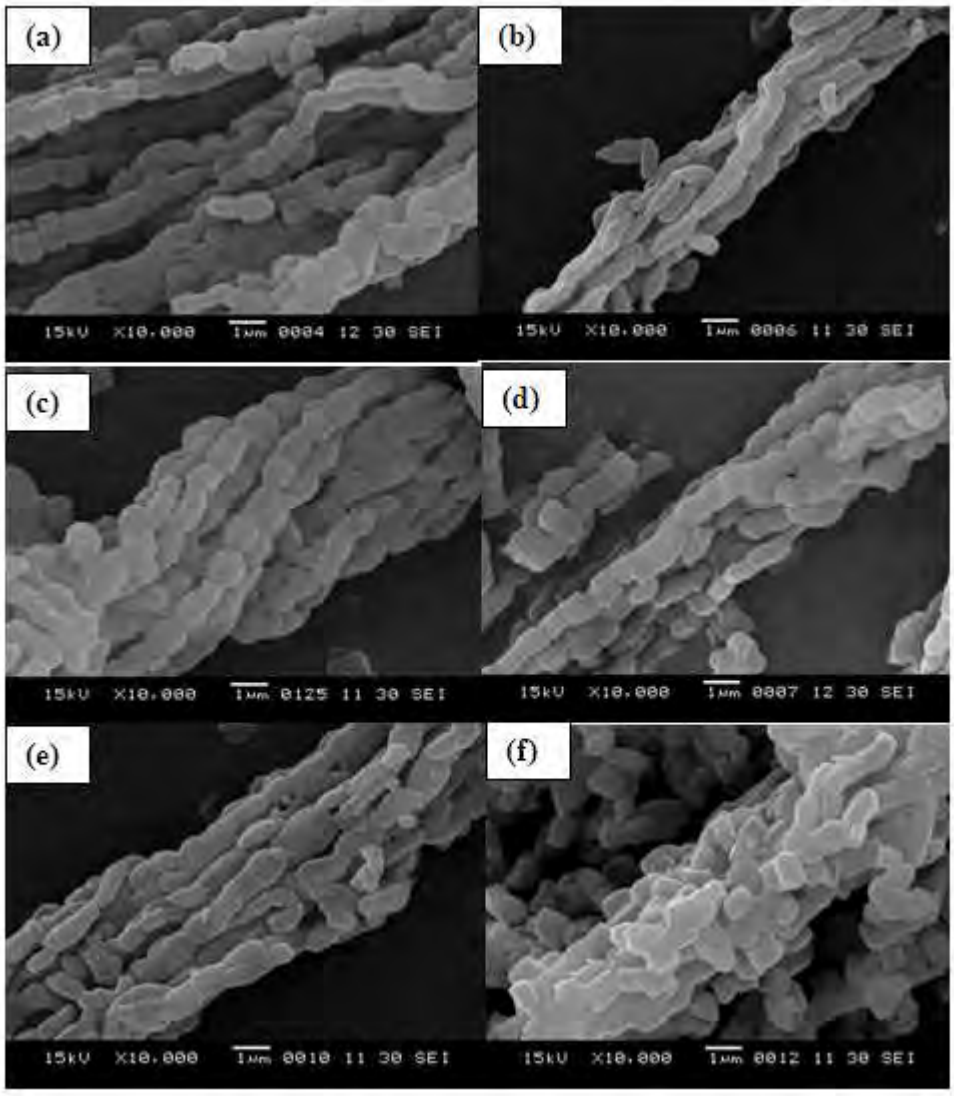

Figure 4.4 Representative SEM images × 10,000 of (a) parent rp-SBA-15, (b) (d) rp-SBA-15-Pr-SO_3H, (c) (p) rp-SBA-15-Pr-SO_3H, (d) used (p) rp-SBA-15-Pr-SO_3H, (e) regenerated (p) rp-SBA-15-Pr-SO_3H and (f) used regenerated (p) rp-SBA-15-Pr-SO_3H.

4.1.1.4 Transmission electron microscopy (TEM)

The transmission electronic microscopy technique was used to confirm the mesoporous tube silica structure. TEM images (Figure 4.5) of all samples evidenced the presence of well-ordered hexagonal arranged of one-dimensional mesoporous channels. The distance from high-dark contrast in the TEM image of rp-SBA-15 and all propyl sulfonic functionalized rp-SBA-15 samples was estimated to be ~10 nm, in agreement with that determined from the XRD data.

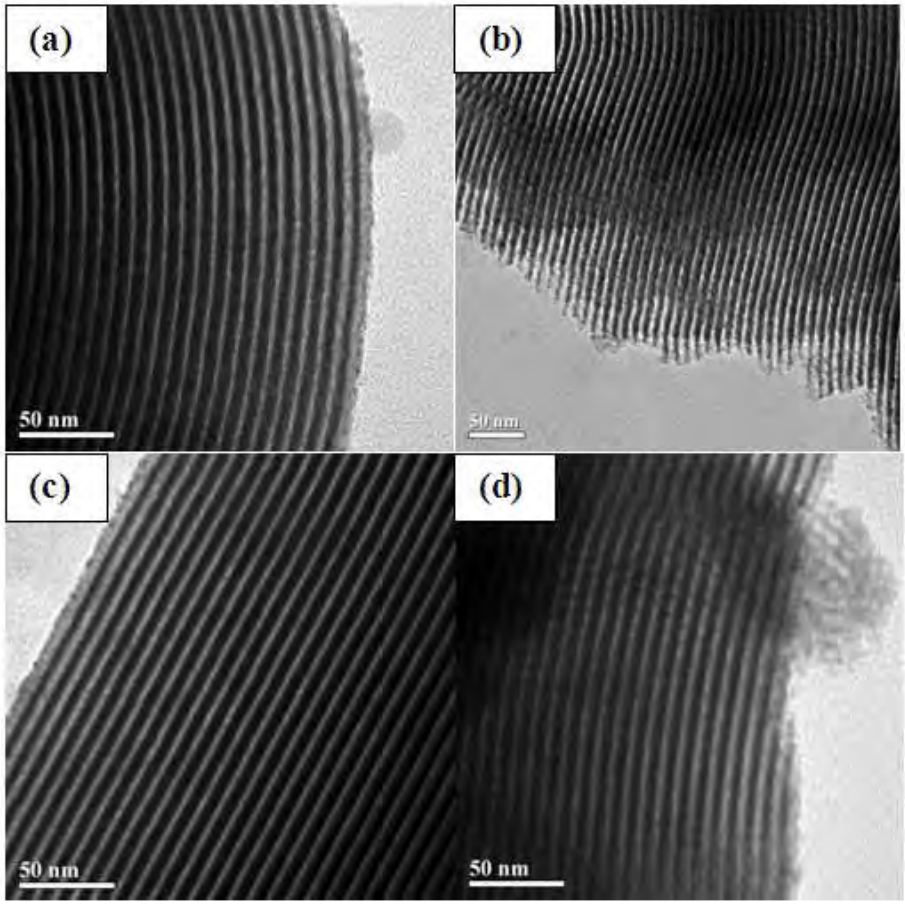

Figure 4.5 Representative TEM images of the (a) rp-SBA-15, (b) (d) Rp-SBA-15-Pr-SO_3H, (c) (p) rp-SBA-15-Pr-SO_3H and (d) regenerated (p) Rp-SBA-15-Pr-SO_3H.

4.1.2 Catalytic activity test of propyl sulfonic acid functionalized rp-SBA-15 catalyst in esterification of oleic and palmitic free fatty acid

4.1.2.1 Esterification of palmitic acid and methanol

The synthesized propyl sulfonic acid functionalized rp-SBA-15 materials, which were prepared by using direct synthesis and post synthesis grafting methods, were tested to study catalytic activity in esterification of palmitic acid and methanol. Furthermore, the catalytic activity of synthesized samples was compared with commercial Amberlyst-15 catalyst. The reaction condition was 9:1 methanol to palmitic acid mole ratio, 60^{o}C for 0.5-6 h and 10 wt.% catalyst amount.

The effect of reaction time was investigated. The catalytic activities of both direct synthesized and post grafted propyl sulfonic acid functionalized rp-SBA-15 and Amberlyst-15 samples were performed. The results were showed in Table 4.2 and the corresponding plot methyl palmitate yield was shown in Figure 4.6. As a result, when reaction time was increased the methyl palmitate yield was increased significantly until 4 h, resulted as 94%, 100% and 98 % directed (d) rp-SBA-15-Pr-SO_3H, posted (p) rp-SBA-15-Pr-SO_3H and Amberlyst-15, respectively. Thus, the posted (p) rp-SBA-15-Pr-SO_3H was a better catalyst than the directed one because (p) rp-SBA-15-Pr-SO_3H catalyst contained higher BET surface area and acid active site. These concluded that the optimum condition for esterification of palmitic acid was methanol to palmitic acid mole ratio of 9:1, catalyst amount of 10wt% at 60°C for 6 h.

Table 4.2 Catalytic activity of directed and posted propyl sulfonic functionalized rp-SBA-15 and Amberlyst-15 catalysts in esterification of palmitic acid

Reaction time (h) at 60°C	**Methyl palmitate yield (%)**		
	(d) rp-SBA-15-Pr-SO_3H	**(p) rp-SBA-15-Pr-SO_3H**	**Amberlyst-15**
0.5	66.10	84.41	68.11
1	67.44	85.79	70.65
2	68.56	86.54	72.57
3	83.67	90.56	87.98
4	85.12	92.46	92.32
6	94.12	100	98.25

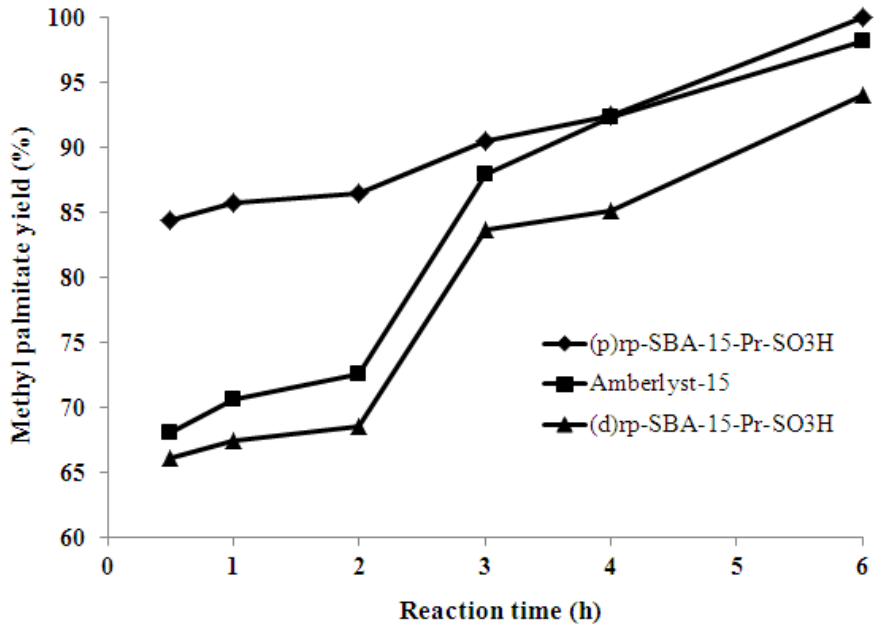

Figure 4.6 Representative catalytic activity of directed and posted propyl sulfonic functionalized rp-SBA-15 and Amberlyst-15 catalysts in esterification of palmitic acid.

4.1.2.2 Esterification of oleic acid and methanol

The directed and posted propyl sulfonic acid functionalized rp-SBA-15 materials were also investigated to study catalytic activity in esterification of oleic acid and methanol. Furthermore, the catalytic activity of synthesized samples was compared with commercial Amberlyst-15 catalyst. The reaction condition was 9:1 methanol to oleic acid mole ratio, 60^{o}C for 0.5-6 h and 10 wt.% catalyst amount.

The effect of reaction time on methyl oleate yield was studied. The catalytic activities of synthesized materials in the esterification of oleic acid at different reaction time were shown in Table 4.3. The corresponding plot of methyl oleate yield versus reaction time was shown in Figure 4.7. As a result, when reaction time was increased the methyl oleate yield was increased significantly until 3 h, resulted as 100% for both posted (p) rp-SBA-15-Pr-SO_3H and Amberlyst-15 except directed (d) rp-SBA-15-Pr-SO_3H. The directed (d) rp-SBA-15-Pr-SO_3H catalyst provided highest methyl oleate yield when reaction time was reached to 4 h. However, when increasing the reaction time to 6 h, the methyl oleate yield was decreased because of backward reaction to the starting material. Therefore, the posted (p) rp-SBA-15-Pr-SO_3H was a good catalyst and appropriated for esterification of FFA. These could be concluded that the optimum condition for esterification of oleic acid was methanol to oleic acid molar ratio of 9:1, catalyst amount of 10 wt.% at 60°C for 3 h. This optimized condition was applied in further study with other catalysts.

Table 4.3 Catalytic activity of directed and posted propyl sulfonic functionalized rp-SBA-15 and Amberlyst-15 catalysts in esterification of oleic acid

Reaction time (h) at 60°C	**Methyl oleate yield (%)**		
	(d) rp-SBA-15-Pr-SO_3H	**(p) rp-SBA-15-Pr-SO_3H**	**Amberlyst-15**
0.5	69.83	80.39	70.85
1	75.33	83.09	75.32
2	85.21	87.32	87.69
3	95.89	100	100
4	100	99.58	98.85
6	95.76	98.00	97.20

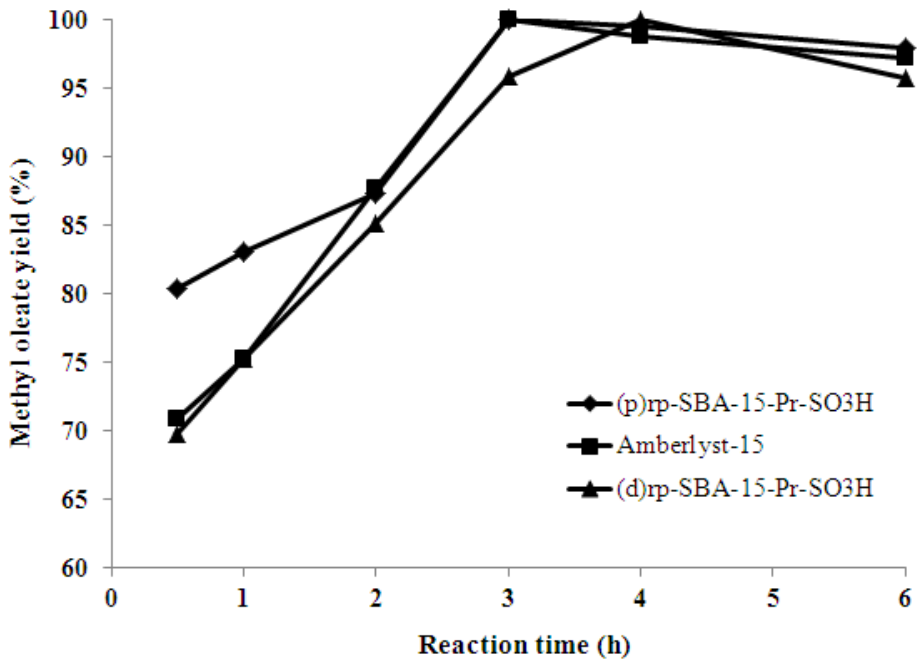

Figure 4.7 Representative catalytic activity of directed and posted propyl sulfonic functionalized rp-SBA-15 and Amberlyst-15 catalysts in esterification of oleic acid.

4.1.3 Catalytic activity test of reused and regenerated posted (p) rp-SBA-15-Pr-SO_3H catalyst in esterification of oleic acid and palmitic acid (FFA)

The catalytic activities test of fresh, reused and regenerated (p) rp-SBA-15-Pr-SO_3H catalysts in the esterification of palmitic acid and oleic acid were shown in Table 4.4. The esterification condition was 9:1 methanol to FFA, at 60^{o}C for 3 h and 10 wt.% catalyst amount. The catalytic activities of both catalysts were decreased after reaction run. The loss in activities of catalyst might be from the deactivation of catalytic active site. The methyl palmitate yield was decreased from 90.5% to 63.2% and methyl oleate yield was decreased from 100% to 71.1% after reaction run using (p) rp-SBA-15-Pr-SO_3H catalyst. For Amberlyst-15, the methyl palmitate yield and methyl oleate yield were decreased from 87.9% to 66.7% and from 100% to 79.8%, respectively. However, the used (p) rp-SBA-15-Pr-SO_3H catalyst was developed in order to improve its performance. After used, catalyst was regenerated, which was previously described in topic 3.3.2.2. The methyl palmitate yield and methyl oleate yield were improved from 63.2% to 89% and from 71.1% to 100%, nearly the fresh one. Therefore, the (p) rp-SBA-15-Pr-SO_3H catalyst could be regenerated successfully.

Table 4.4 Catalytic activity of reused and regenerated posted (p) rp-SBA-15-Pr-SO_3H and reused Amberlyst-15 catalysts in esterification of FFA

Catalyst	**Methyl palmitate yield (%)**	**Methyl oleate yield (%)**
Fresh (p) rp-SBA-15-Pr-SO_3H	90.56	100
Reused (p) rp-SBA-15-Pr-SO_3H	63.29	71.15
Regenerated (p) rp-SBA-15-Pr-SO_3H	89.05	99.55
Amberlyst-15	87.98	100
Reused Amberlyst-15	66.74	79.86

4.2 Rope, rod and fiber-like mesoporous (rp-SBA-15, rd-SBA-15 and f-SBA-15) silica and MCM-41 catalysts

All of propyl sulfonic acid functionalized mesoporous silica samples were prepared by using post synthesis grafting method.

4.2.1 Characterization of catalysts

4.2.1.1 X-ray diffractmetry (XRD)

Low angle X-ray powder diffraction patterns of sulfonic functionalized mesoporous materials were shown in Figure 4.8. The three SBA-15 samples (Figure 4.8a – 4.8f) showed three characteristic peaks that were one very intense peak and two weak peaks corresponding to (100), (110) and (200) diffraction planes, indicating the prepared materials contained well-ordered hexagonal structure [59]. However, the difference of each pattern was 2 theta positions of diffraction planes, that f-SBA-15 indicated largest pore diameter follow by rd-SBA-15, rp-SBA-15 and MCM-41 with smallest pore diameter. In comparison of sulfonic acid functionalized mesoporous silica samples (rp-SBA-15-Pr-SO_3H, rd-SBA-15-Pr-SO_3H, f-SBA-15-Pr-SO_3H and MCM-41-Pr-SO_3H) with their parent samples (rp-SBA-15, rd-SBA-15, f-SBA-15 and MCM-41), the diffraction peaks of sulfonic functionalized SBA-15 materials were slightly shifted to lower 2 theta values. From the results indicated that the presence of organic functional group on the surface of mesoporous matters would decrease pore volume because wall thickness was increased (the results were shown in Table 1). Moreover, the propyl sulfonic acid functionalized samples exhibited lower crystallinity compared to pure mesoporous silica samples due to incorporation of organo sulfonic group in mesoporous structure. From XRD result, the MCM-41 and MCM-41-Pr-SO_3H materials showed (100), (110) and (200) diffraction planes at higher 2 theta values than rp-SBA-15, rd-SBA-15 and f-SBA-15 samples. This observation was assumed that MCM-41 contained lower pore diameter than others due to smaller surfactant micelle. When compared XRD patterns of rp-SBA-15 with rd-SBA-15 and f-SBA-15, the result exhibited that the pore diameter of rp-SBA-15 was lower than rd-SBA-15 and f-SBA-15 because heptane in the presence of NH_4F, which were used in rod and fiber synthesis, enhanced more swelling micelle resulting in larger pore size.

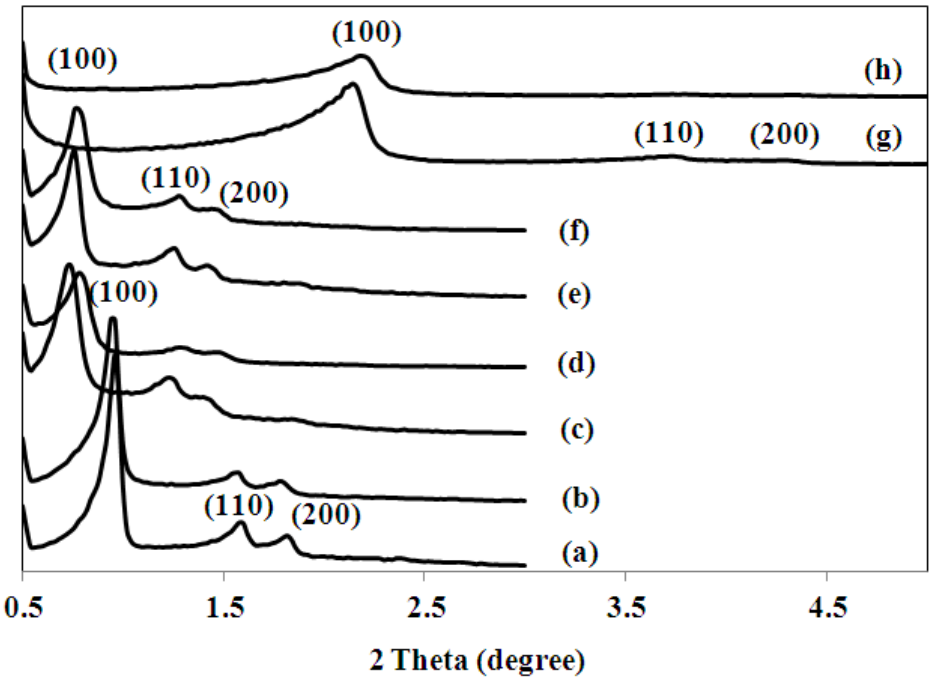

Figure 4.8 Representative XRD patterns of (a) rp-SBA-15, (b) rp-SBA-15-Pr-SO_3H, (c) rd-SBA-15, (d) rd-SBA-15-Pr-SO_3H, (e) f-SBA-15, (f) F-SBA-15-Pr-SO_3H (g) MCM-41 and (h) MCM-41-Pr-SO_3H.

4.2.1.2 Sorption properties and acid amount analysis

The specific BET surface area (A) and total pore volume (V) of samples were obtained from the standard BET (Brunauer, Emmett and Teller) method and the Barret-Joyner-Halender (BJH) equation, respectively. Moreover, the internal surface area was obtained from *t-plot* equation. The textural properties of mesoporous silica and propyl sulfonic functionalized materials were shown in Table 4.5. The rp-SBA-15 that was prepared from using no heptane co-solvent exhibited rope-like structure. The rod and fiber SBA-15 materials were obtained from additional heptane co-solvent in synthesis step. The 350 and 412 heptane to pluronic P123 molar ratio provided rod and fiber SBA-15 materials, respectively. The swelling micelle of pluronic P123 template was increased by adding organic co-solvent. Moreover, MCM-41 was synthesized by using hexadecylamine (HDA) template; thus, the pore size was smaller than rope, rod and fiber SBA-15 samples because the HDA contained lower swelling micelle than pluronic P123 [54, 55]. Therefore, the MCM-41 exhibited smaller pore diameter (2.4 nm) than rope-like SBA-15 (9 nm), rod and fiber-like SBA-15 (12 nm).

On the other hand, the rp-SBA-15 was found to be a mesoporous material with BET surface area 874 m^2/g with large internal surface area as 820 m^2/g and an average pore size diameter 9.2 nm. After the post-synthesis functionalization, the rp-SBA-15-Pr-SO_3H contained BET surface area of 733 m^2/g, internal surface area 699 m^2/g and an average pore diameter of 8.0 nm that were smaller compared to those of the parent rp-SBA-15 material. The analysis results of rd-SBA-15, f-SBA-15, MCM-41 materials and its propyl sulfonic functionalized materials were similar trend to rp-SBA-15 and rp-SBA-15-Pr-SO_3H materials. The decrease in the BET surface area, the internal surface area and the pore size after the functionalization indicated that the preparation conditions used allowed the organo sulfonic acid group incorporated in mesoporous structure and incorporated on the mesoporous surface at the same time. Furthermore from XRD and nitrogen adsorption analysis, the rp-SBA-15-Pr-SO_3H provided higher pore wall thickness than rd-SBA-15-Pr-SO_3H and f-SBA-15-Pr-SO_3H resulting in high thermal stability.

Table 4.5 BET surface area, total pore volume, average pore diameter and acid amount of propyl sulfonic acid functionalized mesoporous silica and Amberlyst-15 samples.

Catalyst	**BET surface area (m^2/g) (A)**	**Internal surface area (m^2/g)**	**Total pore volume (cm^3/g) (V)**	**Average pore diameter (nm)**	**Wall thickness (nm)**	**Acid amount (mmol/g)**
rp-SBA-15	874	820	1.14	9.2	1.69	0.24
rp-SBA-15-Pr-SO_3H	733	699	1.04	8.0	2.83	1.58
rd-SBA-15	407	236	1.21	12.1	1.72	0.32
rd-SBA-15-Pr-SO_3H	303	187	1.13	10.5	2.58	1.54
f-SBA-15	462	379	1.21	12.1	1.38	0.58
f-SBA-15-Pr-SO_3H	387	313	1.07	10.5	2.56	1.28
MCM-41	954	918	0.89	2.4	2.28	0.54
MCM-41-Pr-SO_3H	696	655	0.50	2.0	2.37	1.42
Amberlyst-15	37	12	0.06	2.4	-	3.00

As shown in Figure 4.9, nitrogen adsorption-desorption isotherm curves for the parent mesoporous silica and propyl sulfonic functionalized mesoporous silica exhibited characteristic type IV isotherms resulting from a capillary condensation take place in mesopore and difference in pore size [40]. A slight hysteresis loop and sharp adsorption step at relative pressures around 0.6-0.8 identify characteristic of this isotherm [41]. Pore size of materials has also been confirmed by adsorption-desorption isotherm. From the result, rd-SBA-15 and f-SBA-15 samples exhibited hysteresis loop at higher relative pressures than rp-SBA-15 and MCM-41 indicated that rd-SBA-15 and f-SBA-15 have been contained larger pore size.

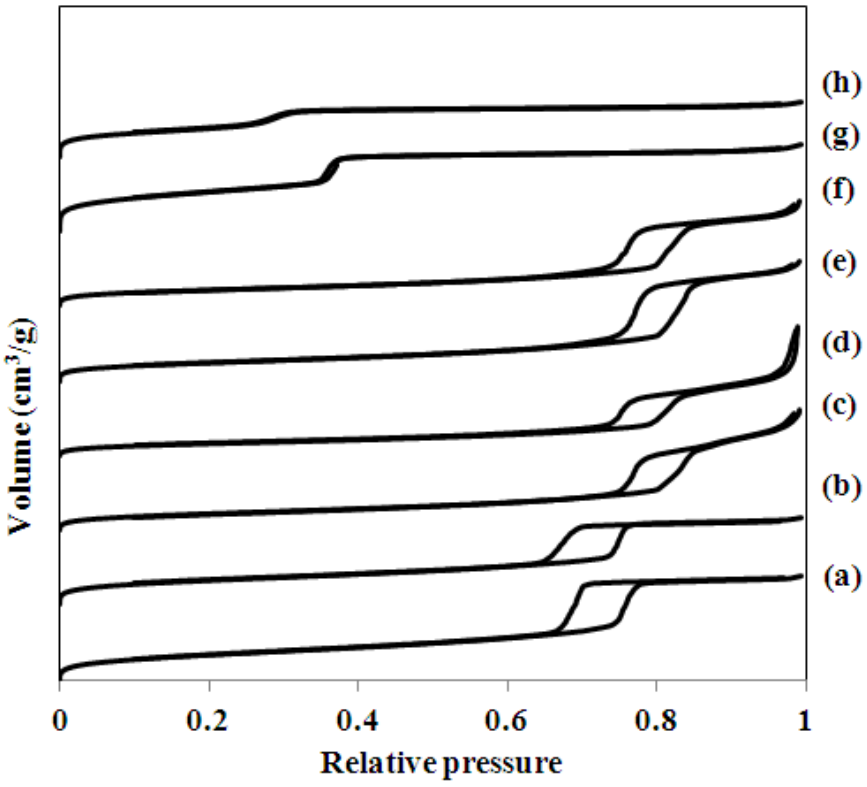

Figure 4.9 Representative N_2 adsorption/desorption isotherms of (a) rp-SBA-15, (b) rp-SBA-15-Pr-SO_3H, (c) rd-SBA-15, (d) rd-SBA-15-Pr-SO_3H, (e) f-SBA-15, (f) f-SBA-15-Pr-SO_3H, (g) MCM-41 and (h) MCM-41-Pr-SO_3H.

The acid amount values of the parent mesoporous silica and propyl sulfonic functionalized mesoporous silica materials were shown in Table 4.5. It was significant that acid amount values of the materials were found to increase when functionalized with sulfonic acid groups. After propyl sulfonic acid functionalization, the acid amount of RpSBA-15-Pr-SO_3H was increased almost 7-fold from 0.24 to 1.58 mmol/g when compare with parent RpSBA-15. The rd-SBA-15-Pr-SO_3H, f-SBA-15-Pr-SO_3H and MCM-41-Pr-SO_3H materials were similar trend to RpSBA-15-Pr-SO_3H.

4.2.1.3 Scanning electron microscopy (SEM)

The SEM images of all samples at 5,000 magnifications were illustrated in Figure 4.10. The rp-SBA-15 (Figure 4.10a) performed regular dispersion containing small rod particles, which agglomerated to rope-liked structure. The rp-SBA-15-Pr-SO_3H sample (Figure 4.10b) was aggregated particles with rope-like structure similar to parent rp-SBA-15. Figure 4.10 (c) and (d) exhibited the formation of small rod-like structure whereas Figure 4.10 (e) and (f) showed the formation of fiber-like structure. In addition, the particle size of rod-like structure materials was smaller than rope-like structure and fiber-like structure samples. The propyl sulfonic acid functionalized mesoporous silica samples showed more aggregate particle due to incorporation of organo sulfonic group in mesoporous structure.

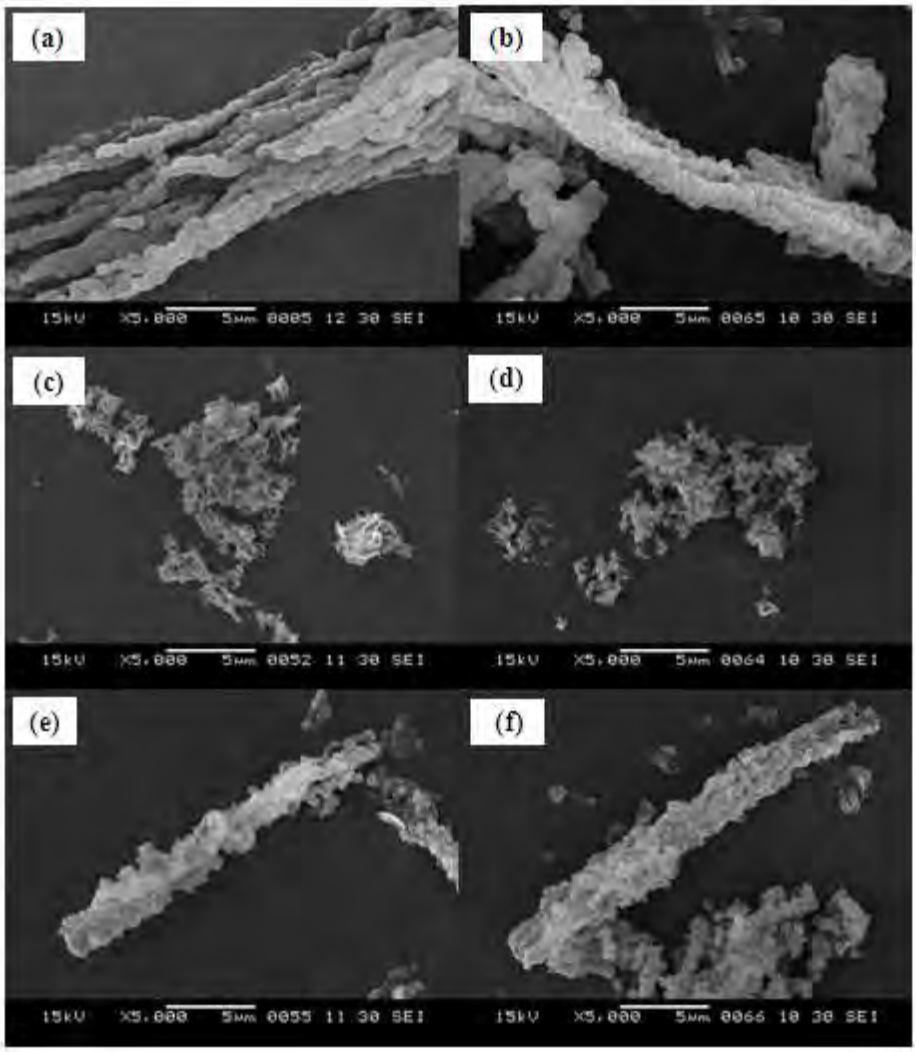

Figure 4.10 Representative SEM images of (a) rp-SBA-15, (b) rp-SBA-15-Pr-SO_3H, (c) rd-SBA-15, (d) rd-SBA-15-Pr-SO_3H, (e) f-SBA-15 and (f) f-SBA-15-Pr-SO_3H.

4.2.1.4 Transmission electron microscopy (TEM)

The mesoporous tube silica material structure has also been confirmed by transmission electronic microscopy. TEM images (Figure 4.11) of all samples evidenced the presence of well-ordered hexagonal arranged of one-dimensional mesoporous channels. From high-dark contrast in the TEM image of rp-SBA-15-Pr-SO_3H samples, the distance between hexagonal tube was estimated to be ~10 nm, in agreement with that determined from the N_2 adsorption experiments. However, the distance between mesopore of rd-SBA-15-Pr-SO_3H and f-SBA-15-Pr-

SO_3H was slightly higher than rp-SBA-15-Pr-SO_3H that confirmed to pores size result.

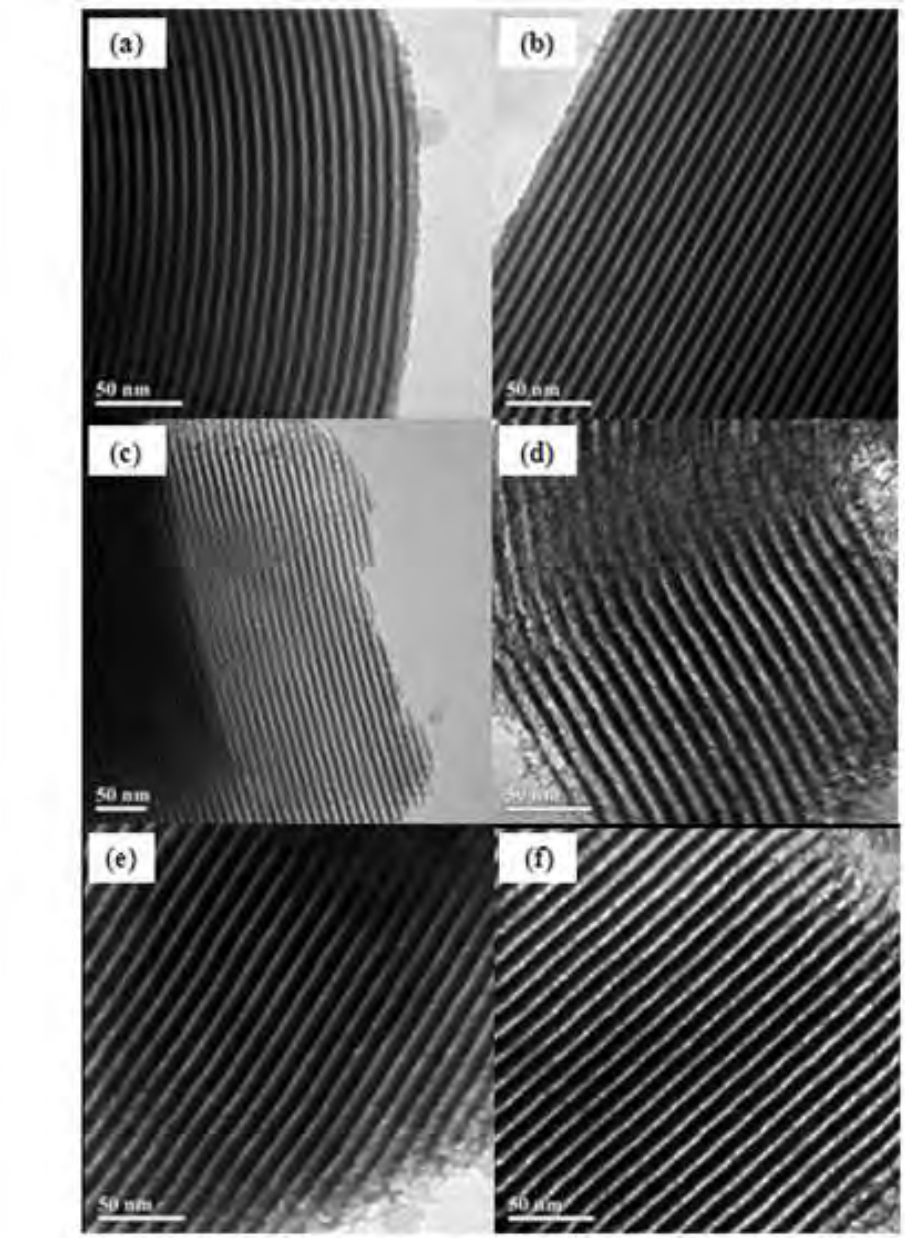

Figure 4.11 Representative TEM images of the (a) rp-SBA-15, (b) rp-SBA-15-Pr-SO_3H, (c) rd-SBA-15, (d) rd-SBA-15-Pr-SO_3H (e) f-SBA-15 and (f) f-SBA-15-Pr-SO_3H.

4.2.2 Catalytic activity test

4.2.2.1 Esterification of oleic acid and methanol

The esterification of a 1:9 mole ratio of oleic acid: methanol at 60^{o}C, which was optimal reaction condition from previous studied, was performed with the different catalysts and the commercial Amberlyst-15 at 0.5 wt. % catalytic amount. The relationship between the obtained % methyl oleate yield (%MO yield) and the reaction time was evaluated at 15 to 180 min (Figure 4.12). The reaction time had a clearly marked effect upon the esterification efficiency. All catalysts displayed essentially catalytic activity, increasing in MO yield when compared with without any catalyst. The rp-SBA-15-Pr-SO_3H catalyst exhibited the highest MO yield because it contained the highest acid amount, high specific BET surface area, large pore diameter (Table 4.5) and high crystallity (XRD). Moreover, this catalyst also gave a superior MO yield that was even higher than that obtained with the commercial Amberlyst-15 catalyst. The f-SBA-15-Pr-SO_3H, rd-SBA-15-Pr-SO_3H and MCM-41-Pr-SO_3H also exhibited % MO yield higher than Amberlyst-15 due to high specific surface area and high pore volume.

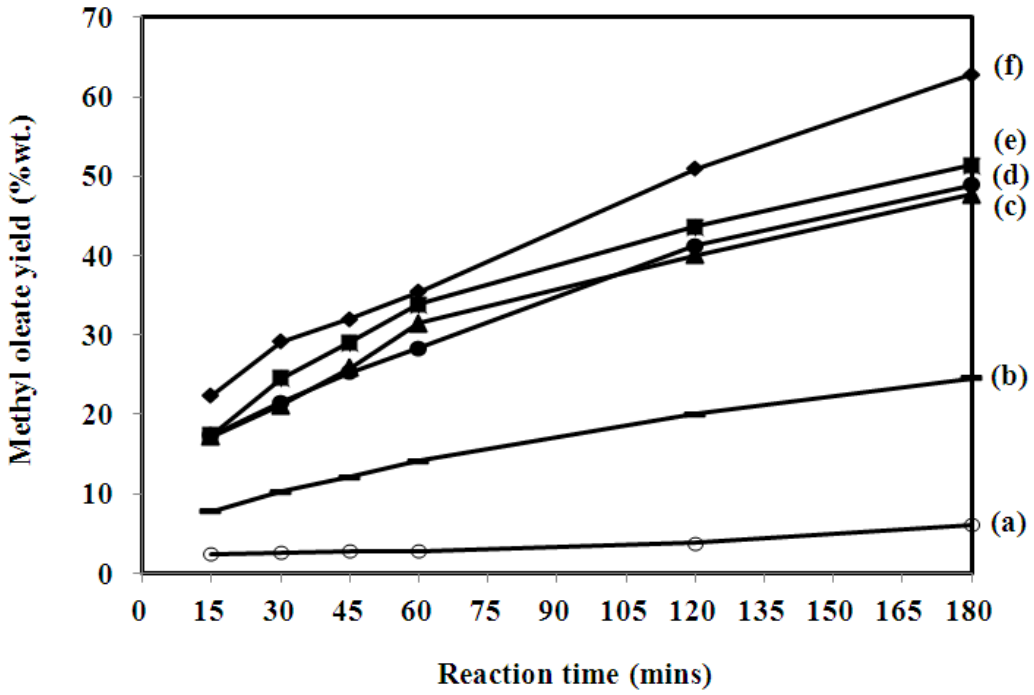

Figure 4.12 Kinetic study of the different propyl sulfonic acid functionalized mesoporous silica catalysts, compared to the blank test, for the esterification of a 1:9 molar ratio of oleic acid: methanol at 60°C for 15-180 min with 0.5 wt.% of catalyst. Shown is the data for (a, ○) no catalyst, (b, ▬) Amberlyst-15, (c, ▲) f-SBA-15-Pr-SO_3H, (d, ●) Rd-SBA-15-Pr-SO_3H, (e, ■) MCM-41-Pr-SO_3H and (f, ♦) rp-SBA-15-Pr-SO_3H.

4.2.2.2 Esterification of oleic acid and glycerol

The catalytic activity of propyl sulfonic acid functionalized mesoporous silica was also studied in esterification similar to topic 4.2.2.1 but one of reactant was changed to larger structure. The molecular flow depended on size and shape of both catalyst and substrates. Therefore, the methanol reactant was taken place by glycerol that was larger structure to prove the effect of catalytic pore size to substrate conversion and product yield. The structural size (length × wide), which was determined using Chemdraw program and HyperChem program, of oleic acid, methanol and glycerol starting materials was 1.76 × 1.27 nm, 0.12 × 0.12 nm and 0.37 × 0.29 nm, respectively. Furthermore, the structural size of methyl oleate, mono-, 1,2-

di- and tri-glyceride products were 1.61 × 1.27 nm, 1.19 × 0.91 nm, 2.15 × 1.20 nm and 3.94 × 2.59 nm, respectively. The tri-glyceride product was used as indicator to study pore size of large mesoporous catalysts (rp-SBA-15-Pr-SO_3H, rd-SBA-15-Pr-SO_3H, f-SBA-15-Pr-SO_3H and Amberlyst-15) and small mesoporous catalyst (MCM-41-Pr-SO_3H). The results from the oleic acid and glycerol esterification at 6:1 oleic acid to glycerol mol ratio, 110^oC, 15 min to 24 h of reaction time with 5 % (w/w) catalyst based on total reactant weight were shown in Table 4.6. Reaction time was a major effect on conversion and product yield. It was obvious that at short reaction time 15 to 30 min were not enough to complete the esterification of oleic acid. At reaction time 45 to 60 min, the oleic acid could convert to highest value about 99% by using rp-SBA-15-Pr-SO_3H, Amberlyst-15 and f-SBA-15-Pr-SO_3H catalysts, which were higher oleic acid conversion than rd-SBA-15, MCM-41 and no catalytic reactions. This indicated that the reaction could be completed within 60 min if high effective catalysts were used. However, it decreased with increasing reaction time because of backward reaction to the intermediate mono- and di-ester or starting material. Furthermore, the large mesoporous catalysts (rp-SBA-15-Pr-SO_3H, rd-SBA-15-Pr-SO_3H and f-SBA-15-Pr-SO_3H) exhibited higher tri-glyceride (TG) yield than small mesoporous catalyst (MCM-41-Pr-SO_3H). This result was a very important evidence to prove that tri-glyceride product could not produce in the pore of MCM-41-Pr-SO_3H catalyst due to larger of tri-glyceride structure than pore size of MCM-41 catalyst. The tri-glyceride could be occurred only on the surface of MCM-41-Pr-SO_3H catalyst. For high oleic acid conversion and TG yield of Amberlyst-15 catalyst, the reaction could be occurred on surface active site because this catalyst contained highest acid amount. The rp-SBA-15-Pr-SO_3H catalyst gave highest tri-glyceride yield of 64.3% at one hour reaction time, which showed higher catalytic activity than commercial Amberlyst-15 catalyst. When catalytic efficiency of large pore catalysts was compared, the rp-SBA-15-Pr-SO_3H showed higher TG yield than rd-SBA-15-Pr-SO_3H and f-SBA-15-Pr-SO_3H due to higher BET surface area, internal surface area, acid amount and high thermal stability (pore wall thickness). Furthermore, fiber mesoporous catalyst (f-SBA-15-Pr-SO_3H) provided higher TG yield than rod catalyst because of higher structure crystallity (XRD result, Figure 4.8).

Table 4.6 Kinetic study using propyl sulfonic acid functionalized mesoporous silica and Amberlyst-15 in the esterification of oleic acid with glycerol at 6:1 oleic acid to glycerol mol ratio, 110^{o}C, 15 min - 24 h of reaction time and 5 % (w/w) catalyst based on total reactant weight.

Reaction time (mins)	**Catalyst**											
	No catalyst		**Rp-SBA-15-Pr-SO_3H**		**Amberlyst-15**		**F-SBA-15-Pr-SO_3H**		**Rd-SBA-15-Pr-SO_3H**		**MCM-41-Pr-SO_3H**	
	Oleic acid conversion (%)	**TG yield (%)**	**Oleic acid conversion (%)**	**TG yield (%)**	**Oleic acid conversion (%)**	**TG yield (%)**	**Oleic acid conversion (%)**	**TG yield (%)**	**Oleic acid conversion (%)**	**TG yield (%)**	**Oleic acid conversion (%)**	**TG yield (%)**
15	-	-	89.1	45.4	22.5	-	88.0	22.9	82.5	17.4	70.2	-
30	-	-	96.6	50.7	83.3	3.1	96.6	40.7	90.4	24.8	77.3	3.9
45	-	-	98.4	53.3	92.3	15.2	99.0	40.2	91.4	29.9	86.2	11.2
60	-	-	99.7	64.3	99.3	25.8	64.2	34.4	98.7	34.2	91.5	13.2
120	9.3	-	97.7	31.2	96.9	44.4	55.3	33.9	88.8	37.8	96.4	14.7
180	16.9	0.4	86.5	30.3	89.4	37.9	49.4	29.8	54.7	22.8	90.9	21.6
360	22.9	1.1	72.6	29.6	69.3	20.1	44.7	25.6	47.8	21.1	81.2	30.5
540	25.2	1.9	65.1	28.9	43.1	20.0	47.4	24.8	44.6	20.9	50.4	15.7
720	32.9	2.5	61.4	27.3	40.2	17.9	33.8	15.3	40.7	19.7	46.4	13.8
1440	72.8	14.3	60.5	27.1	31.5	11.3	27.5	10.6	36.9	18.1	40.0	11.3

4.3 Acid-activated clay catalyst

4.3.1 Characterization of catalysts

4.3.1.1 X-ray diffractometry (XRD)

From XRD patterns in Figure 4.13, the raw bentonite consisted of the montmorillonite (Mt) (d001-value = 1.29 nm) and a substantial amount of the crystalline quartz (Q), similar to that previously reported by Noyan et al. [60]. The crystallinity of montmorillonite decreased as the bentonite was activated with increasing concentrations of H_2SO_4, being essentially lost after activation with 1 and 2 M H_2SO_4. In addition, the intensity of the quartz reflection was also decreased with increasing H_2SO_4 concentrations. In contrast, the XRD pattern of TBN-0.5 still revealed the montmorillonite and quartz phases that were almost the same as in the raw bentonite, except that the lazulite (L) phase was found. The acid-activated kaolin samples (TKN-0.5 and TKS-0.5) both displayed the kaolinite (K) same as raw kaolin with small amount of montmorillonite and quartz phases.

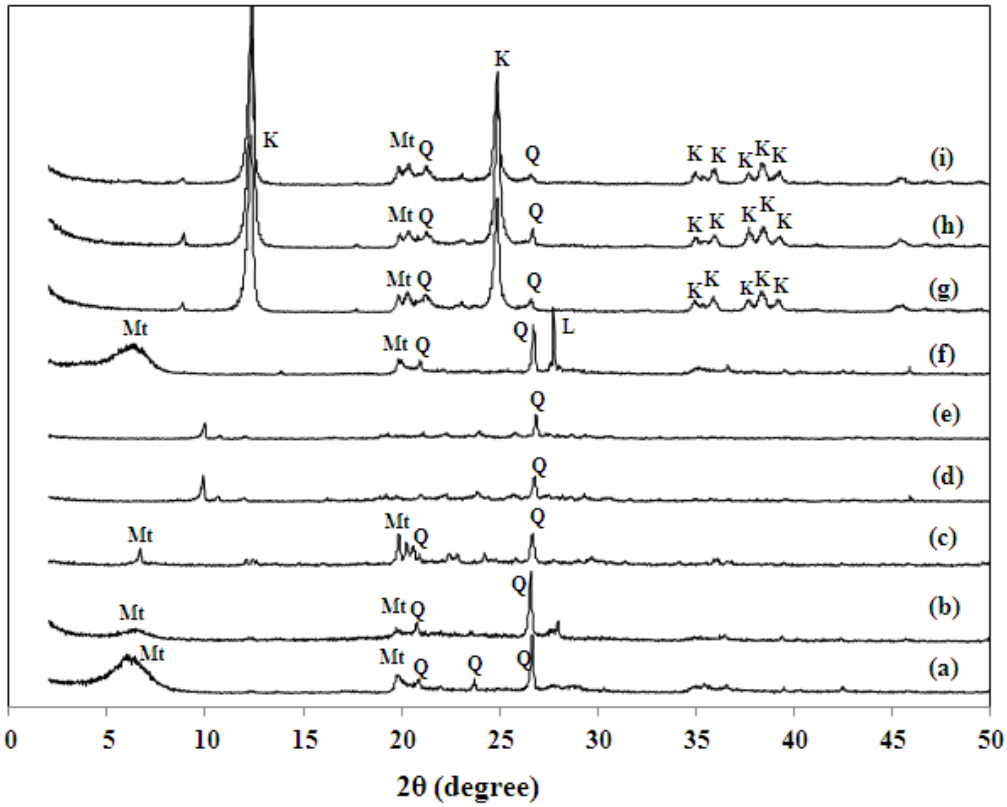

Figure 4.13 Representative XRD patterns of (a) raw bentonite, (b) TBS-0.25, (c) TBS-0.5, (d) TBS-1.0, (e) TBS-2.0, (f) TBN-0.5, (g) raw kaolin (h) TKN-0.5 and (i) TKS-0.5. Mt, Q, L and K represent montmorillonite, quartz, lazulite and kaolinite, respectively.

4.3.1.2 Chemical composition by x-ray fluorescence spectrometry (XRF)

A decrease in the R_xO_y% composition, where R was one of Na^+, K^+, Ca^{2+}, Mg^{2+}, Al^{3+} or Fe^{3+} cations, with increasing H_2SO_4 concentrations was observed (Table 4.7). However, this was not linear, but was more marked (especially for Na^+, Mg^{2+} and Al^{3+}) with the initial increase from 0 to 0.25 M H_2SO_4 than with subsequent further increases in the H_2SO_4 concentration up to 2 M. This was because as the concentration of H_2SO_4 was increased from zero to 0.25 M, the exchangeable cations between the crystal layers were replaced by protons. The K^+, Mg^{2+}, Fe^{3+} and Al^{3+} cations were more easily dissolved from the montmorillonite structure. As the

concentration of H_2SO_4 was increased as 0.25, 0.5 1.0 and 2.0 M, the decrease in amount of R_xO_y% was occurred respectively because the H^+ and SO_3^+ cations could be easily replaced in the montmorillonite structure, as suggested Salem et al. [61]. Thus, the low residual cations still remained in the montmorillonite crystal layers after acid activation. The observed increase in the -SO_3 was simply from the increasing concentration of H_2SO_4 in the activation.

Table 4.7 The chemical composition of raw bentonite and acid-activated bentonite samples

Catalyst	**Mass %**								
	SiO_2	**Al_2O_3**	**Fe_2O_3**	**TiO_2**	**MgO**	**CaO**	**Na_2O**	**K_2O**	**SO_3**
Raw bentonite	68.5	17.0	4.9	1.1	2.8	0.9	3.0	1.3	0.2
TBS-0.25	58.6	13.3	4.1	1.1	1.7	0.5	0.9	1.1	18.6
TBS-0.5	42.3	10.0	3.1	0.8	1.4	0.3	0.5	0.8	40.7
TBS-1.0	38.7	9.1	2.6	0.8	1.3	0.2	0.4	0.9	45.9
TBS-2.0	36.0	8.0	2.3	0.7	1.1	0.1	0.3	0.9	45.7

4.3.1.3 Sorption properties and acid amount analysis

The specific surface area (A) and pore volume (V) of all acid-activated bentonite samples were higher than those for the raw bentonite, but did not increase with all increasing H_2SO_4 concentrations, showing instead peak values at 0.5 M H_2SO_4, and decreasing thereafter with higher H_2SO_4 concentrations, which corresponded to the acid strength (Table 4.8). The maximum obtained value of A and V was due to the electrical layer around the particles, whereas the concentration of H_2SO_4 was increased from 0 to 0.25 M, the exchangeable Na^+, K^+ and Ca^{2+} cations at the interlayer were replaced by protons, and so the A and V values were slightly increased. Increasing the H_2SO_4 concentration from 0.25 M to 0.5 M caused the Mg^{2+}, Fe^{2+} and Al^{3+} cations to dissolve more easily from the octahedral structure and so the increase in the A and V values were larger [62]. That the A and V values then

decreased with increasing H_2SO_4 concentrations above 0.5 M was because of the decomposition of the montmorillonite structure. Thus, the concentration of used H_2SO_4 plays an important role in the activation process in order to obtain the maximum A and V values.

The acid amount of the samples was higher for all the acid activated-bentonite samples than the raw bentonite (Table 4.8), which is consistent with the previously reported increase in the IR spectrum of the O-H band at 2980.22 cm^{-1} (broad) after acid activation [62]. The acid amount of the TBS-0.5 was the highest and that it was higher than that for TBN-0.5 was due to divalent proton nature of H_2SO_4 compared to HNO_3 (1.0 vs. 0.5 M). That the acid strength of TBS-0.5 was also significantly higher than that for TKS-0.5 was because the H^+ ion could be more easily replaced in the montmorillonite layer of TBS-0.5 than in the TKS-0.5.

Table 4.8 BET surface area, total pore volume, average pore diameter and acid strength of raw bentonite, acid-activated bentonite and acid-activated kaolin samples.

Catalyst	**BET surface area (m^2/g) (A)**	**Total pore volume (cm^3/g) (V)**	**Average pore diameter (nm)**	**Acid strength (mmol/g)**
Raw bentonite	20	0.07	12	0.2
TBS-0.25	29	0.10	12	1.6
TBS-0.5	42	0.16	21	2.5
TBS-1.0	32	0.16	21	2.2
TBS-2.0	25	0.14	21	2.1
TBN-0.5	51	0.09	24	1.1
Raw kaolin	13	0.07	12	0.6
TKN-0.5	13	0.06	12	1.1
TKS-0.5	8	0.05	12	1.2
Amberlyst-15	36	0.06	2.4	3.0

4.3.1.4 Scanning electron microscopy (SEM)

SEM analysis was used to probe the change in the morphological features of raw bentonite and acid-activated bentonite samples. From SEM images in Figure 4.14, the surface morphology of the activated bentonite was clearly different to that of the raw bentonite. The corrosion of the bentonite surface by the acid activation resulted in a higher specific surface area. The TBS-0.5 sample showed the best smectite layers, in terms of having an even dense array of aggregated thin sheets, followed by the TBS-1.0 and TBS-2.0 samples, which corresponds to their high specific surface area (Table 4.8).

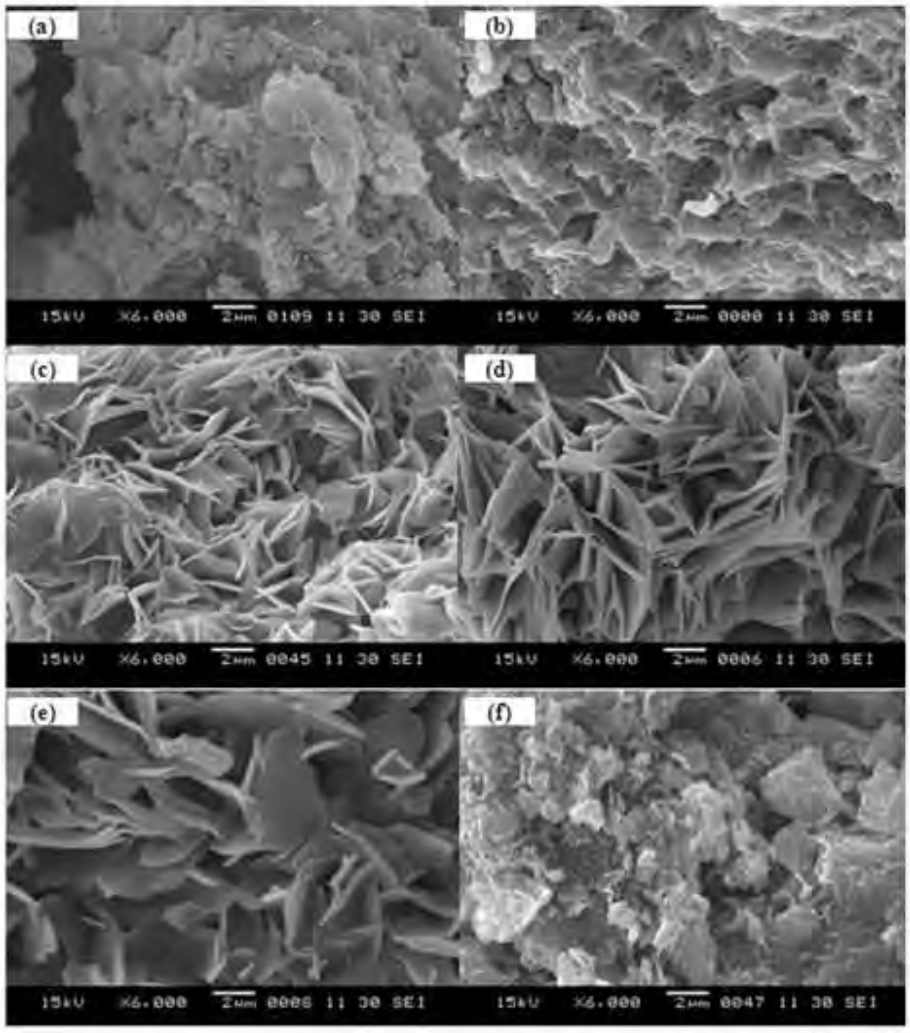

Figure 4.14 Representative SEM images of the (a) raw bentonite, (b) TBS-0.25, (c) TBS-0.5, (d) TBS-1.0, (e) TBS-2.0 and (f) TBN-0.5.

4.3.2 Catalytic activity test

4.3.2.1 Esterification of oleic acid and methanol

The catalytic activity of each of the acid-activated bentonite catalysts was far superior to the essentially ineffective raw bentonite, and so acid activation clearly increased the number of active sites of bentonite (Table 4.9). The highest methyl oleate (MO) yield was obtained using TBS-0.5, followed by TBS-1.0. That the TBS-0.5 catalyst gave the highest MO yield because it contained a higher acid strength and specific surface area than the other catalysts. The TBS-0.5 catalyst also exhibited a higher MO yield than TKN-0.5 and TKS-0.5. Furthermore, the TBS-0.5 catalyst provided the same maximal yield as the Amberlyst-15 catalyst. Therefore, the esterification reaction was further evaluated using TBS-0.5 and Amberlyst-15 as the catalysts.

Table 4.9 Catalytic activity of different clays and acid-activated clays for the esterification of oleic acid and methanol at a 9:1 methanol: oleic acid mole ratio, 60^{o}C, 3 h and 10% (w/w) catalyst.

Catalyst	**Methyl oleate yield (% wt.)**
Raw bentonite	8
TBS-0.25	85
TBS-0.5	100
TBS-1.0	96
TBS-2.0	90
TBN-0.5	80
Raw kaolin	7
TKN-0.5	80
TKS-0.5	23
Amberlyst-15	100

4.3.2.2 Esterification of high acid content oil with methanol

The catalytic activity of TBS-0.5 was equal to or higher than that for the Amberlyst-15 catalyst in all tested reactions (Figure 4.15). For the esterification of the mixed refined palm oil and oleic acid, both catalysts yielded over a 99% FFA conversion with methanol, but whilst the yield with ethanol was lower, that obtained with TBS-0.5 was slightly higher than that with the Amberlyst-15 catalyst. With respect to the esterification of Jatropha oil or waste cooking oil with methanol, the TBS-0.5 catalyst gave significantly higher % FFA conversion in both cases than Amberlyst-15 catalyst. The comparison between methanol and ethanol in the esterification of the mixed palm oil and oleic acid was performed in order to study the stearic effect of the alcohol structure. As expected and mentioned above, a higher % FFA conversion (about 12%) was obtained with methanol than with ethanol, and this is likely to be due to the sterical hindrance of ethanol that impeded or limited the access of reactants to active site [63].

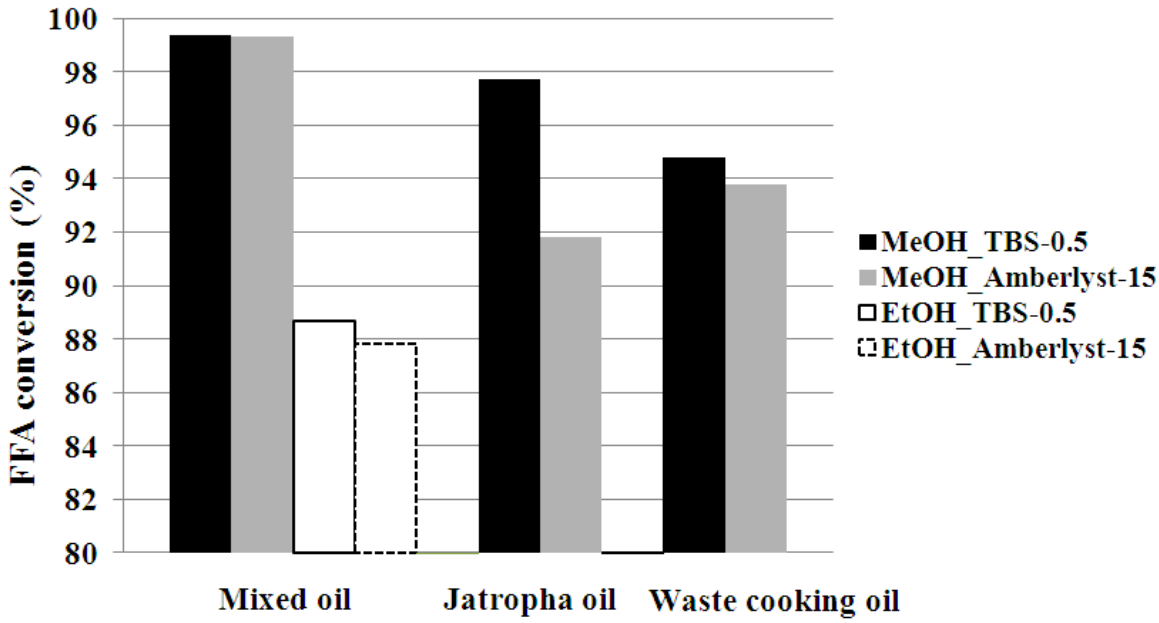

Figure 4.15 Comparison of the catalytic activity of TBS-0.5 and Amberlyst-15 in the esterification of different oils at a methanol: oil mole ratio of 23:1, in a 60^{o}C, 1 h reaction with 10% (w/w) catalyst (based on total weight of reactants).

4.3.3 Optimal reaction condition for esterification

4.3.3.1 Effect of oil to methanol molar ratio

The oil: methanol mole ratio in the esterification reaction was found to significantly affect the FFA conversion obtained in 1 h reaction (Figure 4.16). The stoichiometric mole ratio for the esterification reaction was 1:1 (methanol: FFA), but in practice an excess amount of alcohol was needed in order to shift the reaction equilibrium to the formation of the fatty acid methyl ester products. At a mole ratio of methanol: oil of 9:1, the % FFA conversion was 82%, and this was increased to 99% by increasing the mole ratio to 23:1. Increasing the methanol: oil mole ratio above 23:1 exhibited slightly decreasing the resultant % FFA conversion since the excess methanol might be reduced the catalytic efficiency of sulfonic group.

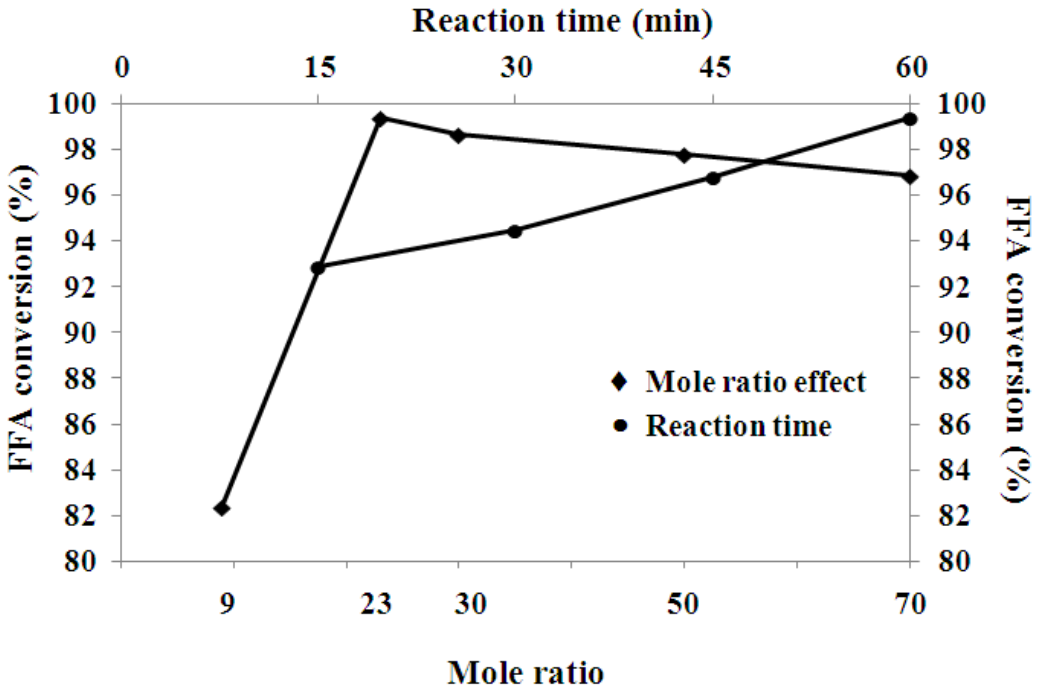

Figure 4.16 The effect of the methanol: oil mole ratio and the reaction time on the efficiency of the esterification reaction of the mixed palm oil and oleic acid with methanol at 60^{o}C and with 10 wt.% TBS-0.5 as the catalyst.

4.3.3.2 Effect of reaction time

The relationship between the obtained % FFA conversion and the reaction time was evaluated at a methanol: oil mole ratio of 23:1. The reaction time had a clearly marked effect upon the esterification efficiency (Figure 4.16), where it was clear that a reaction time of 15 to 45 min was insufficient to complete the esterification of the acidified oil at 60°C. At a reaction time of 60 min (longest tested time) the % FFA conversion reached about 99%, and so the reaction was essentially completed within 60 min.

4.3.3.3 Effect of catalytic amount

The effect of varying the amount of catalyst revealed that the reaction efficiency increased considerably with increasing amounts of catalyst (Table 4.10). However, whilst dramatic increases in the reaction efficiency were noted with increases in the catalyst level from 0.125 to 0.5% (w/w) (21 to 82% FFA conversion), further 5- or 10-fold increases in the catalyst level from 1% to 5 or 10% (w/w) resulted in a less marked increase in the yield of biodiesel. Nevertheless, to obtain the commercially desired >99% FFA conversion then a 10% (w/w) catalyst addition was required. The TBS-0.5 catalytic activity was also determined from the % FFA conversion with respect to the number of acidic sites, in terms of the turnover number (TON). Here, the highest TON at 309 was obtained with 0.25% (w/w) of TBS-0.5 catalyst (Table 4). Therefore, a small amount of catalyst exhibited the highest effectiveness of the TBS-0.5 active sites.

Table 4.10 The obtained % FFA conversion and TON using varying amounts of TBS-0.5 catalyst at a 23:1 methanol: acidified oil mole ratio, 60^{o}C and 1 h reaction time

Amount of catalyst (wt.%)	% FFA conversion	TON
0.125	21	224
0.25	57	309
0.5	82	220
1	94	126
5	96	25
10	99	13

4.4 Acid-activated pillar bentonite

4.4.1 Characterization of catalysts

4.4.1.1 X-ray diffractometry (XRD)

The pillar porous bentonite formation was illustrated in Scheme 4.1. The smectite layers were first substantially expanded by replacing the labile cations (Na^{+}, K^{+}, Mg^{2+}, Ca^{2+}) by micelles of cetyltrimethylammonium cations (CTA^{+}) surfactant with an intercalated co-surfactant, hexadecylamine (HDA). The expansion of clay sheets was best evidenced by XRD patterns featuring an important shift of the associated reflection at low 2 theta angles. In the presence of silicon precursor (TEOS), the material was a good candidate for promoting the formation of an ordered pillar silica structure together with the surfactant and co-surfactant micelle induced the mesostructural order. After the pillars were formed, the organic molecules were removed two methods, i.e. only calcination or acidic refluxing before calcination. The high porous pillar bentonite materials were obtained with their specific surface areas higher than parent bentonite as shown in Table 4.11.

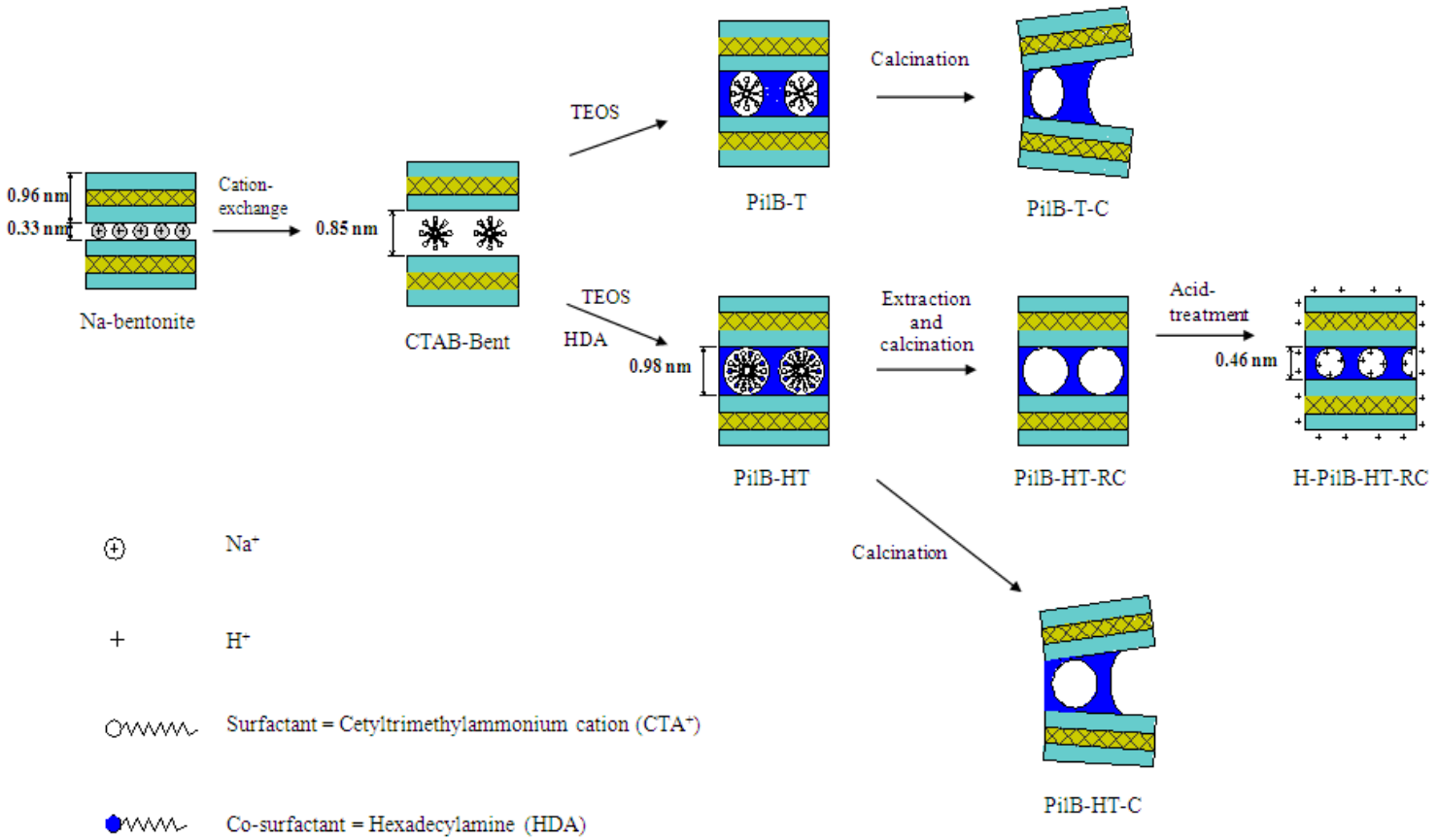

Scheme 4.1 The mechanism of formation of the silica pillar bentonites with the CTAB surfactant alone (PilB-T and PilB-T-C), or also with the co-surfactant HDA (PilB-HT, PilB-HT-C and PilB-HT-RC), and the H_2SO_4-activated pillar bentonite (H-PilB-HT-RC).

The four pillar bentonite samples were characterized their structure by XRD as shown in Figure 4.17. For Na-bentonite, the 001 reflection ascribed to the ordering of clay layers, present at the position of 6.8^{o} related to the basal spacing of 1.29 nm and two dimentional diffractions *h k* were found at 19.9^{o} and 35.1^{o} [64]. Moreover, the reflection at 2 theta of 19.7^{o} corresponded to diffraction from (100) layers of montmorillonite (Mt) and the reflection at 27^{o} ascribed to the presence of quartz (Q) impurity were detected [64]. The basal spacing of the layer clay minerals depended on the thickness of the smectite layer and interlayer space. The thickness of the smectite layers was estimated to be around 0.96 nm [65]. Thus, the interlayer space was about 0.33 nm in case of hydrated bentonite clay [66]. The deposition of surfactant and co-surfactant as well as the formation of the silica pillars in the interlayer space of montmorillonite resulted in a shift of the d_{001} peak in direction of the lower value of 2 theta angle. This effect could relate to an increase of the interlayer distance in the clay materials. For the CTAB-Bent containing the intercalation surfactant micelle in the interlayer space of montmorillonite resulted in an expanding of its spacing from 0.33 to 0.85 nm. For the PilB-T-C and PilB-HT-C samples, which surfactants were removed by calcination only, the montmorillonite plane at low 2 theta peak was disappeared due to the partial delamination of the pillar structure. However, the silica pillar sample (PilB-HT-RC) that surfactant was removed by acidic reflux with ethanol prior calcination, the montmorillonite characteristic peak were retained. Therefore, acid wash and calcination were dual selected steps to remove surfactant and co-surfactant due to sustainable Mt structure. In additional, the interlayer space of PilB-HT-RC matter was further expanded from 0.85 to 0.98 nm by effect of added HDA co-surfactant due to the increasing of critical micelle concentration (CMC). However, H-PilB-HT-RC sample, which was treated with sulfuric acid solution in order to rising acidic property, the montmorillonite characteristic peak was clearly attained and the interlayer space was decreased.

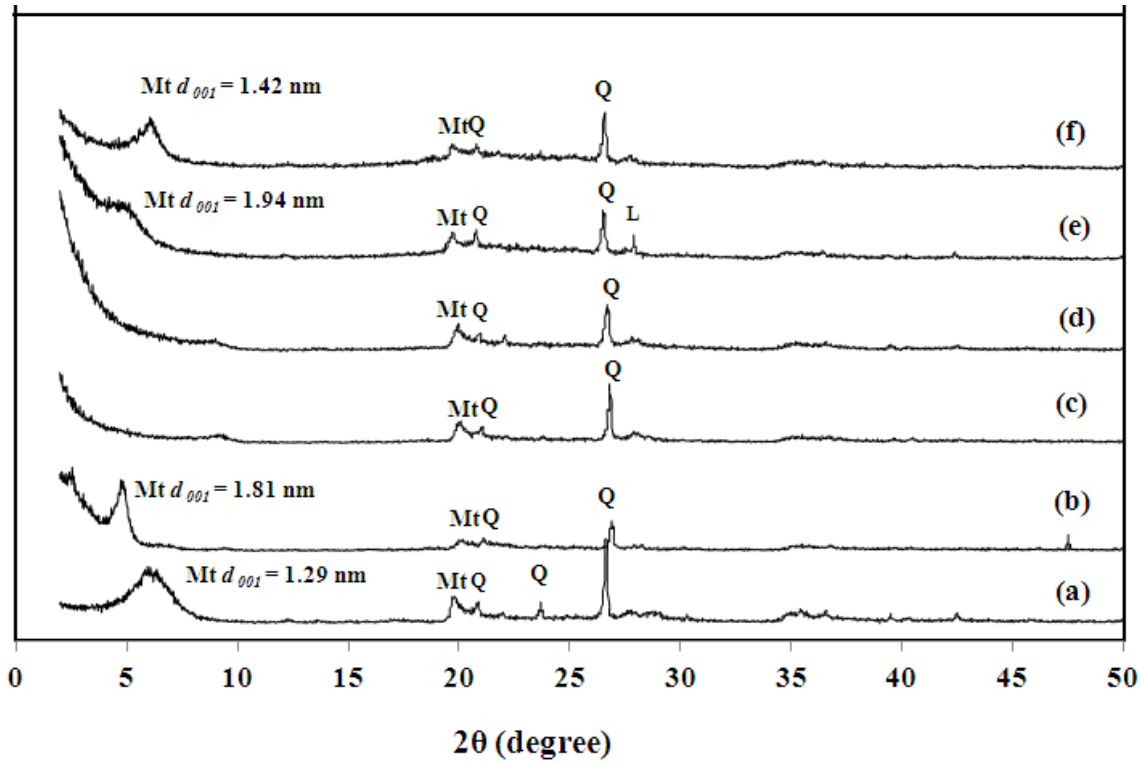

Figure 4.17 Representative XRD patterns of the (a) raw Na-bentonite, the (b) CTAB-Bent, the as-prepared pillar bentonites (c) PilB-T-C, (d) PilB-HT-C and (e) PilB-HT-RC and (f) the H_2SO_4-activated pillar bentonite H-PilB-HT-RC. Mt, Q and L represent montmorillonite, quartz and lazulite, respectively.

4.4.1.2 Sorption properties and acid amount analysis

The specific surface area (A) and pore volume (V) of samples were obtained from standard Brunauer, Emmett and Teller (BET) method and BJH equation, respectively. The A, V and pore diameter of pillar bentonite and acid-treated pillar bentonite samples were higher than raw bentonite as shown in Table 4.11. That was claimed about the pillar bentonite preparation was successfully and significantly increased the parent specific surface area. The highest values of specific surface area (A), pore volume (V) and pore diameter were found in PilB-HT-RC sample, while acid-treated pillar bentonite sample (H-PilB-HT-RC) resulted in smaller of A, V and pore diameter values. That might be result from acid corroded some part of pillar

bentonite structures that brought to the shrinkage of interlayer. However, the acid treatment was very important in order to increase acidity of pillar material.

The acid amount values of all related samples were shown in Table 4.11, non-acidified pillar samples (PilB-T, PilB-HT and PilB-HT-RC) exhibited acid amount lower than raw bentonite due to deprotonation of acidic working site. After acid treatment, the acid amount of H-PilB-HT-RC was raised close to twenty times from 0.1 to 1.96 mmol/g.

Table 4.11 BET surface area, total pore volume, average pore diameter and acid amount of the raw Na-bentonite, pillar bentonites and H_2SO_4-activated pillar bentonite.

Catalyst	**BET surface area (m^2/g) (A)**	**Total pore volume (cm^3/g) (V)**	**Average pore diameter (nm)**	**Acid amount (mmol/g)**
Raw bentonite	20	0.07	1.2	0.20
PilB-T-C	290	0.52	2.4	0.09
PilB-HT-C	335	0.71	2.4	0.08
PilB-HT-RC	412	0.80	2.6	0.10
H-PilB-HT-RC	212	0.59	2.4	1.96
Used H-PilB-HT-RC	67	0.31	1.5	1.24
Amberlyst-15	37	0.06	2.4	3.00

N_2 adsorption/desorption isotherms of the raw bentonite, pillar bentonite and acid-treated pillar bentonite samples were shown in Figure 18. All the adsorption isotherms were exhibited type II, characteristic of non-porous materials. However, the hysteresis loops of all samples, associated with capillary condensation, were presented type IV mesopores indicated the existing of silicon oxide pillar structure and smectite

layers [66]. The large amount of hysteresis loop in PilB-T, PilB-HT, PilB-HT-RC and H-PilB-HT-RC samples could refer to the increasing number of mesopore and larger pore diameter in the samples. Nevertheless, the used H-PilB-HT-RC catalyst exhibited smaller pore volume than others, which corresponding to their total specific surface area and pore diameter.

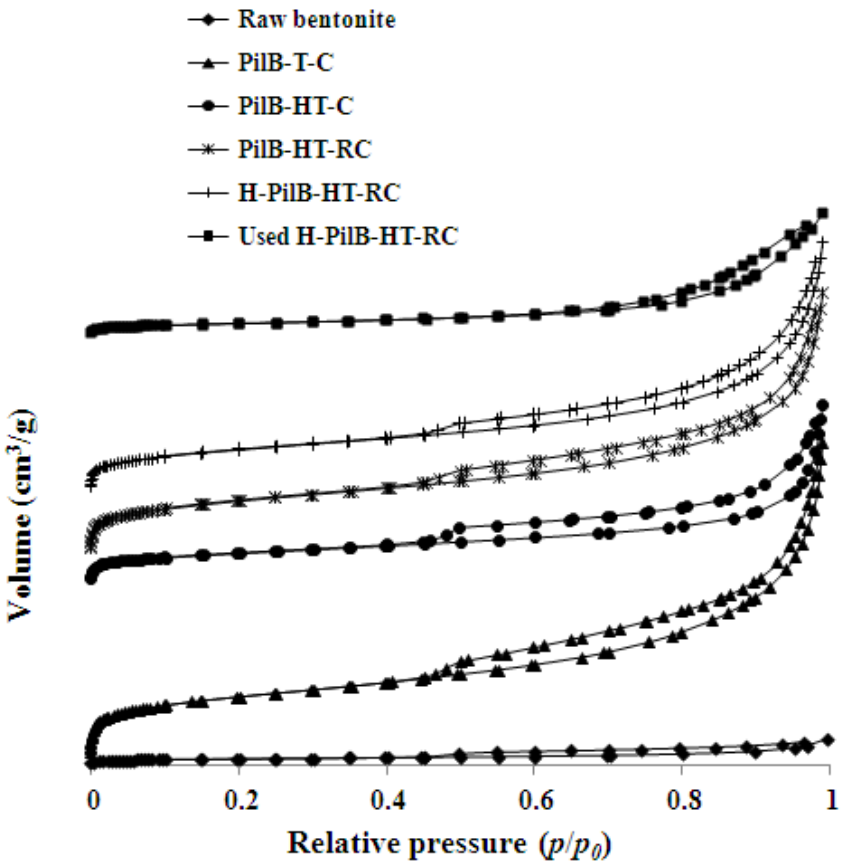

Figure 4.18 Representative N_2 adsorption/desorption isotherms of the raw Na-bentonite, the as-prepared pillar bentonites (PilB-T-C, PilB-HT-C and PilB-HT-RC) and the as-prepared and used H_2SO_4-activated pillar bentonite (H-PilB-HT-RC).

4.4.1.3 Scanning electron microscopy (SEM)

SEM analysis was used to probe the change in the morphological features of raw bentonite, pillar bentonite (PilB-HT-RC) and acid-treated pillar bentonite (H-PilB-HT-RC) samples. From SEM micrographs in Figure 4.19 (a), the raw bentonite exhibited large aggregated of platelets. The surface morphology of the PilB-HT-RC sample in Figure 4.19 (b) was slightly different from the raw bentonite. Intercalation of the silica pillar into the interlayer space of the clay could combine the thin sheets at surface to the unique morphology, which corresponded to its high specific surface area. The acid-treated sample in Figure 4.19 (c) showed the similar surface morphology close to the pillar one.

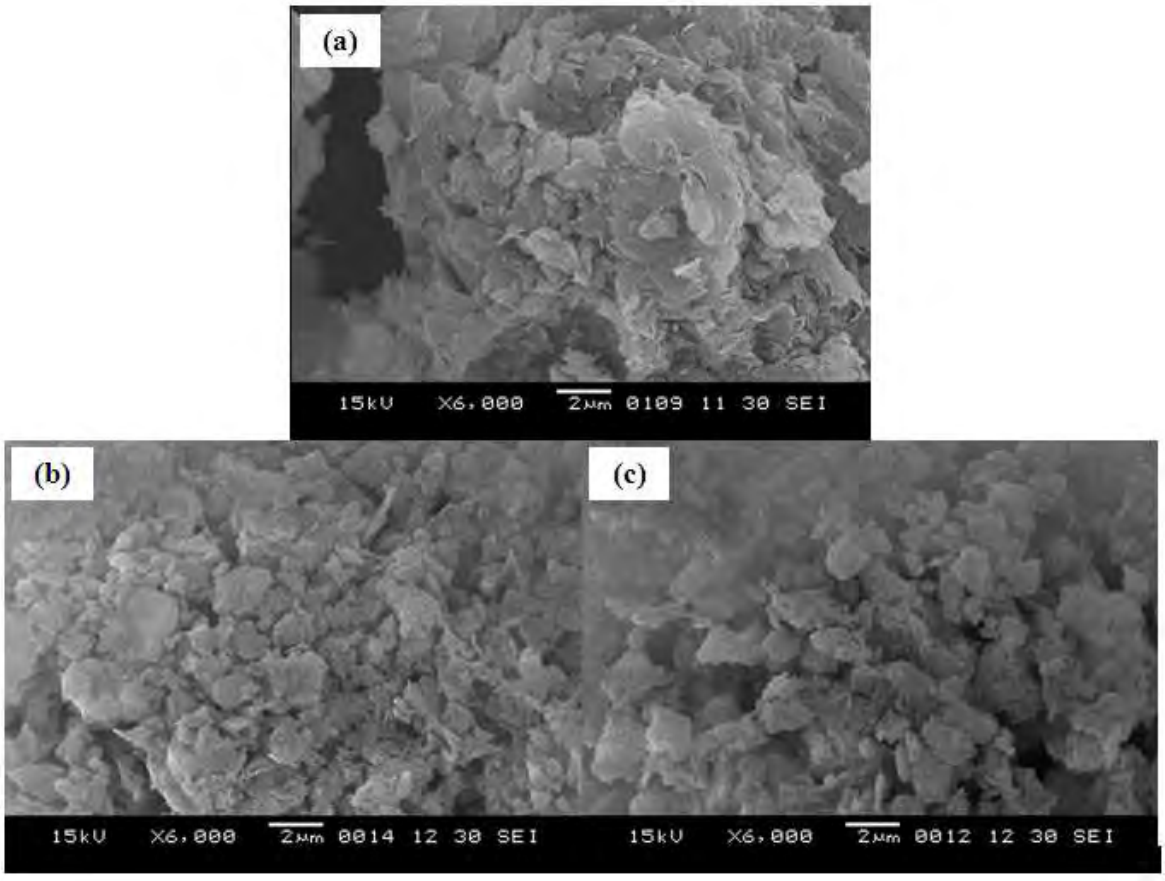

Figure 4.19 Representative SEM images (6,000 × magnification) of the (a) raw Na-bentonite and the as-prepared (b) PilB-HT-RC pillar bentonite and (c) its H_2SO_4-activated counterpart (H-PilB-HT-RC).

4.4.2 Catalytic activity test

4.4.2.1 Esterification of oleic acid and methanol

The esterification of oleic acid and methanol was carried out over different catalysts and the results were shown in Figure 4.20. The results showed that the raw bentonite catalyst gave methyl oleate yield nearly blank test (no catalyst). When compared catalytic activity between raw bentonite and pillar bentonite catalysts (PilB-T-C, PilB-HT-C and PilB-HT-RC), the methyl oleate (MO) yield of all pillar bentonite was higher than raw bentonite about two to four times. Whilst, PilB-HT-RC catalyst that surfactant was removed by acid wash and calcination exhibited 43.5 mol% of MO yield higher than another surfactant removable method. This is because PilB-HT-RC sample contained highest specific surface area and largest pore diameter. However, the MO yield was further increased by acid treatment. The H-PilB-HT-RC catalyst showed the superior MO yield high as 100 mol%. Furthermore, the acid treated pillar clay catalyst provided the same catalytic activity to the commercial Amberlyst-15.

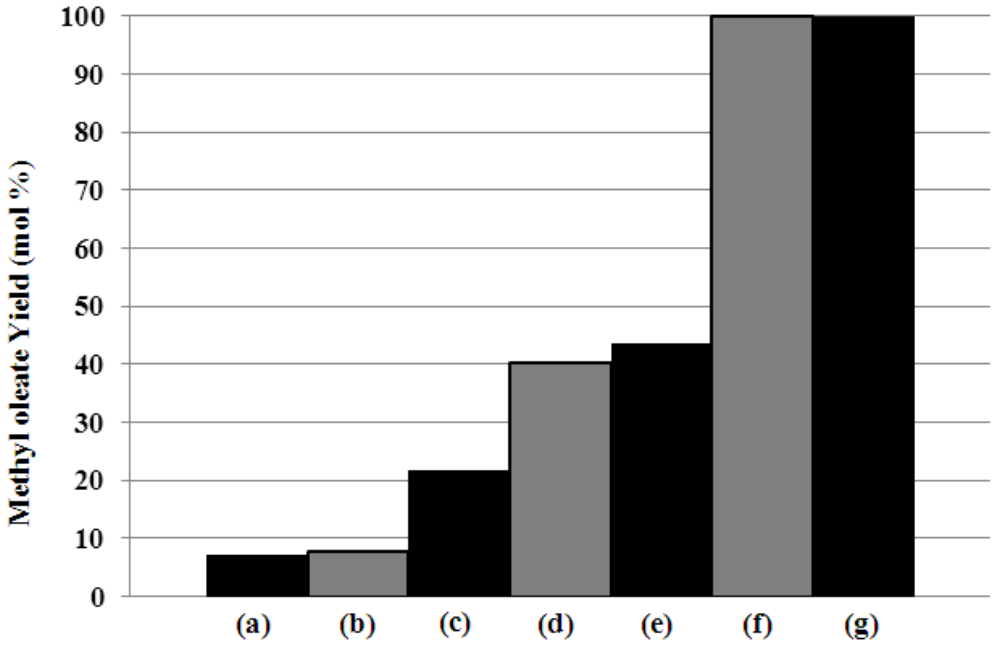

Figure 4.20 Catalytic activity of the different pillar bentonites and the H_2SO_4-activated pillar bentonite, compared to the commercial Amberlyst-15 catalyst, for the esterification of a 1:9 molar ratio of oleic acid: methanol at 60^{o}C for 3 h with 10 wt.% of catalyst. Shown is the data for (a) no catalyst, (b) raw bentonite, the pillar bentonites (c) PilB-T-C, (d) PilB-HT-C, (e) PilB-HT-RC, (f) the H_2SO_4-activated pillar bentonite H-PilB-HT-RC and (g) Amberlyst-15.

4.4.2.2 Esterification of high acid content palm oil and methanol

The catalytic activity of different catalysts were also test in esterification of high acid content palm oil and methanol in term of oleic free fatty acid (FFA) conversion and the results were shown in Figure 4.21. From the results, catalytic activity trend of all catalysts exhibited FFA conversion similar to previous test in esterification of oleic acid with methanol. The H-PilB-HT-RC catalyst revealed highest FFA conversion as 99.7 mol%, which provided the same maximal FFA conversion as the commercial catalyst. Furthermore, FFA conversion of two reused catalysts was also studied. The used H-PilB-HT-RC and Amberlyst-15 catalysts were filtered from the reaction mixture and then soaked in acetone for 10 minute to remove

the esters present on the surface. At the final step, the catalyst was dried overnight at 100^{o}C and reused for esterification of high acid content palm oil with methanol. The FFA conversions of two reused catalysts were decreased when compared with the fresh ones. The loss of activity could explain by acid leaching out after first run. The acid amount of used pillar clay that was decreased around 35 % as shown in Table I. Moreover, reused H-PilB-HT-RC catalyst exhibited high tolerant than reused Amberlyst-15.

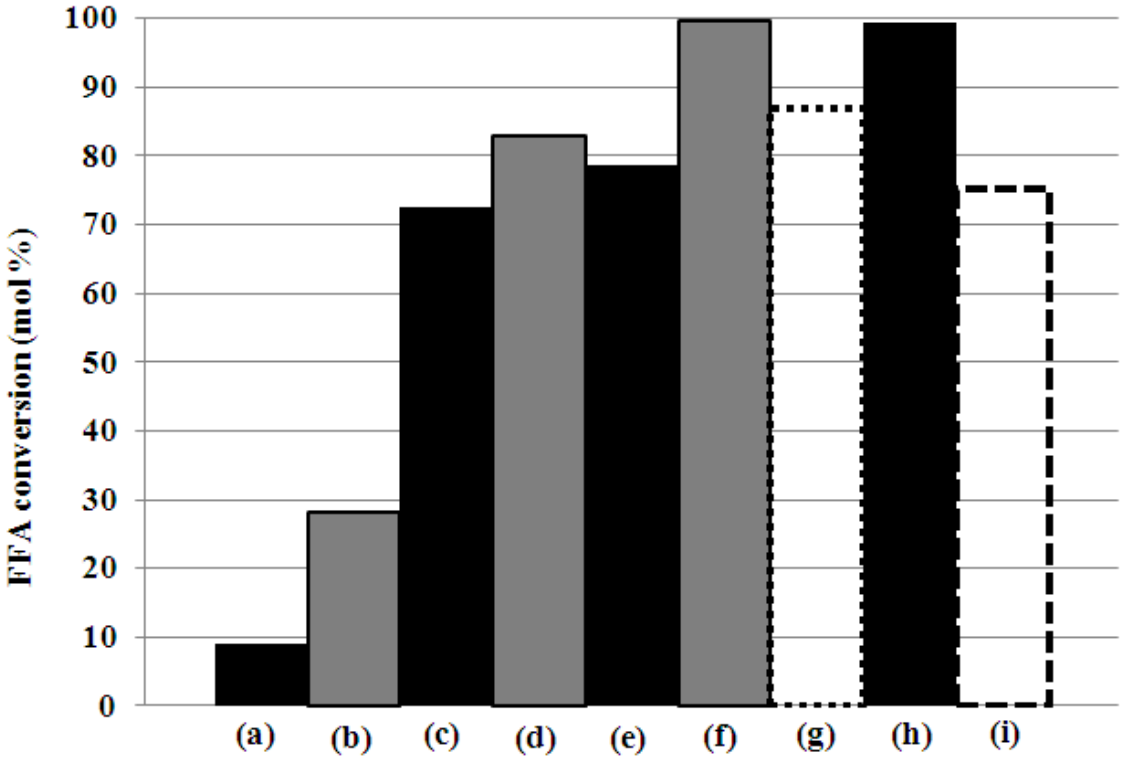

Figure 4.21 Catalytic activity of the different bentolite catalysts, compared to the commercial Amberlyst-15 catalyst, for the esterification of a 1: 23 molar ratio of high acid RPO: methanol at 60^{o}C for 1 h with 10 wt.% catalyst. Shown is the data for (a) no catalyst, (b) raw Na-bentonite, the as-prepared pillar bentonites (c) PilB-T-C, (d) PilB-HT-C and (e) PilB-HT-RC, (f) the H_2SO_4-activated pillar bentonite (H-PilB-HT-RC) as-prepared, and (g) reused H-PilB-HT-RC, (h) the as-bought commercial Amberlyst-15 and (i) the reused Amberlyst-15.

4.4.2.2.1 Effect of catalyst amount

The effect of H-PilB-HT-RC loading on esterification of high acid content palm oil with methanol was studied as shown in Figure 4.22. The rising in catalytic loading from 1.0 to 5.0 wt.% showed an increase of the FFA conversion from 88 to 98 mol%. These results could be attributed to an increase in the number of catalytic active sites [31, 32]. However, the conversion was further increased to 99 mol% FFA conversion when push up the catalytic amount to 10.0 wt.%. Therefore, the suitable catalyst loading in this esterification was 10.0 wt.% based on total reactants weight.

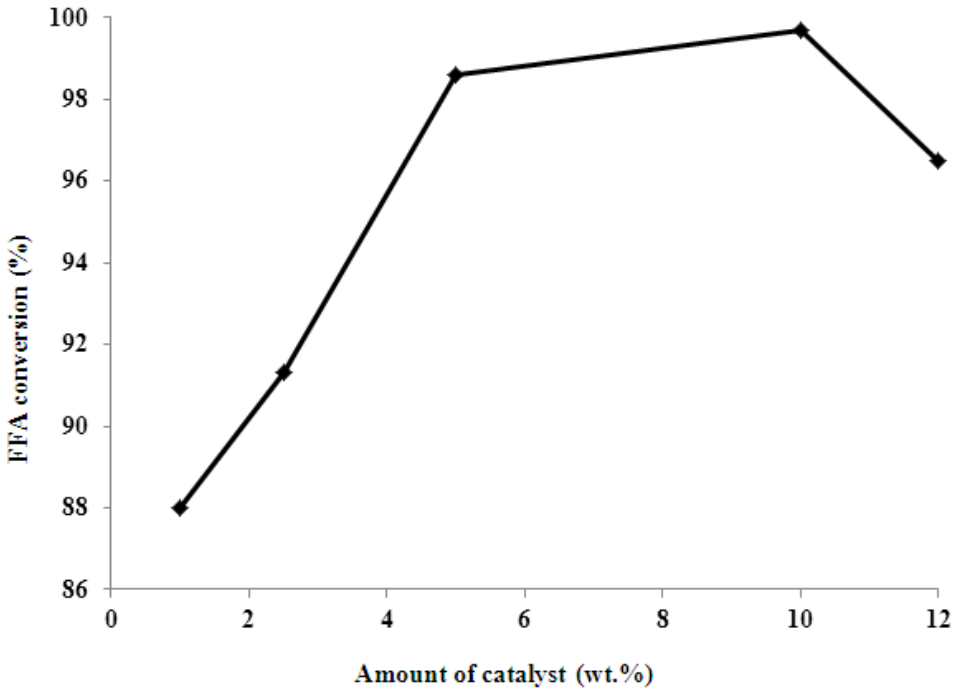

Figure 4.22 The FFA conversion level (mol %) obtained with varying amounts of the H_2SO_4-activated pillar bentonite H-PilB-HT-RC catalyst of a 1:23 mole ratio of acidified RPO: methanol at 60^{o}C for 1 h.

4.5 The optimal esterification condition study over (p) rp-SBA-15-Pr-SO_3H, TBS-0.5 and Amberlyst-15 catalysts

4.5.1 Effect of methanol to oleic mole ratio

The esterification reaction was performed at constant temperature, 60^oC, for 1 h over 5-10 wt% of post synthesized (p) rp-SBA-15-Pr-SO_3H, TBS-0.5 and Amberlyst-15 catalysts based on reactant weight. The mixed oil (acidified RPO) of refined palm oil and 15 wt.% oleic acid was used as starting oil in esterification. The mole ratio of methanol to acidified RPO oil was varied from 9:1 to 70:1. The corresponding plot of FFA conversion versus methanol to oil mole ratio was shown in Figure 4.23. The stoichiometric mole ratio requires one mole of methanol and a mole of oleic acid and three moles of methanol to a mole of triglyceride that included in palm oil. However, in real practice the excess amount of alcohol was needed in order to shift the equilibrium to the right-hand side to produce more methyl ester product. From results, the methanol to oil mole ratio was increased from 9:1 to 23:1, resulting to the FFA conversion considerably increased. Beyond the molar ratio of 23:1, the excessively added methanol had decreasing FFA conversion, due to the difficulty of methoxide nucleophile to react with carboxyl group. When conversion of 10 wt.% of three catalysts ((p) rp-SBA-15-Pr-SO_3H, TBS-0.5 and Amberlyst-15) was compared, it was found that the (p) rp-SBA-15-Pr-SO_3H catalyst exhibited highest FFA conversion at all mole ratios. Furthermore, (p) rp-SBA-15-Pr-SO_3H and TBS-0.5 provided higher FFA conversion than commercial Amberlyst-15 at the same catalyst amount used. A 10 wt.% amount of TBS-0.5 catalyst gave higher FFA conversion than 5 wt.% amount catalyst at all methanol to oil mole ratios due to higher active site. From the experimental results in all catalysts, methanol to oil ratio of 23:1 was the most appropriate one to give the highest FFA conversion around 99%.

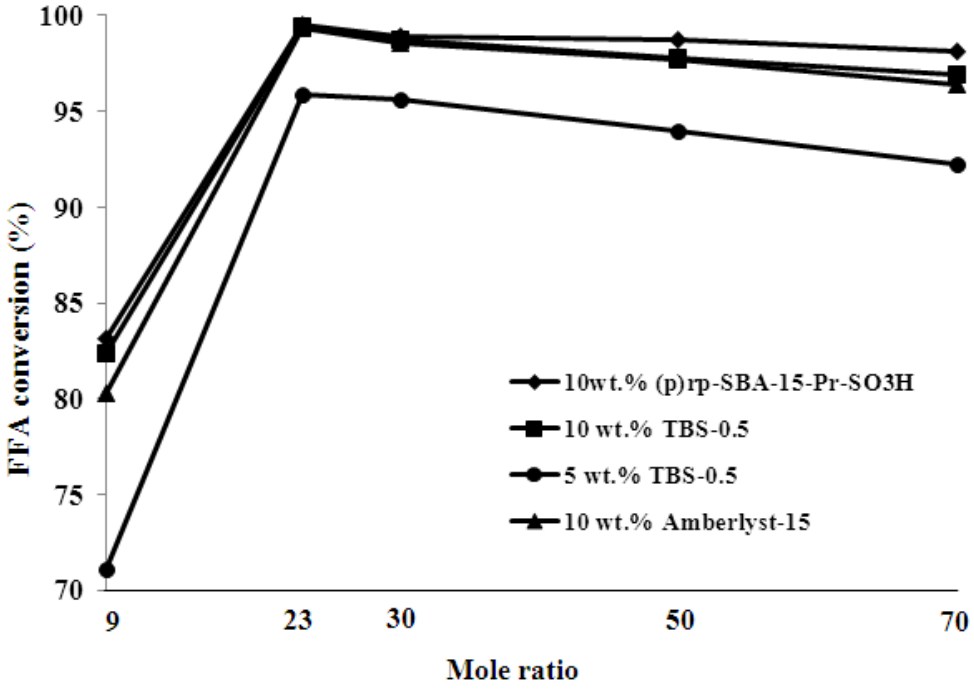

Figure 4.23 The FFA conversion level obtained with varying mole ratio of methanol to acidified RPO oil using the (p) rp-SBA-15-Pr-SO_3H, TBS-0.5 and Amberlyst-15 catalysts at 60^{o}C for 1 h.

4.5.2 Effect of catalytic amount

The optimizing catalyst amount based on limiting reactant was studied. The esterification condition was methanol to acidified RPO oil mole ratio of 23:1, 60^{o}C for 1 h. The effect of the catalyst amount over the FFA conversion was presented in Figure 4.24. The catalytic activities of catalyst at various catalyst amounts of 0.5, 1.0, 2.5, 5.0, 7.5 and 10 wt% in the esterification could be observed the FFA conversion which increased by rising the catalyst amount. This result is expected because of catalyst loading increment was proportional to availability of active sites. From results, it was observed that the catalyst amount between 0.5 to 1.0 wt.% provided highest reaction rate. Furthermore, (p) rp-SBA-15-Pr-SO_3H and TBS-0.5 catalysts showed higher FFA conversion than commercial Amberlyst-15 at small catalyst amount. The catalyst amount of 10 wt.% exhibited highest FFA conversion of 99% at all of catalyst. According to the FFA conversion, 10 wt% of the catalytic amount to reactant mixture was chosen for further study.

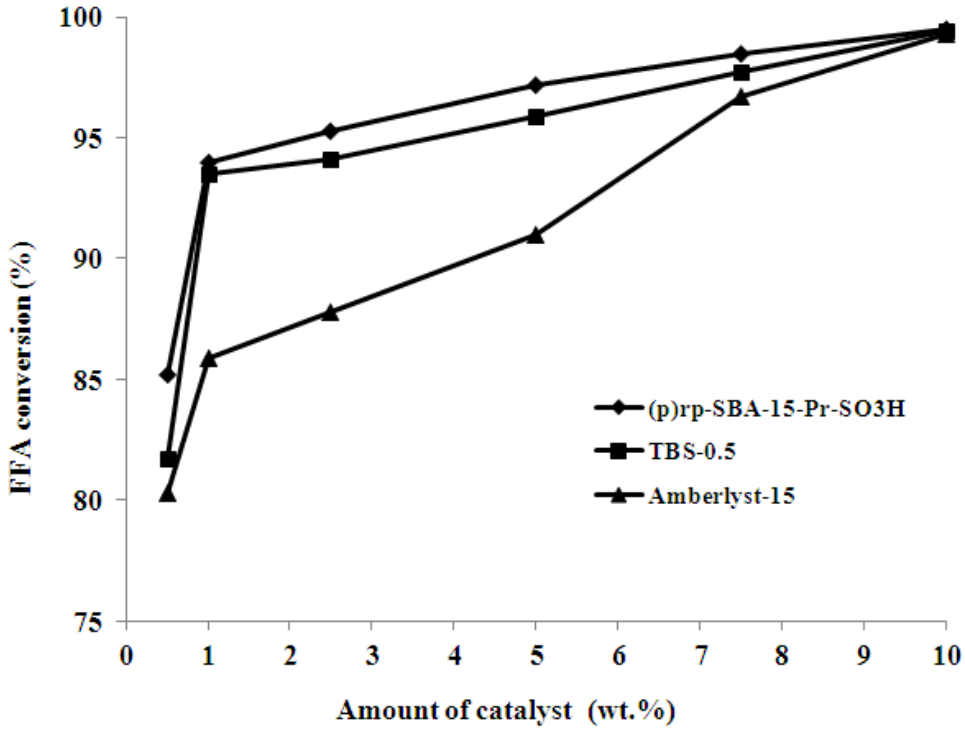

Figure 4.24 The FFA conversion level obtained with varying amounts of (p) rp-SBA-15-Pr-SO_3H, TBS-0.5 and Amberlyst-15 catalyst of a 23:1 mole ratio of methanol : acidified RPO at 60^{o}C for 1 h.

4.5.3 Effect of reaction time

The kinetic rate in esterification was investigated using post synthesized (p) rp-SBA-15-Pr-SO_3H, TBS-0.5 and Amberlyst-15 catalysts. Two types of starting oil, which were acidified RPO oil and Jatropha oil, were used to study effect of amount of FFA content in oil to conversion. The acidified RPO oil contained of only 15 wt.% oleic free fatty acid whereas Jatropha oil included of 32 wt.% FFA. The esterification condition was 23:1 methanol to oil mole ration, 60oC and 10 wt.% amount of catalyst. The reaction time was varied in range of 15-90 mins.

4.5.3.1 Esterification of acidified RPO oil

The catalytic activities of post synthesized (p) rp-SBA-15-Pr-SO_3H, TBS-0.5 and Amberlyst-15 catalysts were presented in Figure 4.25. The reaction time was varied in the range of 15-60 mins. As a result, the FFA conversion was increased when the reaction time was raised. At the reaction time of 60 min, all of catalysts could reach high FFA conversion to 99.5% indicating the reaction was complete within 60 mins. However, (p) rp-SBA-15-Pr-SO_3H and TBS-0.5 catalysts showed higher initial reaction rate than Amberlyst-15. The (p) rp-SBA-15-Pr-SO_3H catalyst exhibited highest FFA conversion at all reaction time. Therefore, the optimum reaction time of all catalysts was 60 min for esterification of acidified RPO oil and methanol.

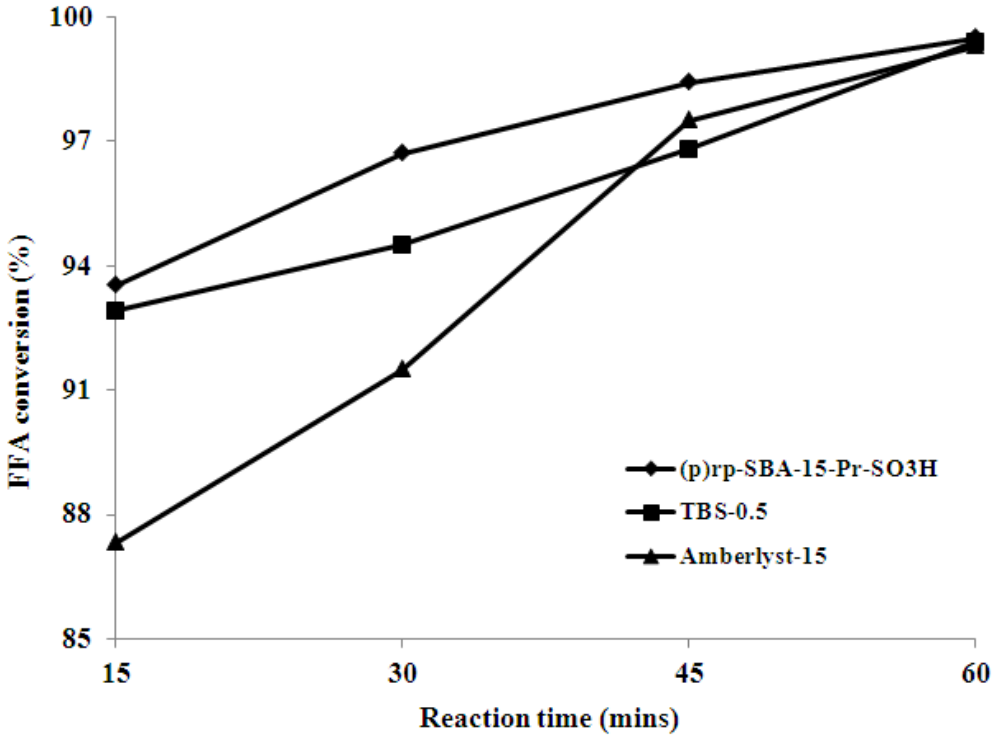

Figure 4.25 The effect of reaction time on the efficiency of the esterification reaction of the acidified RPO oil with methanol at 60^{o}C and with 10 wt.% (p) rp-SBA-15-Pr-SO_3H, TBS-0.5 and Amberlyst-15 as the catalyst.

4.5.3.2 Esterification of Jatropha oil

The catalytic activities of post synthesized (p) rp-SBA-15-Pr-SO_3H, TBS-0.5 and Amberlyst-15 catalysts in the esterification of Jatropa oil at reaction temperature 60^oC with different reaction time are shown in Figure 4.26. The reaction time was studied in the range of 15-90 mins. From the results, the FFA conversion was raised by increasing in reaction time. At the reaction time of 90 min, all of catalysts gave high FFA conversion 96-99% indicating the reaction was complete within 90 mins. The reaction time in esterification of Jatropha oil was higher than esterification of acidified RPO oil because Jatropha oil contained higher FFA content. However, (p) rp-SBA-15-Pr-SO_3H catalyst provided higher initial reaction rate than other at 15-30 mins. Therefore, the optimum reaction time in esterification of Jatropha oil was 60 min.

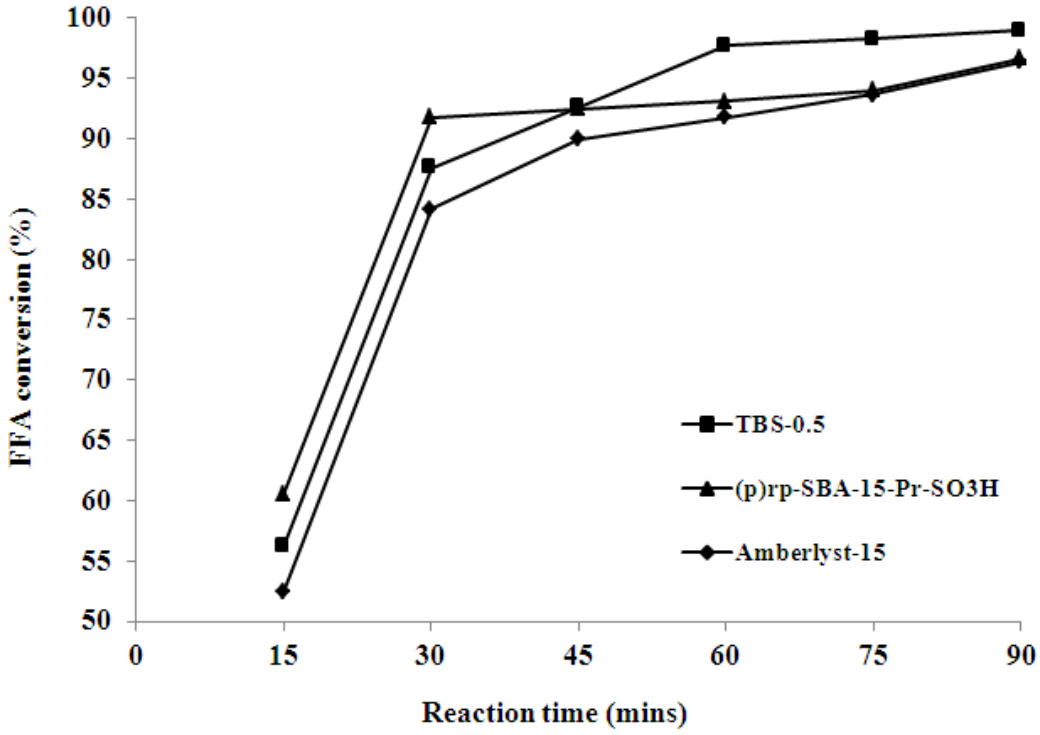

Figure 4.26 The effect of reaction time on the efficiency of the esterification reaction of the Jatropha oil with methanol at 60^oC and with 10 wt.% (p) rp-SBA-15-Pr-SO_3H, TBS-0.5 and Amberlyst-15 as the catalyst.

4.6 Catalytic activity of reused and regenerated post synthesized (p) Rp-SBA-15-Pr-SO_3H, TBS-0.5 and Amberlyst-15 catalysts

One of the main advantages of using heterogeneous catalysts is the ease of separation and reusability in the successive catalytic cycles. From all studies, it was found that (p) rp-SBA-15-Pr-SO_3H, acid-activated bentonite (TBS-0.5) and Amberlyst-15 catalysts provided a good catalytic activity in esterification of FFA and high acid content oil. Therefore, these catalysts were chosen to study reuse and regeneration in esterification of acidified RPO oil (refined palm oil mixed with 15 wt.% oleic acid) and methanol.

For reuse catalyst, the used catalysts that were catalyzed in esterification were tested for their activity again without any treatment except washing with acetone and dry in air at 60-100^oC for 24 h before reuse in next batch reaction. For regeneration of (p) rp-SBA-15-Pr-SO_3H, the used catalyst was washed with acetone, dried at 60^oC for 24 h and incorporated with propyl sulfonic acid group by using post synthesis grafting method, which was described in topic 3.3.2.2. For regeneration of acid-treated clay, the used catalyst was washed with acetone, dried at 100^oC for 24 h and acid activated by 0.5 M H_2SO_4 aqueous solution that was described in topic 3.3.3.

4.6.1 Physical and chemical properties study

4.6.1.1 X-Ray diffractometry (XRD)

The XRD patterns of 1st, 2nd, 3rd, 4th and 5th used post synthesized (p) rp-SBA-15-Pr-SO_3H catalysts were showed in Figure 4.27. As a result, all materials still exhibited three characteristic peaks of hexagonal phase similar to the fresh catalyst. The characteristic peaks were slightly shifted to higher 2 theta values, indicating the presence of bulky reactant and products on the surface and in the pore of catalyst would decrease void volume, then *d*-spacing was decreased. Moreover, the crystal structure was decreased after each reaction run because the reactants and product could be adsorbed on surface and in pore of catalyst although washing with acetone in several times. Furthermore, some characteristic properties of reused post synthesized (p) rp-SBA-15-Pr-SO_3H were exhibited in topic 4.1.1-4.1.4.

For regeneration of post synthesized (p) rp-SBA-15-Pr-SO_3H, the some physical and chemical characterizations were described and were showed in topic 4.1.1-4.1.4.

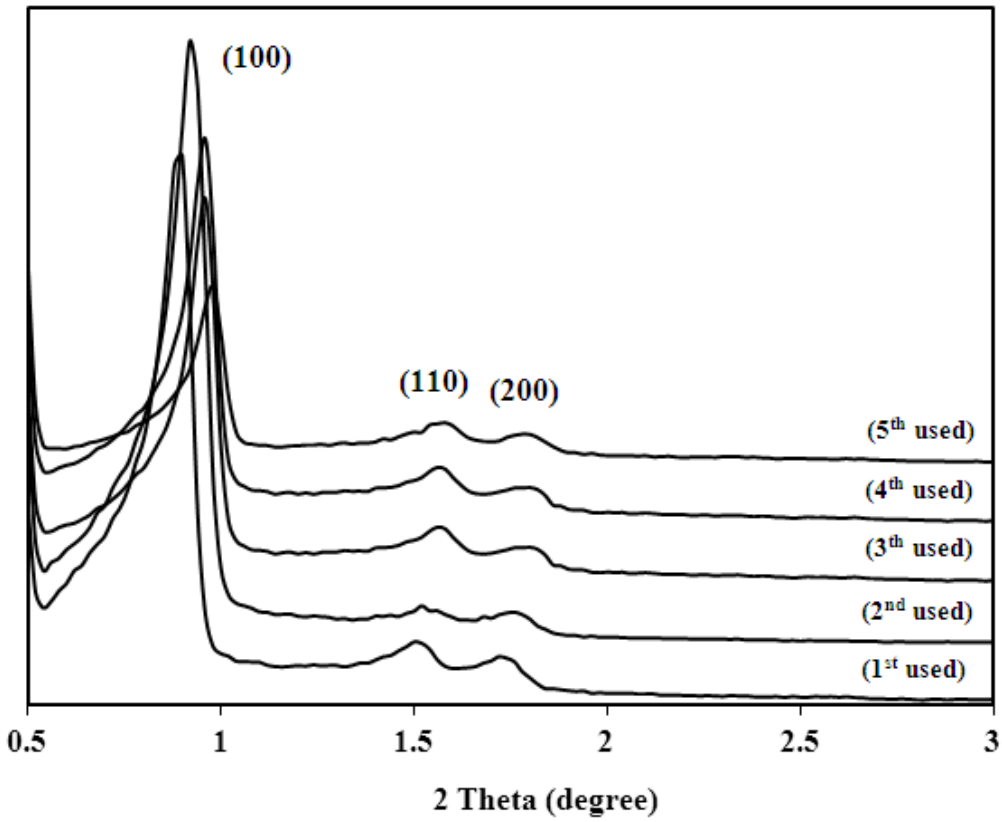

Figure 4.27 Representative XRD patterns of reused post synthesized (p) Rp-SBA-15-Pr-SO_3H catalysts.

The XRD patterns of 1st, 2nd, 3rd, 4th and 5th used acid-activated bentonite (TBS-0.5) catalysts were illustrated in Figure 4.28. The all samples still provide characteristic peaks that consisted of montmorillonite and crystalline quartz similar to fresh one. In addition, the intensity of the quartz reflection was also increasing with increasing reaction run.

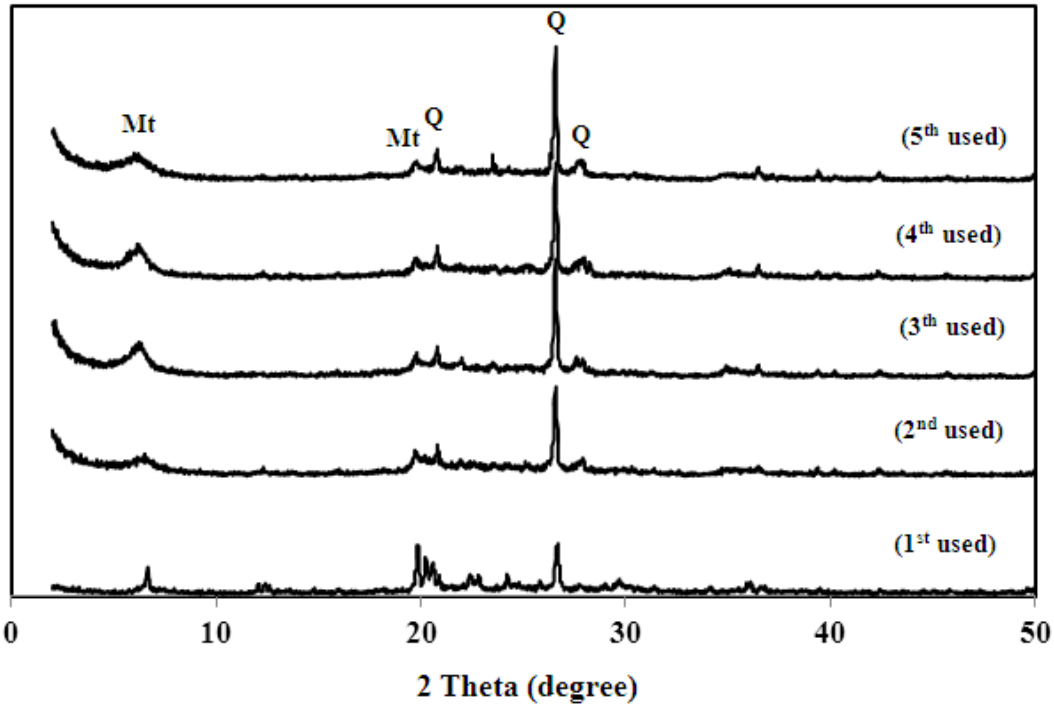

Figure 4.28 Representative XRD patterns of reused acid-activated bentonite (TBS-0.5) catalysts.

4.6.2 Catalytic activity test of reused and regenerated post synthesized (p) rp-SBA-15-Pr-SO_3H, TBS-0.5 and Amberlyst-15 catalysts

The catalytic activities test of fresh and reused (p) rp-SBA-15-Pr-SO_3H, TBS-0.5 and Amberlyst-15 catalysts in the esterification of acidified RPO oil were shown in Table 4.12 and Figure 4.29. The esterification condition was 23:1 methanol to acidified RPO oil, 60^{o}C for 1 h and 10 wt.% catalyst amount. The catalytic activities of all catalysts were continually decreased after each esterification run. The loss in activities of catalyst might be from the deactivation of catalytic active site. The (p) rp-SBA-15-Pr-SO_3H catalyst showed less catalytic activity loss than TBS-0.5 and commercial Amberlyst-15 catalysts. All catalyst provided a significant drop in activity from 99% FFA conversion of fresh to 51-56 % FFA conversion of 5th used catalysts under the same operational condition.

However, the used catalyst was developed in order to improve its performance. After 3rd used, catalysts were regenerated that was previously described.

The catalytic activities of regenerated (p) rp-SBA-15-Pr-SO_3H and TBS-0.5 catalysts were presented in Figure 4.30. The FFA conversion was improved from 78% to 98% for regenerated (p) rp-SBA-15-Pr-SO_3H catalyst, nearly the fresh one. Furthermore, the FFA conversion of regenerated TBS-0.5 was increased from 71% to 98%, nearly the fresh one. Therefore, the (p) rp-SBA-15-Pr-SO_3H and acid-activated bentonite (TBS-0.5) catalysts could be regenerated successfully.

Table 4.12 Catalytic activities of reused catalyst in esterification of acidified RPO oil and methanol

Catalyst	**FFA conversion (%)**
1^{st} used (p) rp-SBA-15-Pr-SO_3H	99.5
1^{st} used treated bentonite	99.4
1^{st} used Amberlyst-15	99.3
2^{nd} used (p) rp-SBA-15-Pr-SO_3H	88.9
2^{nd} used treated bentonite	82.8
2^{nd} used Amberlyst-15	75.2
3^{rd} used (p) rp-SBA-15-Pr-SO_3H	78.0
3^{rd} used treated bentonite	71.0
3^{rd} used Amberlyst-15	66.2
4^{th} used (p) rp-SBA-15-Pr-SO_3H	66.9
4^{th} used treated bentonite	63.4
4^{th} used Amberlyst-15	61.4
5^{th} used (p) rp-SBA-15-Pr-SO_3H	56.5
5^{th} used treated bentonite	55.1
5^{th} used Amberlyst-15	51.0

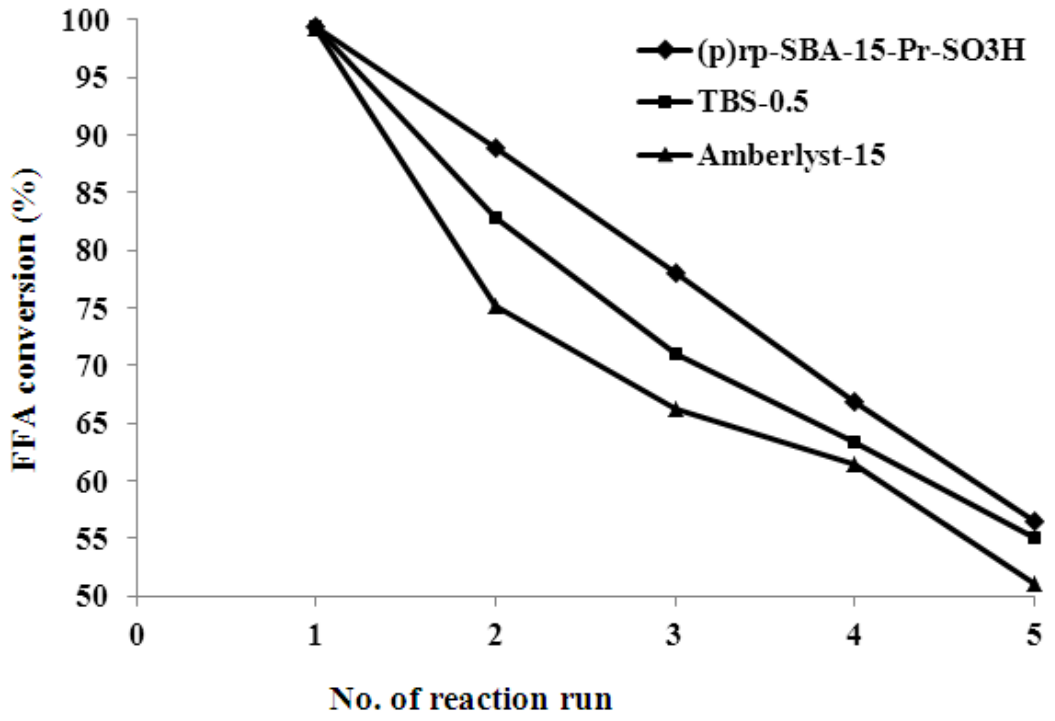

Figure 4.29 Representative catalytic activities of reused catalyst in esterification of acidified RPO oil and methanol at 23:1 methanol to oil mole ratio, 60^{o}C for 1 h and 10 wt.% catalyst amount.

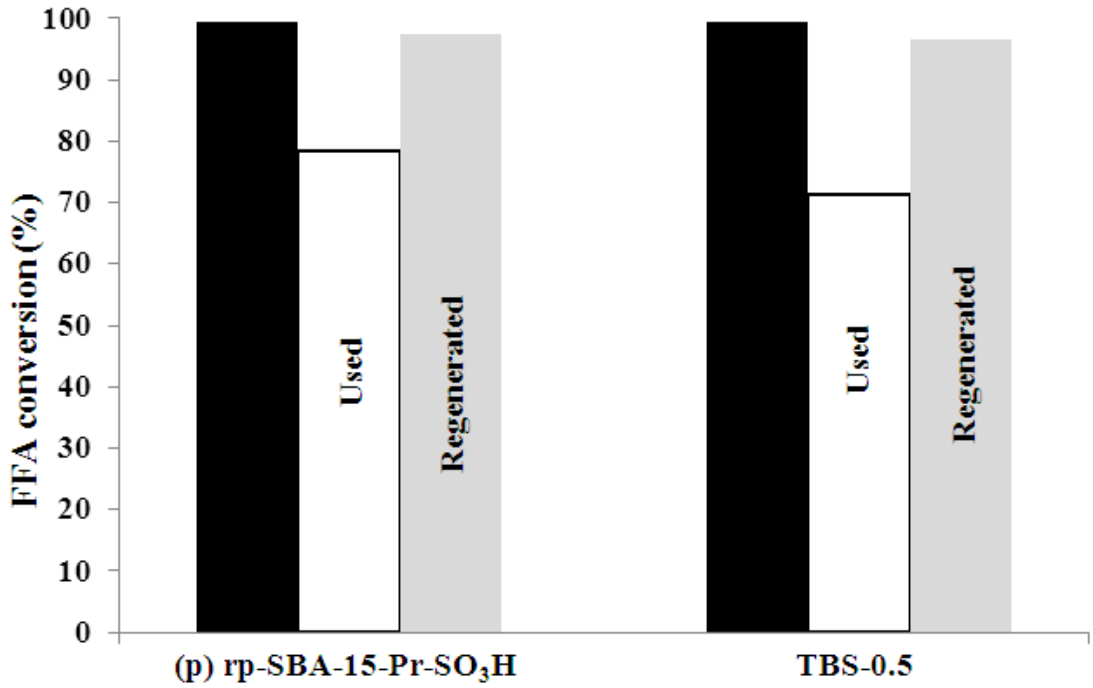

Figure 4.30 Representative catalytic activities of regenerated catalyst in esterification of acidified RPO oil and methanol at 23:1 methanol to oil mole ratio, 60^{o}C for 1 h and 10 wt.% catalyst amount.

CHAPTER V

CONCLUSIONS

Propyl sulfonic acid functionalized mesoporous silica materials, (d) SBA-15-Pr-SO_3H and (p) SBA-15-Pr-SO_3H, were synthesized using direct synthesis method and post synthesis grafting method, respectively. The SBA-15 material, which was prepared by using no additional organic co-solvent, showed rope-like structure. From catalytic activity results in esterification, the propyl sulfonic functionalized mesoporous silica, which was synthesized from post synthesis grafting method, exhibited higher catalytic activity than direct synthesis method. This (p) SBA-15-Pr-SO_3H catalyst exhibited 100% methyl palmitate and methyl oleate yields under reaction condition of 9:1 methanol to FFA mole ratio, 60^oC, for 3-6 h and 10 wt.% amount of catalyst. The (p) SBA-15-Pr-SO_3H catalyst showed higher catalytic activity than commercial Amberlyst-15 in the same esterification condition. Moreover, (p) SBA-15-Pr-SO_3H could be regenerated, whereas reusability of Amberlyst-15 was limited. The catalytic activity of the regenerated (p) SBA-15-Pr-SO_3H catalyst exhibited no significant difference in the product yield when compared to the fresh one.

In addition, the rope-like mesoporous SBA-15 was synthesized by non-additional heptane co-solvent whereas rod and fiber-like SBA-15 materials were prepared by using heptane to pluronic P123 template molar ratio as 350 and 412, respectively. The heptane co-solvent helped increasing in swelling template micelle resulting in larger pore diameter of porous matter. Furthermore, MCM-41, which was synthesized by using hexadecylamine (HDA) template, showed smaller pore diameter than rope, rod and fiber SBA-15 samples because HDA exhibited lower swelling micelle than pluronic P123. The rod and fiber-like SBA-15 parent matters showed a larger pore diameter (12 nm) than rope-like SBA-15 (9 nm) and MCM-41 (2.4 nm). The physical and chemical properties of mesoporous silica materials were modified

using organo-sulfonic acid group functionalized by post-synthesis grafting method. The behaviors of methanol or glycerol with oleic acid in esterification using propyl sulfonic functionalized mesoporous silica catalysts were successfully determined. The rp-SBA-15-Pr-SO_3H catalyst exhibited the higher catalytic activity than rd-SBA-15-Pr-SO_3H, f-SBA-15-Pr-SO_3H and MCM-41-Pr-SO_3H catalysts not only in oleic acid and methanol esterification but also in oleic acid and large structural alcohol as glycerol esterification. Moreover, rp-SBA-15-Pr-SO_3H catalyst also showed a greater efficiency than the Amberlyst-15 catalyst.

Furthermore, other interesting heterogeneous catalysts were found. The one of heterogeneous catalyst was bentonite and kaolin that are natural clay. The acid activation method was used to modify physical and chemical properties of clay. The acid-activated bentonite catalyst preparation was successful and significantly increasing the acidity of the starting bentonite material. The results of catalytic tests indicated the importance of acid activation given the derivatized catalyst was high effective in the esterification reaction of oleic free fatty acid with methanol and esterification of high acid content palm oil with methanol or ethanol. The optimal condition in esterification was methanol to oil mole ratio of 23:1, reaction temperature 60^{o}C, reaction time for 1 h and catalytic amount of 10 wt.%.

Moreover, the bentonite was also modified to be a pillar for increasing in specific surface area and then H_2SO_4-activated for rising acidity. The pillar bentonite has been synthesized by surfactant and co-surfactant directed assembly of silica between interlayer of montmorillonite. In the last step of synthesis, the surfactants were removed by reflux with ethanol and calcination, respectively. The refluxed and calcined materials contained higher specific surface area, pore volume and pore diameter than the parent. The acid-activated pillar bentonite sample found to be significantly more active in oleic acid esterification than non-acid activation bentonites due to an increase in the number of catalytic sites. Additionally, the acid-activated pillar bentonite catalyst was proved to be higher deactivated tolerance in term of catalytic stability and reusability than commercial acid-exchange resin catalyst.

The suggestion for future work

1. Modify mesoporous silica material by incorporation of other organo-sulfonic acid such as polystyrene sulfonic acid to improve the acidity and water tolerance of catalyst.

2. Modify removal template method that is milder way in order to achieve larger pore diameter mesoporous material.

3. Find the other clays in Thailand such as sepiolite and illite that can be used as catalyst.

REFERENCES

[1] Schuchardt, U., Sercheli, R., Vargas, R. M. Transesterification of vegetable oils: A review. *J. Braz. Chem. Soc*. 9(1998) : 199.

[2] Michael, S. G., McCormick, R. L. Combustion of fat and vegetable oil derived fuels in diesel engines. *Prog. Energy Combust. Sci*. 24(1998) : 125.

[3] Ma, F., Hanna, M. A. Biodiesel production: A review. *Biores. Tech.* 70(1999) : 1.

[4] Barnwal, B. K., Sharma, M. P. Prospects of biodiesel production from vegetable oils in India. *Renew. Sustain. E. Rev*. 9(2005) : 363.

[5] Michael, S. G., McCormick, R. L. Combustion of fat and vegetable oil derived fuels in diesel engines. *Prog. Energy Combust. Sci*. 28(1998) : 125.

[6] Naik, S. N., Meher, L. C., Vidya Sagar, D. Technical aspects of biodiesel production by transesterification: a review. *Renew. Sustain. E. Rev.* 10(2004) : 1.

[7] Pintoa, A. C., Guarieiroa, L. L. N., Rezendea, M. J. C., Ribeiroa, N. M., Torresb, E. A., Lopesc, W. A., Pereirac, P. A. P., Andrade, J. B. Biodiesel: An Overview. *J. Braz. Chem. Soc.* 16(2005) ; 131.

[8] Dorado, M. P., Ballesteros, E., Arnal, J. M., Gomez, J., Lopez, F. J. Exhaust emissions from a diesel engine fuelled with transesterified waste olive oil. *Fuel* 82(2003) : 1311.

[9] Krawczyk, T. Biodiesel-alternative fuel makes inroads but hurdles remain. INFORM 7(1996) : 801.

[10] Labeckas, G., Slavinskas, S. The effect of rapeseed oil methyl ester on direct injection diesel engine performance and exhaust emissions. *Energy Convers Manage.* 47(2006) : 1954.

[11] Srivastava, A., Prasad, R. Triglycerides based diesel fuels. *Renew Sustain Energy Rev.* 4(2000) : 111.

[12] Ulusoy, Y., Tekin, Y., Cetinkaya, M., Karaosmanoglu, F. The engine tests of biodiesel from used frying oil. *Energy Sources* 26(2004) ; 927.

[13] Royon, D., Daz, M., Ellenrieder, G., Locatelli. Enzymatic production of biodiesel from cotton seed oil using *t*-butanol as a solvent. *Biores. Tech.* 28(2006) : 648.

[14] Yadav, G. D., Lathi, P. S. Lipase catalyzed transesterification of methyl acetoacetate with *n*-butanol. *Mol. Cat. B* 32(2005) : 107.

[15] Aracil, J., Vicente, G., Martinez, M. Integrated biodiesel production: a comparison of different homogeneous catalysts systems. *Biores. Tech.* 92 (2004) : 297.

[16] Basu, H. N., Norris, M. E. US patent 5,525,126, 1996.

[17] Koono, S., Moriya, O., Noguchi, T., Okamura, H. EP patent 566,047, 1993.

[18] Zhao, D., Feng, J., Huo, Q., Melosh, N., Fredrickson, G. H., Chmelka, F. B., Stucky, G. D. Triblock copolymer syntheses of mesoporous silica with periodic 50 to 300 angstrom pores. *Science* 279(1998) : 548.

[19] Mbaraka, I. K., Radu, D. R., Lin, V. S., Shanks, B. H. Organosulfonic acid-functionalized mesoporous silicas for the esterification of fatty acid. *Catal*. 219(2003) : 329.

[20] Mbaraka, I. K., Shanks, B. H. Design of multifunctionalized mesoporous silicas for esterification of fatty acid. *Catal*. 229(2005) : 365.

[21] Hart, M. P., Brown, D. R. Surface acidities and catalytic activities of acid-activated clays. *Mol. Catal., A* Chem. 212(2004) : 315.

[22] Murray, H. H. Traditional and new applications for kaolin, smectite, and palygorskite: a general overview. *Appl. Clay Sci*. 17(2000) : 207.

[23] Breen, C., Watson, R. Acid-activated organoclays: preparation, characterisation and catalytic activity of polycation-treated bentonites. *Appl. Clay Sci*. 12(1998) : 479.

[24] Grim, R. E., Clay Mineralogy, McGraw-Hill, New York, 1968.

[25] Komadel, P., Schmidt, D., Madejova, J., Cicel, B. Alteration of smectites by treatments with hydrochloric acid and sodium carbonate solutions. *Appl. Clay Sci*. 5(1990) : 113.

[26] Zhaohua, L., Hartmann, M., Zhao, D., Zhou, D., Kevan, L. Alumination and ion exchange of mesoporous SBA-15 molecular sieve. *Chem. Mater.* 11(1999) : 1621.

[27] Melero, J. A., Margolese, D., Christiansen, S. C., Chemelka, B. F., Stucky, G. D. Direct syntheses of ordered SBA-15 mesoporous silica containing sulfonic acid groups. *Chem. Matter.* 12(2000) : 2448.

[28] Melero, J. A., Stucky, G. D., Grieken, R. V., Morales, G. Direct syntheses of ordered SBA-15 mesoporous materials containing arenesulfonic acid groups. *Matter. Chem.* 12(2002) : 1664.

[29] Luo, Y. J., Yang, L. M., Wang, G. S., Dal, Y. Y. Functionalization of SBA-15 mesoporous silica with thiol or sulfonic acid groups under the crystallization conditions. *Micropor. Mesopor. Mat.* 84(2005) : 275.

[30] Cheng, S., Chen, C., Jang, L. Dual-functionalized large pore mesoporous silica as an efficient catalyst for bisphenol-A synthesis. *Micropor. Mesopor. Mat.* 109(2008) : 258.

[31] Kureshy, R. I., Ahmad, I., Pathak, K., Khan, N. H., Abdi, S. H. R., Jasra, R. V. Sulfonic acid functionalized mesoporous SBA-15 as an efficient and recyclable catalyst for the synthesis of chromenes from chromanols. *Catal. Comm*. 10(2009) : 572.

[32] Galarneau, A., Barodawalla, A., Pinnavaia, T. J. Study of the surface charge of a porous clay heterostructure (PCH) and its adsorption capacity of alkaline metals. Nature 374(1995) : 529-531.

[33] Nascimento, L. A. S., Angelica, R. S., Costa, C. E. F., Zamian, J. R., Filho, G. N. Comparative study between catalysts for esterification prepared from kaolins. *Appl. Clay Sci*. 51(2011) : 267.

[34] Moraes, D. S., Angélica, R. S., Costa, C. E. F., Filho G. N. R., Zamian, J. R. Bentonite functionalized with propyl sulfonic acid groups used as catalyst in esterification reactions. *Appl. Clay Sci*. 51(2011) : 209.

[35] Juan, J. C., Zhang, J., Yarmo, M. A. Structure and reactivity of silica-supported zirconium sulfate for esterification of fatty acid under solvent-free condition. *Appl. Catal. A* 287(2005) : 209.

[36] Ni, J., Meunier, F. C. Esterification of free fatty acids in sunflower oil over solid acid catalysts using batch and fixed bed-reactors. *Appl. Catal. A* 333(2007) : 122.

[37] Marchetti, J. M., Miguel, V. U., Errazu, A. F. Heterogeneous esterification of oil with high amount of free fatty acids. *Fuel* 86(2007) : 906.

[38] Morales, G., Grieken, R., Martin, A., Martinez, F. Sulfonated polystyrene-modified mesoporous organosilicas for acid-catalyzed processes. *Chem. Eng*. 161(2010) 388.

[39] Melero, J. A., Bautista, L. F., Morales, G., Iglesias, J., Sanchez-Vazquez, R. Biodiesel production from crude palm oil using sulfonic acid-modified mesostructured catalysts, *Chem. Eng. J.* 161(2010) : 323.

[40] BOND, G. C. Heterogeneous Catalysis: Principles and Applications, Clarendon, Oxford, 1974.

[41] Lepage, J. F., Cosyns, J., Courty, P. Applied Heterogeneous catalysis: Design Manufacture and Use of solid catalysts, Technip, Paris, 1987.

[42] Analysis software user's manual, BELSORP, BEL JAPAN, INC, 57.

[43] Grim, R.E., Guven, N., Bentonites, Geology, Mineralogy, Properties and Uses, Development in Sedimentology, vol. 24, Elsevier, Amsterdam, 1978.

[44] Soler-Illia, G. J. A. A., Sanchez, C., Lebeau, B., Patarin, J. Chemical strategies to design textured materials: from microporous and mesoporous oxides to nanonetworks and hierarchical structures. *Chem. Rev.* 102(2002) : 4093.

[45] Ying, J. Y., Mehnert, C. P., Wong, M. S. Synthesis and applications of supramolecular-templated mesoporous materials. *Angew. Chem. Int. Ed.* 38(1999) : 56.

[46] Melosh, N.A., Lipic, P., Bates, F.A., Stucky, G.D. Molecular and mesoscopic structure of transparent block copolymer silica monoliths. *Macromolecules* 32(1999) : 4332.

[47] Soler-Illia, G. J. A. A., Crepaldi, E. L., Grosso, D., Sanchez, C. Block copolymer-templated mesoporous oxides. *Curr. Opin. Colloid Interface Sci.* 8(2003) : 109.

[48] Beck, J. S., Leonowicz, M. E., Roth, W. J., Vartuli, J. C., Kresge, C. T. A new family of mesoporous molecular sieves prepared with liquid crystal templates. *Am. Chem. Soc.,* 114(1992) : 10834.

[49] Nesaretnam, K.; Muhammad, B.; Chong, C. L.; Tan, Y. A. Selected readings on palm oil and its uses, Kuala Lumpur, Palm Oil Research Institute of Malaysia, 1994.

[50] Available from: Wikipedia, the free encyclopedia, http://en.wikipedia.org/wiki/Fatty_acid

[51] Song, C., Hsu, C. S., Mochida, I. Chemistry of Diesel Fuels, New York, Taylor & Francis, 2000.

[52] Naik, S. N., Meher, L. C., Vidya Sagar, D. Technical aspects of biodiesel production by transesterification: a review. *Renew. Sustain. E. Rev.* 10(2004) : 1.

[53] Robson, H. Verified synthesis of zeolitic materials, 2nd Edition, Elsevier Science, Amsterdam, 2001.

[54] Johansson, E. M., Córdoba, J. M., Odén, M. Synthesis and characterization of large mesoporous silica SBA-15 sheets with ordered accessible 18 nm pores. *Mater. Lett.* 63(2009) : 2129.

[55] Johansson, E. M., Córdoba, J. M., Odén, M. The effects on pore size and particle morphology of heptane additions to the synthesis of mesoporous silica SBA-15. *Micropor. Mesopor. Mater*. 133(2010) : 66.

[56] Tuel, A., Gontier, S. Synthesis and characterization of a hexagonal mesoporous silica with enhanced thermal and hydrothermal stabilities. *Chem. Mater*. 8 (1996) : 114.

[57] Raju, B. D., Reddy, S. S., Kumar, V.S., Padmasri, A. H., Narayanan, S., Rao, K. S. R. Sulfonic acid functionalized mesoporous SBA-15 for selective synthesis of 4-phenyl-1,3-dioxane. *Catal. Commun*. 8(2007) : 261.

[58] Pangma, W. *Preparation of tungstic oxide supported on SBA-15 for metathesis of 1-hexene*, Master's Thesis, Program of Petrochemistry and Polymer Science, Fauclty of Science, Chulalongkorn University, 2003.

[59] Fan, J., Lei, J., Wang, L., Yu, C., Bo, T., Zhao, D. Controlled Fabrication and Application of Platelet SBA-15 Materials. *Chem. Commun*. 24(2003) 2140.

[60] Noyan H., Onal, M., Sarikaya, Y. The effect of sulphuric acid activation on the crystallinity, surface area, porosity, surface acidity, and bleaching power of a bentonite. *Food Chem.* 105(2007) : 156.

[61] Salem, A., Karimi, L. Physico-chemical variation in bentonite by sulfuric acid activation. *Chem. Eng*. 26(2009) : 980.

[62] Xinfeng, X., Yanfen, D., Zhongzhong, Q., Feng, W., Bin, W., Hu, Z., Shimin, Z., Mingshu, Y. Degradation of poly(ethylene terephthalate)/clay nanocomposites during melt extrusion: Effect of clay catalysis and chain extension. *Polym. Degrad. Stab*. 94(2009) : 113.

[63] Stavarache, C., Vinatoru, M., Nishimura, R., Maeda, Y. Fatty acids methyl esters from vegetable oil by means of ultrasonic energy. *Ultrasonics Sonochemistry* 12(2005) : 367-72.

[64] Chen, J. P., Hausladen, M. C., Yang, R.T. Pillared clays and related catalysts. *Catal.* 151(1995) : 135.

[65] Temuujin, J., Jadambaa, T., Burmaa, G., Erdenechimeg, S., Amarsanaa, J., MacKenzie, K. J. D., Characterisation of acid activated montmorillonite clay from Tuulant (Mongolia). *Ceram. Int*. 30(2004) : 251.

[66] Long, R. Q., Yang, R. T., Kinetics of selective catalytic reduction of NO with NH_3 on Fe-ZSM-5. *Catal*. 190(2000) : 22.

[67] Corma, A., Martín-Aranda, R. M., Sánchez, F. Zeolites as base catalysts: Condensation of benzaldehyde derivatives with activated methylenic compounds on germanium-substituted faujasite. *J. Catal.*, 126(1990) : 192.

[68] Available from: PTT Public Company Limited, http://www.pttplc.com/TH/Default.aspx

[69] Barnwal, B. K., Sharma, M. P. Prospects of biodiesel production from vegetable oils in India. *Renew. Sustain. E. Rev*., 9(2005) : 363.

Appendices

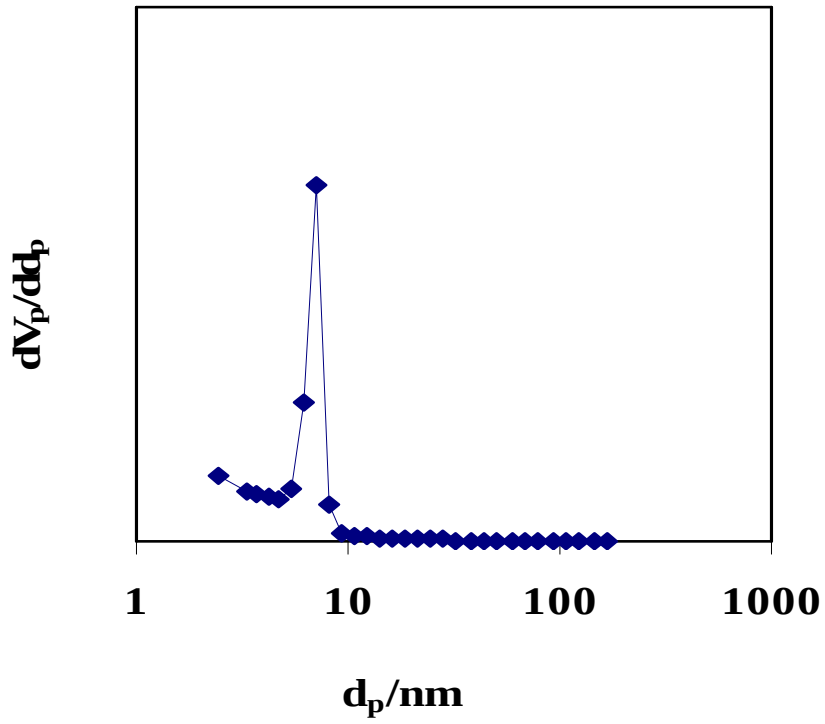

Figure A-1 Pore size distribution of mesoporous silica catalyst.

1. Calculation of methyl oleate and methyl palmitate yield

$$\% \text{ Methyl oleate yield} = \frac{\text{Mole of methyl oleate}}{\text{Mole of starting oleic acid}} \times 100 \quad \text{…..…(A-1)}$$

$$\text{Where ; Mole of starting oleic acid} = \frac{\text{Weight of atarting oleic acid (g)}}{\text{Molecular weight of oleic acid (g/mole)}}$$

$$\text{Mole of methyl oleate} = \text{Mole of methyl oleate for GC analyze} \times \text{sampling factor}$$

$$\text{Mole of methyl oleate for for GC analyze} = \frac{\text{Weight of methyl oleate calculated from standard curve (g)}}{\text{Molecular weight of methyl oleate (g/mole)}}$$

- Yield of methyl palmitate and tri-glyceride was calculated similar to methyl oleate.

2. Calculation of FFA conversion

2.1 %FFA conversion of starting mixed refined palm oil and 15 wt.% oleic acid

- The starting free fatty acid (FFA) value in stating oil = 15 wt.%
- FFA value that was investigated from titration technique after reaction = A wt.%

$$\% \text{ FFA conversion} = 100 - ((100 \times A)/15)$$

2.2 %FFA conversion of starting Jatropha oil

- The starting free fatty acid (FFA) value in stating oil = B wt.%
- FFA value that was determined from titration technique after reaction = C wt.%

$$\% \text{ FFA conversion} = 100 - ((100 \times C)/B)$$

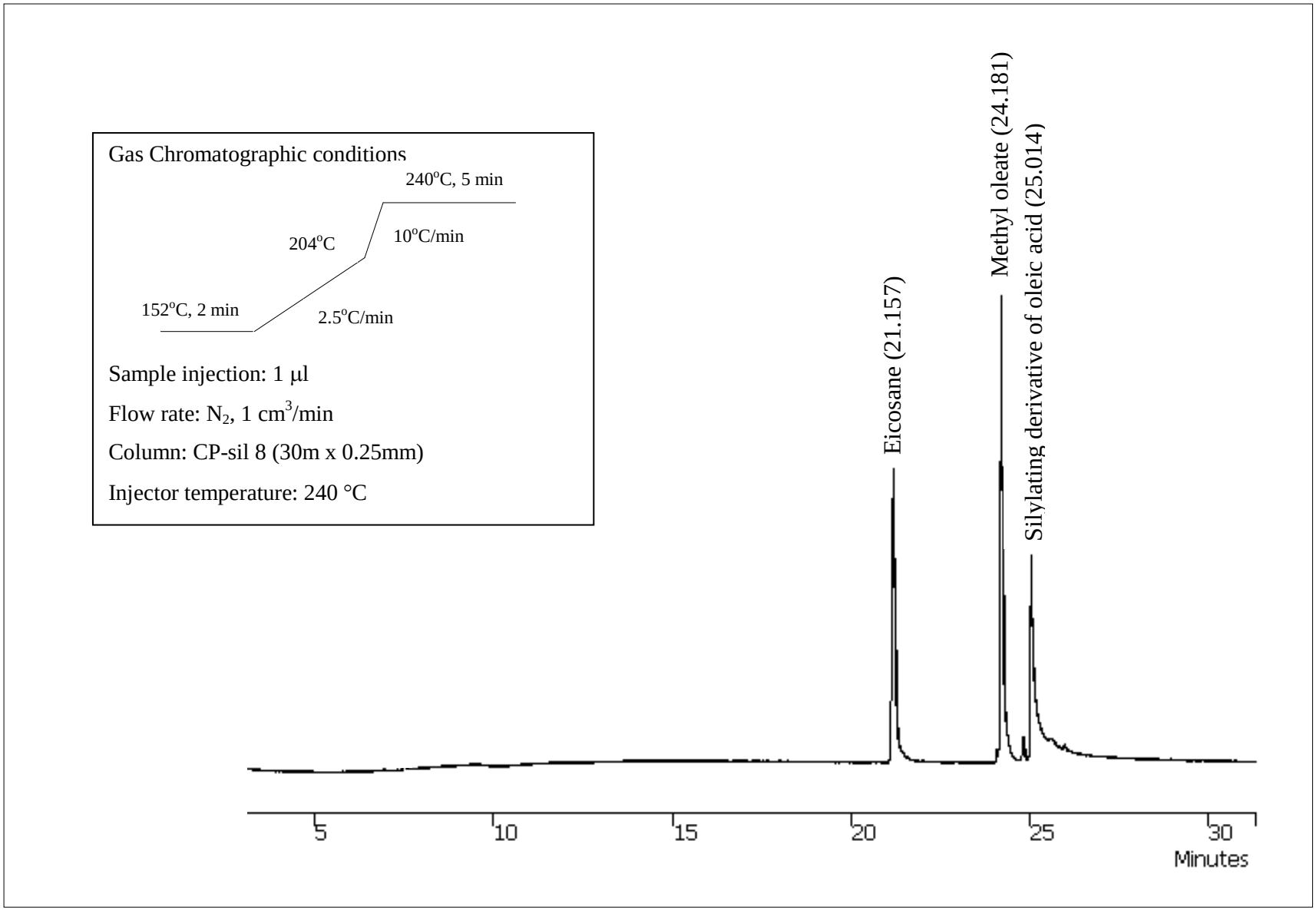

Figure A-2 GC chromatogram of methyl oleate product from esterification reaction.

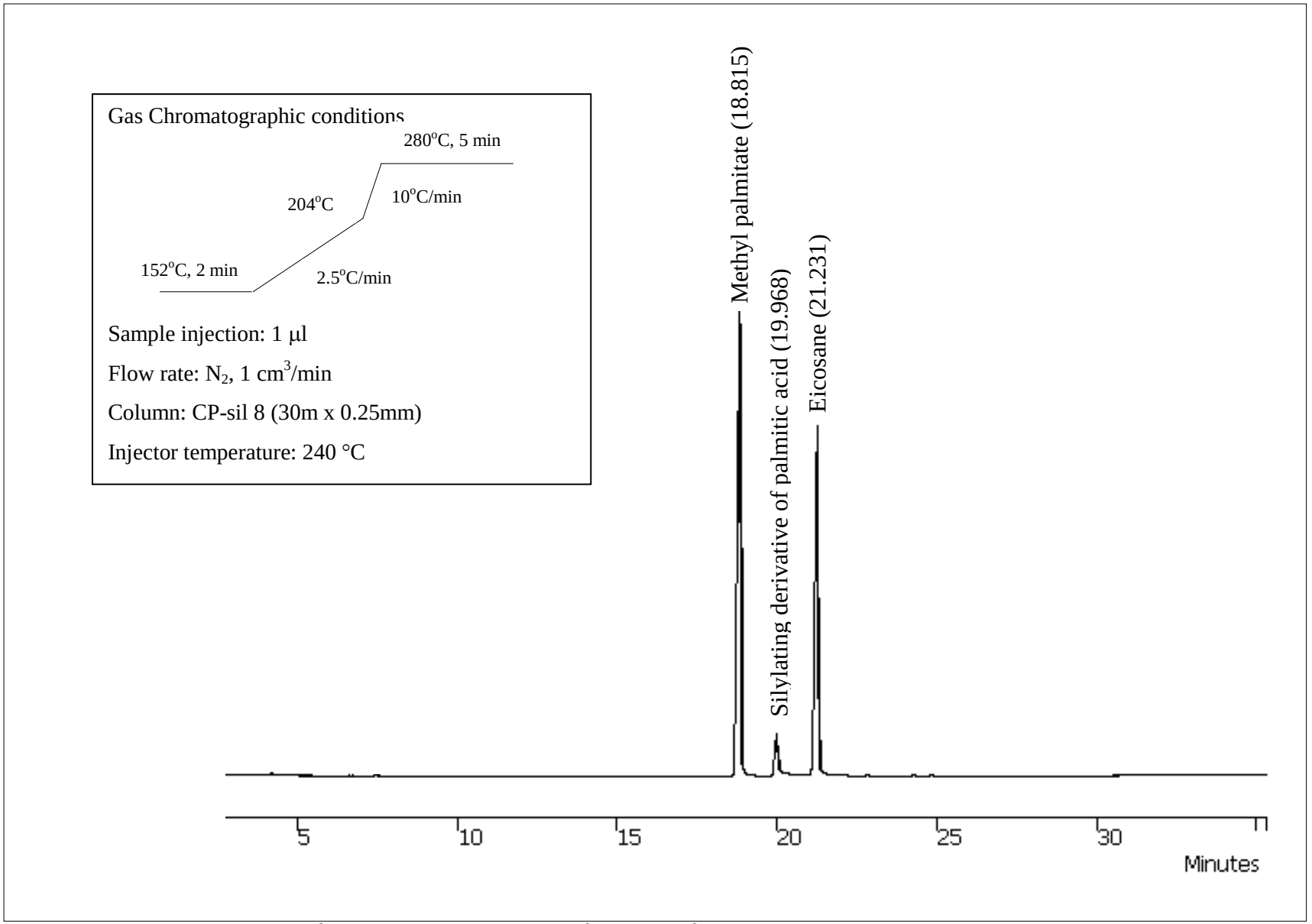

Figure A-3 GC chromatogram of methyl palmitate product from esterification reaction.

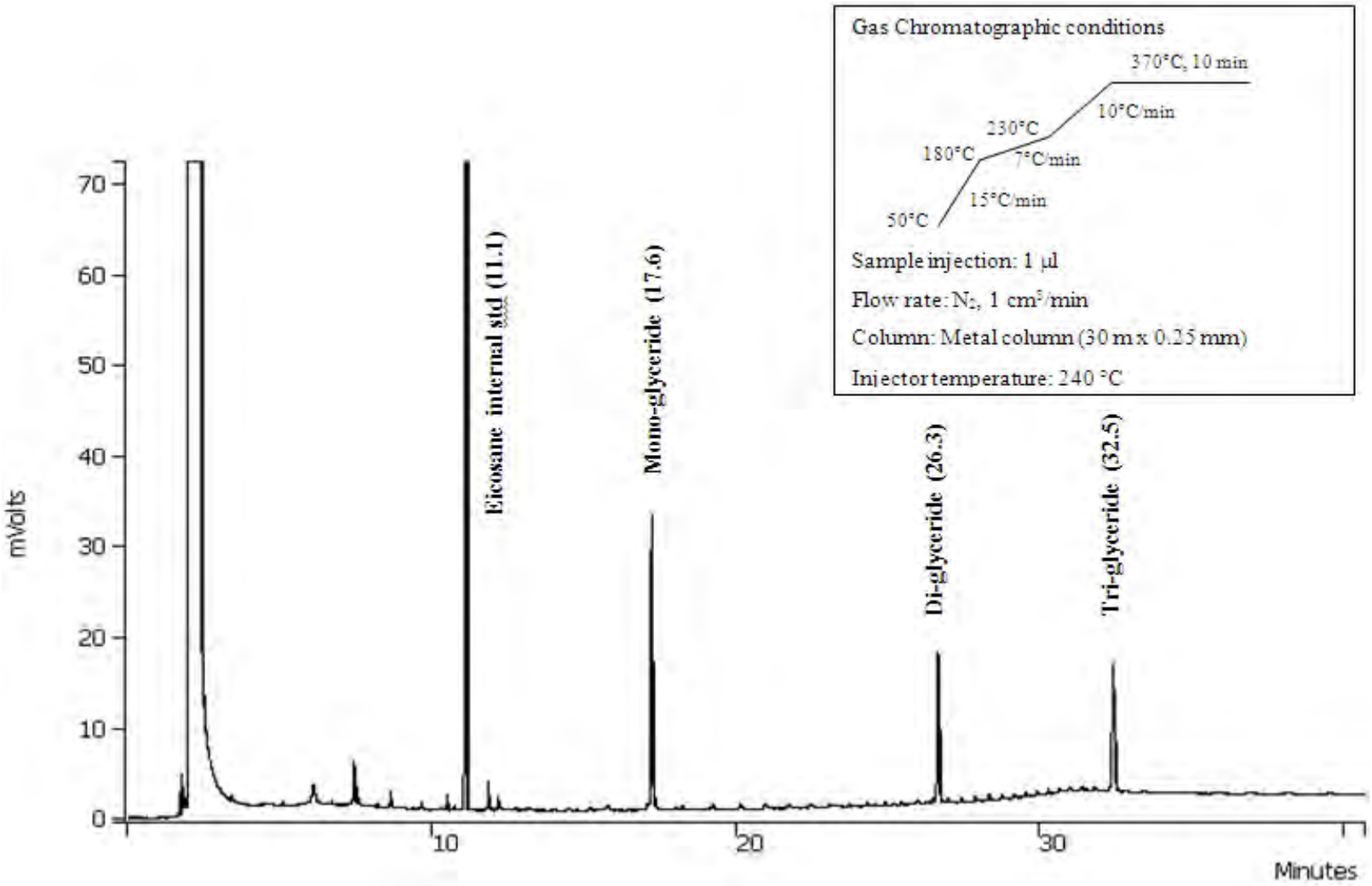

Figure A-4 GC chromatogram of mono-, di- and tri-glyceride product from esterification reaction.

3. Standard calibration curve

3.1 Methyl oleate calibration curve

The concentrations of methyl oleate were prepared as 1.0×10^{-3} M, 5.0×10^{-3} M, 1.0×10^{-2} M, 5.0×10^{-2} M and 1.0×10^{-1} M. The standard calibration curve of methyl oleate was shown in Figure A-5. The standard curve equation is expressed as following

$$y = 1.2247x + 0.0733$$

where y is M_{MO}/M_{Int} ; M_{MO} = Mass of methyl oleate (g)

M_{Int} = Mass of internal standard (g)

x is A_{MO}/A_{int} ; A_{MO} = Peak area of methyl oleate

A_{Int} = Peak area of internal standard

The correlation coefficient R^2 value for methyl oleate calibration curve is 0.9998

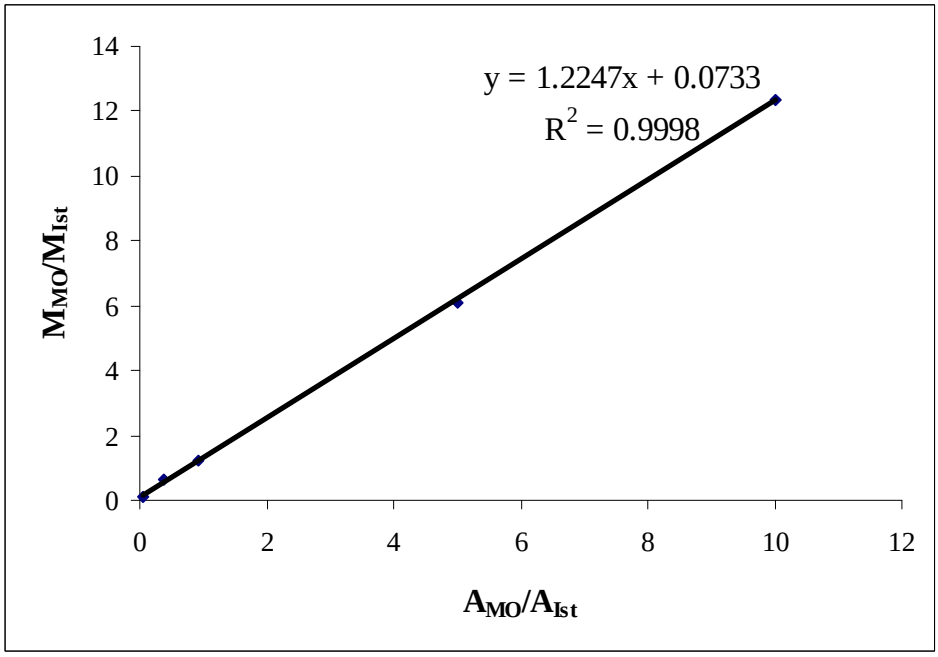

Figure A-5 Calibration curve of methyl oleate.

3.2 Methyl palmitate calibration curve

The concentrations of methyl palmitate were conducted as 1.0×10^{-3} M, 5.0×10^{-3} M, 1.0×10^{-2} M, 5.0×10^{-2} M and 1.0×10^{-1} M. The standard calibration curve of methyl palmitate was shown in Figure A-6. The standard curve equation is expressed as following

$$y = 1.4488x + 0.0181$$

where y is M_{MP}/M_{Int} ; M_{MP} = Mass of methyl palmitate (g)

M_{Int} = Mass of internal standard (g)

x is A_{MP}/A_{int} ; A_{MP} = Peak area of methyl palmitate

A_{Int} = Peak area of internal standard

The correlation coefficient R^2 value for methyl palmitate calibration curve is 0.9997

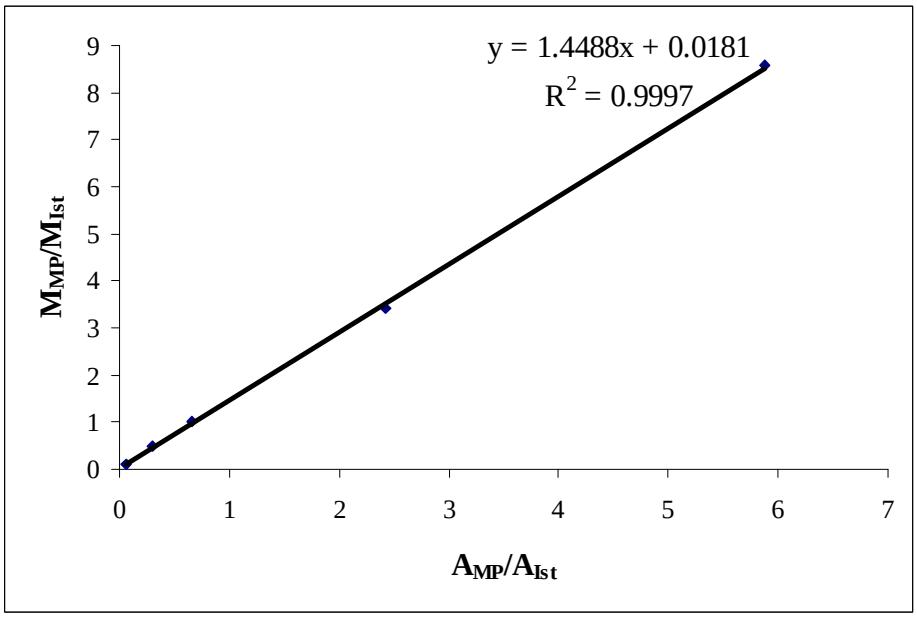

Figure A-6 Calibration curve of methyl palmitate.

3.3 Mono-glyceride calibration curve

The concentrations of mono-glyceride were prepared as 4.21×10^{-5} M, 8.42×10^{-5} M, 4.21×10^{-4} M, 8.42×10^{-4} M and 4.21×10^{-3} M. The standard calibration curve of mono-glyceride was shown in Figure A-7. The standard curve equation is expressed as following

$$y = 2.4787x + 0.0608$$

where y is M_{MG}/M_{Int} ; M_{MG} = Mass of mono-glyceride (g)

M_{Int} = Mass of internal standard (g)

x is A_{MG}/A_{int} ; A_{MG} = Peak area of mono-glyceride

A_{Int} = Peak area of internal standard

The correlation coefficient R^2 value for mono-glyceride calibration curve is 0.9995

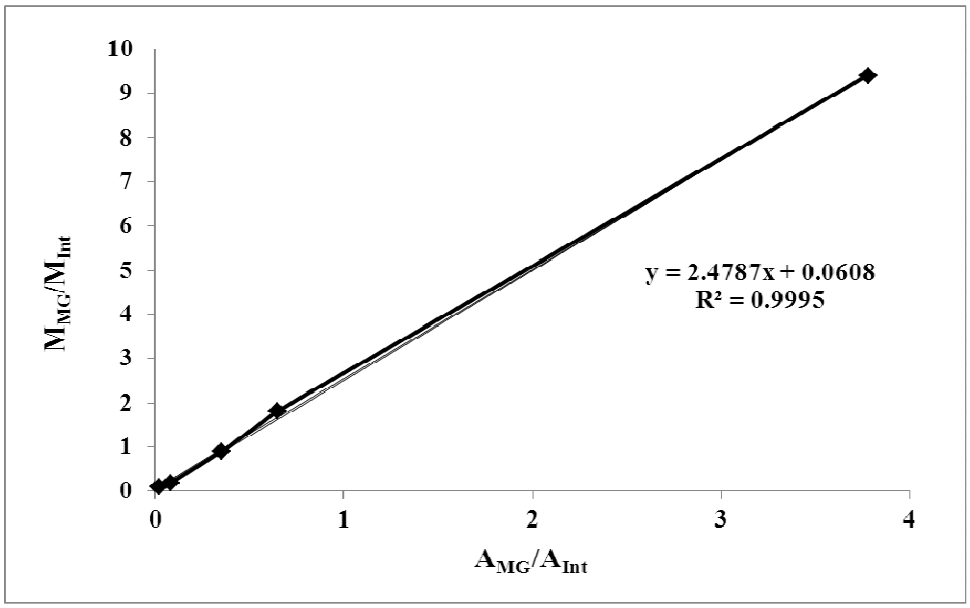

Figure A-7 Calibration curve of mono-glyceride.

3.4 Di-glyceride calibration curve

The concentrations of di-glyceride were performed as 1.61×10^{-5} M, 8.05×10^{-5} M, 1.61×10^{-4} M, 8.05×10^{-4} M and 1.61×10^{-3} M. The standard calibration curve of di-glyceride was shown in Figure A-8. The standard curve equation is expressed as following

$$y = 3.3633x + 0.0064$$

where y is M_{DG}/M_{Int} ; M_{DG} = Mass of di-glyceride (g)

M_{Int} = Mass of internal standard (g)

x is A_{DG}/A_{int} ; A_{DG} = Peak area of di-glyceride

A_{Int} = Peak area of internal standard

The correlation coefficient R^2 value for di-glyceride calibration curve is 0.9999

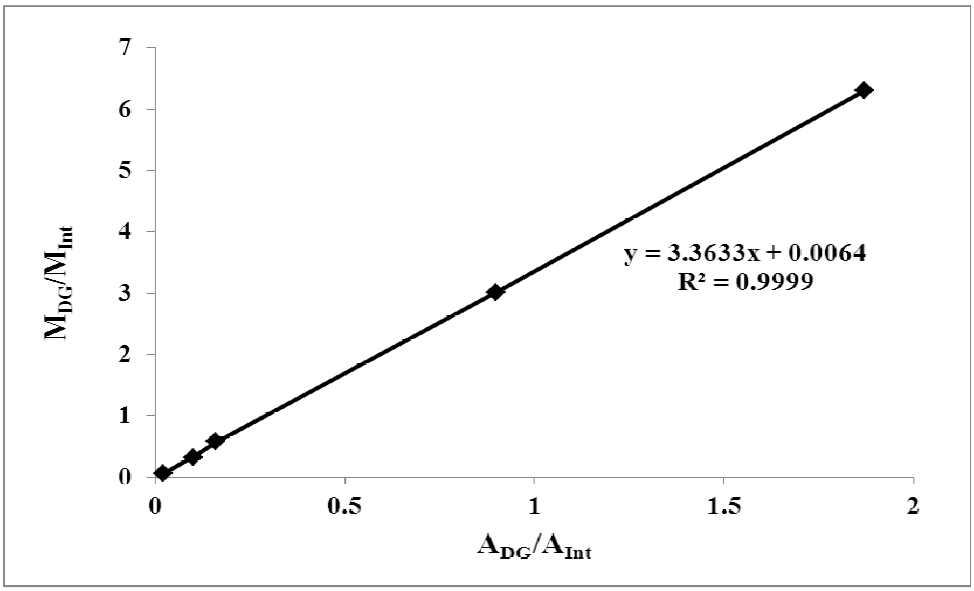

Figure A-8 Calibration curve of di-glyceride.

3.5 Tri-glyceride calibration curve

The concentrations of tri-glyceride were carried out as 1.13×10^{-5} M, 5.65×10^{-5} M, 1.13×10^{-4} M, 5.65×10^{-4} M and 1.13×10^{-3} M. The standard calibration curve of tri-glyceride was shown in Figure A-9. The standard curve equation is expressed as following

$$y = 2.0943x + 0.0069$$

where y is M_{TG}/M_{Int} ; M_{DG} = Mass of tri-glyceride (g)

M_{Int} = Mass of internal standard (g)

x is A_{TG}/A_{int} ; A_{DG} = Peak area of tri-glyceride

A_{Int} = Peak area of internal standard

The correlation coefficient R^2 value for tri-glyceride calibration curve is 0.9999

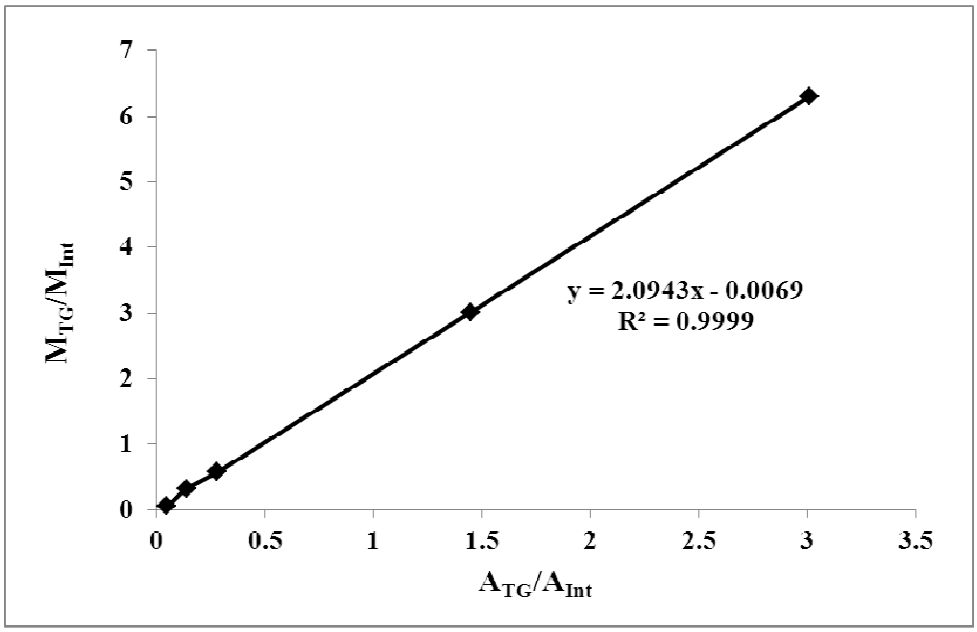

Figure A-9 Calibration curve of tri-glyceride.

Table A-1 EU Specification for automotive diesel [67]

Specification	Units	Year 2000 Limits	Possible Future Limits
Cetane number		51 (min)	55 (min)
Cetane index		No spec	52 (min)
Density@15^{o}C	g/cm^{3}	0.845 (max)	0.84
Distillation			
90% boiling point	^{o}F	No spec	608 (max)
95% boiling point	^{o}F	680 (max)	644 (max)
Final boiling point	^{o}F	No spec	662 (max)
90% boiling point	^{o}C	No spec	320 (max)
95% boiling point	^{o}C	360 (max)	340 (max)
Final boiling point	^{o}C	No spec	350 (max)
Polyaromatic hydrocarbons (PAH)	wt%	11 (max)	2 (max)
Total aromatic	wt%	No spec	15 (max)
Sulfur	wppm	350 (max)*	10 (max)

***** As discussed elsewhere, diesel sulfur will be limited to 50 wppm in 2005

Table A-2 Chemical and physical properties of diesel and biodiesel [68]

Properties	MOC SPEC.	Diesel	Biodiesel
Specific gravity @ 15.6/15.6 °C	0.81-0.87	0.8302	0.8342
Cetane index	Min. 47	58.2	57.2
Viscosity @ 40 °C cSt	1.8-4.1	3.34	3.725
Pour point °C	Max. 10	0	-3
Sulfur content %wt.	Max 0.05	0.037	0.032
Copper strip corrosion (number)	Max. 1	1a	1a
Carbon residue %wt.	Max 0.05	< 0.001	< 0.001
Water and sediment %vol.	Max 0.05	Traces	Traces
Ash %wt.	Max 0.01	0.001	0.001
Flash point °C	Min 52	69	70
Distillation	-	-	-
90% recovered °C	Max. 357	352.0	356.2
Colour	Max. 40	0.5	0.5
Lubricity by HFRR	Max.460	465	204
Gross heating value (J/g)	-	45906	45387
TAN (mgKOH/g)	-	-	-
Total insoluble mg/100 ml	-	-	-
Total aromatics g/100 ml	-	23.2	22.7

Table A-3 Properties of biodiesel from different oils [69]

Vegetable oil methyl esters (biodiesel)	Cetane No.	Kinematic Viscosity at 38°C (mm^2/s)	Lower heating value (MJ/kg)	Clound point (°C)	Pour point (°C)	Flash point (°C)	Density (kg/l)
Peanut	4.9	54	33.6	5	-	176	0.883
Soya bean	4.5	45	33.5	1	-7	178	0.885
Babassu	3.6	63	31.8	4	-	127	0.875
Palm	5.7	62	33.5	13	-	164	0.880
Sunflower	4.6	49	33.5	1	-	183	0.860
Tallow	-	-	-	12	9	96	-
Diesel	3.06	50	43.8	-	-19	76	0.855
20% biodiesel blend	3.2	51	43.2	-	-16	128	0.859

4. Research outcomes

Table A-4 Research outcomes

Type	Title	Patent /Journal	Submitted number/Paper impact factor
Patent	Preparation of Acidic Mesoporous Silicon Oxide Catalyst for Fatty Acid Esterification	Thailand	1201002017
Patent	Preparation of Acid Treated Bentonite Catalyst for Fatty Acid Esterification	Thailand	1201002016
Paper (Published)	Acid-Activated Pillar Bentonite as a Novel Catalyst for the Esterification of High FFA Oil	Powder Technology	2.08
Paper (Submitted)	Esterification of Oleic Acid and High Acid Content Palm Oil over an Acid-Activated Bentonite Catalyst	Applied Clay Science	2.47
Paper (In preparation)	Propyl Sulfonic Acid Functionalized Mesoporous Silica Catalyst for Esterification of Fatty Acid	Microporous and Mesoporous Materials	3.28

Detail:

1. Patent : Preparation of Acidic Mesoporous Silicon Oxide Catalyst for Fatty Acid Esterification

   The preparation of hexagonal mesoporous silica was conducted by varying the synthesis crystallization time. Then mesoporous silica sample was acidified by anchoring 3-mercaptopropyltrimethoxysilane as a propyl-thiol precursor using post-synthesis grafting method. The propyl sulfonic functionalized silica material was catalytic activity tested in esterification of oleic acid, high acid content palm oil, Jatropha oil and waste cooking oil with methanol. This catalyst exhibited highest product yield at the optimal reaction condition.

2. Patent : Preparation of Acid Treated Bentonite Catalyst for Fatty Acid Esterification

   The natural bentonite samples in sodium and calcium form were acid activated by varying the concentration of H_2SO_4 and HNO_3 solution from 0.25 to 2.0 M. The prepared materials were tested in esterification of oleic acid, high acid content palm oil, Jatropha oil and waste cooking oil with methanol. The 0.5 M H_2SO_4 activated Na-bentonite provided highest product yield.

3. Paper : Acid-Activated Pillar Bentonite as a Novel Catalyst for the Esterification of High FFA Oil

   The synthesis process of pillar bentonite materials consisted of three main steps: surfactant intercalation, silica pillar polymerization and surfactant removal. Moreover, the pillar bentonite material was acidic raised by sulfuric acid activation. Raw bentonite was increased in specific surface areas by porous pillar. Acidic pillar bentonite gave highest catalytic activity in biodiesel production. Furthermore, acidic pillar bentonite is tolerant than Amberlyst-15 in reused catalyst testing.

4. Paper : Esterification of Oleic Acid and High Acid Content Palm Oil over an Acid-Activated Bentonite Catalyst

   The esterification reaction of oleic free fatty acid with methanol and esterification of high acid content palm oil with methanol or ethanol catalyzed over acid treated bentonite has been recovered. Na-bentonite was acid activated by H_2SO_4 and HNO_3 solution with varying concentration from 0.25 to 2.0 M. The results indicated that the acid-treated bentonite with 0.5 M H_2SO_4 catalyst exhibited highest methyl oleate yield and FFA conversion. Moreover, this catalyst also gave methyl oleate yield and FFA conversion higher than commercial Amberlyst-15.

5. Paper : Propyl Sulfonic Acid Functionalized Mesoporous Silica Catalyst for Esterification of Fatty Acid

Three morphology types of SBA-15 materials (rope, rod and fiber) were conducted to study their catalytic properties and to compare with MCM-41 smaller pore size sample. Propyl sulfonic acid functionalized mesoporous silica catalysts were synthesized by post-synthesis grafting method using 3-mercaptopropyltrimethoxysilane as a propyl-thiol precursor. Catalytic performances of propyl sulfonic acid functionalized mesoporous silica materials were studied in esterification of oleic acid with small and long chain alcohol molecules, in order to prove the effect of catalytic pore size to substrate conversion and product yield. Propyl sulfonic functionalized mesoporous silica catalysts have been found to be highly active and selective for these esterifications.

VITAE

Miss Sirima Jeenpadiphat was born on May 12, 1983 in Bangkok, Thailand. She graduated with Bachelor's Degree in General Science from Faculty of Liberal Arts & Science, Kasetsart University in 2006. Moreover, she graduated with Master's Degree in Petrochemistry and Polymer Science from Faculty of Science, Chulalongkorn University in 2008. After that, she continued her study in Nanoscience and Technology Program, Faculty of Graduate School, Chulalongkorn University. During her graduate study, she also received a research scholarship from PTT Public Company Limited. She has completed her study leading to a Doctor of Philosophy (Ph.D.) in Nanoscience and Technology Program in 2012.